

Nuclear magnetic resonance spectroscopy: A comprehensive tool for analyzing liquid products in electrochemical CO₂ reduction

Aymen S. Abu Hatab, Yahia H. Ahmad, Mohamed F. Mady, Yasser Hassan, Abdelrahman Zkria, Alessandro Sinopoli, Aboubakr M. Abdullah, Siham Y. Al-Qaradawi, Tsuyoshi Yoshitake, Mazen Khaled

Item type

Journal Contribution

Terms of use

This work is licensed under a [CC BY 4.0](https://creativecommons.org/licenses/by/4.0/) license

This version is available at

https://manara.qnl.qa/articles/journal_contribution/Nuclear_magnetic_resonance_spectroscopy_A_comprehensive_tool_for_analy

Access the item on Manara for more information about usage details and recommended citation.

Posted on Manara – Qatar Research Repository on

2025-04-02



Nuclear magnetic resonance spectroscopy: A comprehensive tool for analyzing liquid products in electrochemical CO₂ reduction

Aymen S. Abu Hatab^a, Yahia H. Ahmad^a, Mohamed F. Mady^a, Yasser Hassan^a, Abdelrahman Zkria^{b,c}, Alessandro Sinopoli^d, Aboubakr M. Abdullah^e, Siham Y. Al-Qaradawi^a, Tsuyoshi Yoshitake^b, Mazen Khaled^{a,*}

^a Department of Chemistry and Earth Sciences, College of Arts and Sciences, Qatar University, Doha 2713, Qatar

^b Department of Advanced Energy Science and Engineering, Faculty of Engineering Sciences, Kyushu University, Kasuga, Fukuoka 816-8580, Japan

^c Center for Japan-Egypt Cooperation in Science and Technology (E-JUST Center), Kyushu University, Kasuga, Japan

^d Qatar Environment and Energy Research Institute (QEERI), Hamad Bin Khalifa University, Doha, Qatar

^e Center for Advanced Materials (CAM), Qatar University, 2713 Doha, Qatar

ARTICLE INFO

Keywords:

Quantitative NMR

CO₂ utilization

Electrocatalysis

CO₂ electroreduction

Value-added multi-carbon compounds

ABSTRACT

The electrochemical reduction of carbon dioxide (eCO₂RR) has become a very promising pathway that can be used in the transformation of CO₂ to important chemical products and, thus, is one of the mitigations of climate change and will contribute toward sustainable chemical production. This review aims at presenting the importance of Nuclear Magnetic Resonance spectroscopy (NMR) to analyze and quantify the liquid-phase products obtained by eCO₂RR. This provides a summary regarding the role that NMR plays in the process of reducing carbon dioxide. The following discusses the benefits: identification, complete elucidation, and follow-up on reactions involving CO₂ electro-reduction. Pulse experiments corresponding to different methods for water signal suppression are considered separately, outlining some recent developments in the interference water signal reduction which is very crucial for the correct NMR data acquisition in aqueous electrolytes. Certain selected products are described, like carbon monoxide (CO)-associated liquids, formic acid, methanol, and formaldehyde as examples of the NMR precision for the characterization of important compounds. Further, the quantification of C₂ products such as ethanol and acetate is discussed in order to illustrate how the technique can be applied in the elucidation of reaction mechanisms and optimization of catalyst performance. This review covers challenges, advanced methodologies, and emerging trends in order to underline the transformative role that NMR plays in advancing CO₂ electrochemical reduction toward sustainable chemical synthesis.

1. Introduction

The interest in the electrochemical reduction reaction of CO₂ (eCO₂RR) has significantly increased owing to its importance in converting CO₂, a key source of greenhouse gas emission, into valuable and environmentally acceptable chemical products [1–4]. This dual-purpose approach, which aims to reduce climate change consequences while also producing economically viable resources, emphasizes the importance of electrochemical CO₂ reduction [5–7]. Essentially, applied electric potential at the interface of an electrode drives a series of chemical changes that CO₂ molecules undergo as processes of electrochemical reduction. Many byproducts are formed out of this multi-step process, often comprising some basic ones like carbon monoxide (CO) [8–11], and

formate (HCOO[−]) [12–17], but sometimes it extends to higher hydrocarbons and oxygenates [18–23]. The selectivity and efficiency of electrochemical pathways to these reactions determine the production of desired products while reducing environmental impact (Fig. 1) [24–27].

The eCO₂RR, as an electrochemical field, becomes the alternative to the traditional carbon-intensive methods in the production of chemicals and fuels, thereby motivating researchers to extensively explore the intricacies of eCO₂RR. This understanding can only be achieved by precise and quantitative analytical methodologies that will give an accurate outcome regarding the products of eCO₂RR [6,21,22]. In the analysis of such products, gaseous and liquid phases are included. The gaseous products formed, like carbon monoxide, methane, ethane, and

* Corresponding author.

E-mail address: mkhalel@qu.edu.qa (M. Khaled).

<https://doi.org/10.1016/j.jelechem.2025.119097>

Received 23 January 2025; Received in revised form 20 March 2025; Accepted 27 March 2025

Available online 28 March 2025

1572-6657/© 2025 The Authors. Published by Elsevier B.V. This is an open access article under the CC BY license (<http://creativecommons.org/licenses/by/4.0/>).

ethylene, can be majorly analyzed by gas chromatography through the separation and quantification of produced components in the electrochemical process [8,9,28–30].

The liquid products can be analyzed by many analytical and spectroscopic methods such as high-performance liquid chromatography

(HPLC), liquid chromatography-mass spectrometry (LC-MS), headspace gas chromatography (HS-GC), and NMR, including proton, and carbon NMR (^1H , ^{13}C NMR, respectively) [12,13,31–36]. HPLC has been conventionally carried out as an analytical tool to elucidate products of eCO_2RR . It leans on high-precision separation, analysis, and

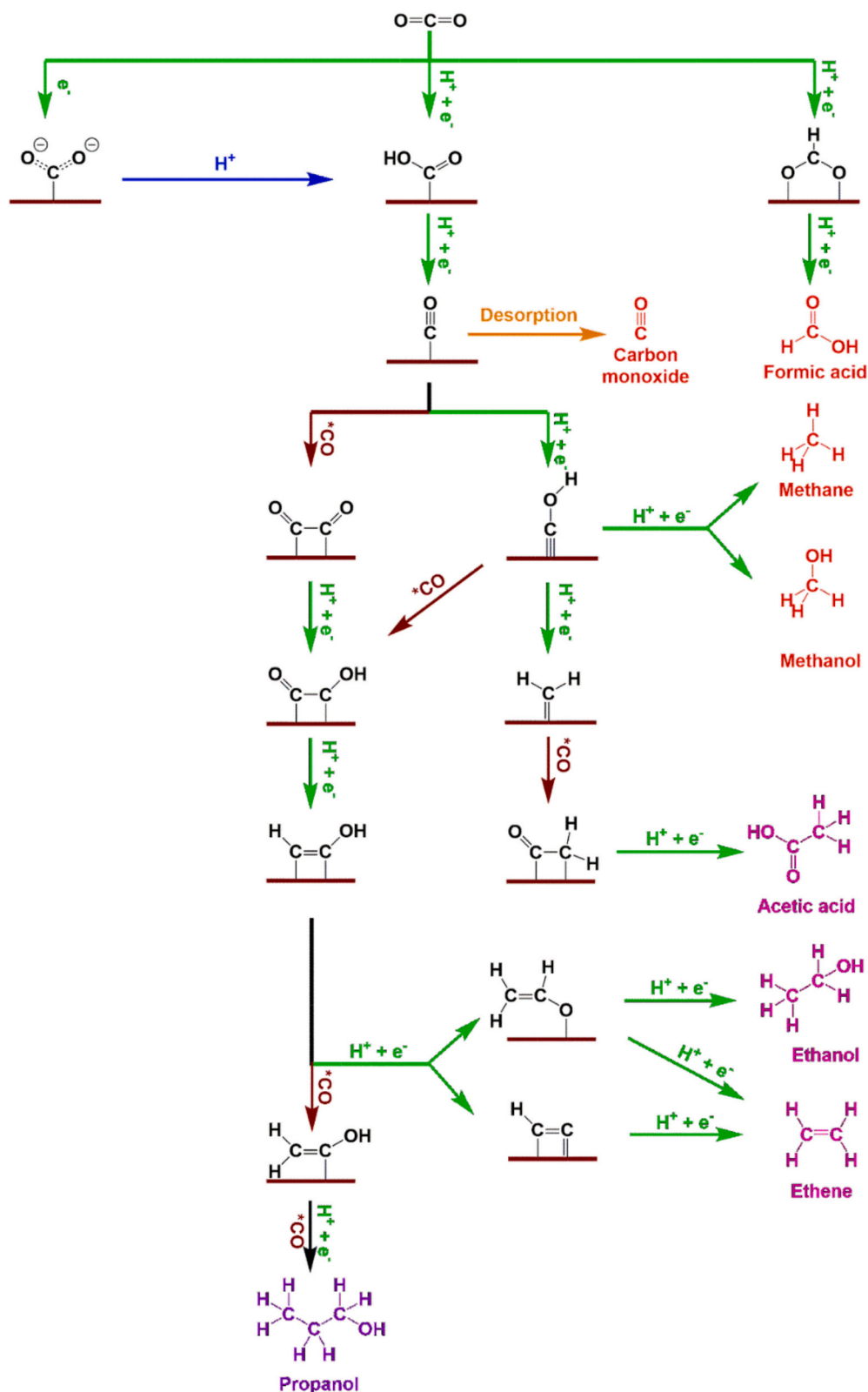


Fig. 1. Mechanism and reaction pathways for eCO_2RR .

quantification of liquid phase products for understanding the reaction mechanism involved in producing sustainable and renewable fuels [12,13,37–39]. LC-MS now becomes a strong candidate as a precise tool for investigation with eCO₂RR products. Such an analytical tool is useful, enabling qualitative and quantitative measurements of the liquid phase products [31,32]. HS-GC, coupled with a downstream flame ionization detector (FID), has found application in the analysis of volatile products. Here, C₁, C₂, and C₃ are methanol, ethanol, and *n*-propanol, respectively [33,34,36]. This combination develops a precise tool for the identification and quantification of liquid products in the eCO₂RR process.

NMR probably represents the most common qualitative methodologies applied to basic analysis such as structure [40–42], purity [43,44], and dynamics of chemical and biochemical entities [45–47]. The principle of the technique rests on the fact that some atomic nuclei, when put in a strong magnetic field, can absorb and immediately re-emit electromagnetic radiation at characteristic frequencies [48,49]. Determination of these frequencies provides comprehensive information from NMR on the local environment of selected nuclei within a molecule: functional groups containing given nuclei can be identified and the bonding between atoms can be determined [50–52]. As a non-destructive technique, NMR is particularly useful to confirm the identity and structure of organic compounds, often complex molecular structures, with high precision [53,54].

Besides organic chemistry, NMR spectroscopy forms an important tool for the investigation of biomolecules such as proteins, nucleic acids, and small metabolites [55,56]. It was with the advent of multidimensional NMR techniques that one could probe into the three-dimensional structure of large biomolecules in solution to gain atomic-level insights into their function and interactions [57–59]. Consequently, NMR can be used in the monitoring of chemical reactions in real time, changes in the conformation of molecules, and dynamic processes such as folding of proteins [60,61]. Because of ease of applicability and the fact that it gives the most relevant structural information without destroying the sample, NMR is an indispensable tool in academia and industry, especially in drug development and materials sciences [53,62,63].

NMR has been applied in an extended way as a trustworthy quantitative technique for liquid products of CO₂ electroreduction [64–66]. Other than the known qualitative tool, it has been used substantially as one of the most effective techniques for monitoring reactions and assessing purity and determination of concentration [44,67,68]. Quantification of liquid products of eCO₂RR based on NMR has recently been utilized by many researchers [69–74]; this can be assigned to its ability to provide structural details, its ability to detect multiple compounds, and simplicity in contrast to other analytical tools [53,54]. To the best of our knowledge, this is the first comprehensive review in the open literature that highlights the utilization of NMR as a quantitative tool for eCO₂RR liquid products. The focus will be given to the role of NMR as a quantitative method of analysis for CO₂ electroreduction liquid products. This will be achieved through a critical review of the recent progress in CO₂ electrochemical reduction reaction, including NMR spectroscopy applied in the analysis of CO₂ reduction products, key parameters measured by NMR, state-of-the-art applications of NMR in studies on CO₂ reduction, challenges and their remedies related to quantitative analysis based on NMR, and finally perspectives and new trends.

2. NMR analysis for electrochemical CO₂ reduction: advances and limitations

Gas chromatography-mass spectrometry (GC-MS) is a general analytical technique for the identification and quantification of volatile organic compounds. GC-MS is extremely sensitive and specific and therefore very effective for the identification of gaseous and volatile liquid products that are generated in electrochemical CO₂ reduction [31,32]. GC-MS is limited by the requirement of pre-calibration with

reference compounds, which might limit detection of new or unknown products [75]. Some compounds would also need to be derivatized to allow for detection, thus complicating the analysis.

Another conventional method of analysis for liquid-phase products is HPLC, a method in which compounds are separated based on the interaction between compounds and the stationary phase, and it employs detectors such as refractive index (RID) or variable wavelength detectors (VWD) typically. HPLC best suits the analysis of non-volatile liquid products such as formate [76] and acetate [77] but is deficient in the capability of detecting unknowns since structural information is not available [75]. Also, the requirement for the chromatographic separation can provide a boost to the analysis time [75].

Ion chromatography (IC) is used primarily to detect ionic analytes such as formate, acetate, and oxalate [78–81]. While IC is very selective for these charged analytes, it can only be used for a restricted class of analytes and is less convenient for neutral or non-polar substances [75]. Moreover, the requirement of special ion-exchange columns and eluent conditions can make the technique less flexible than others [75].

Nuclear magnetic resonance (NMR) spectroscopy is the most appropriate method for analyzing liquid products since it can provide qualitative and quantitative information to a very precise degree [44,64–68]. NMR does not require extensive reference standard calibration, as in the case of GC-MS and HPLC, and is thus particularly valuable in new or unexpected product identification. It allows the simultaneous determination of multiple compounds in a multi-component sample without the need for chromatographic separation, reducing time and labor of analysis [53,54]. NMR is also a non-destructive technique that leaves the sample intact, giving guaranteed and reproducible results [53,54]. While it is less sensitive for very low concentrations and less ideal for very volatile substances, its ability to probe a wide range of liquid products with little pre-treatment makes it the most widespread and reliable means of electrochemical CO₂ reduction studies. For complete characterization, NMR is best supplemented by other techniques like GC-MS for volatile compounds and HPLC for additional confirmation of liquid products.

3. NMR spectroscopy in analyzing CO₂ reduction products

Proton NMR spectroscopy (¹H NMR) has been widely utilized in the analysis of protonated organic compounds [40,41,53]. The high sensitivity of the state-of-art NMR machine is particularly noteworthy, making it a powerful machine for detecting low concentration of trace protonated products in a complex mixture [64,65,82]. In addition, ¹H NMR spectroscopy exhibits distinctive advantages compared to other product identification techniques, this is attributed to the superfluous requirement for comparison with standard references when identifying new compounds [64]. This feature is considered valuable when we have a mixture of products in an aliquot during a chemical reaction, such as in an electrochemical CO₂ reduction reaction [64].

The effective utilization of ¹H NMR spectroscopy for precise quantitative analysis of eCO₂RR products requires tremendous attention to the following factors: First, ¹H NMR analysis requires the use of deuterated solvents to eradicate interference from solvent's active protons [83]. In this regard, the aqueous eCO₂RR electrolyte such as potassium bicarbonate (KHCO₃), sodium bicarbonate (NaHCO₃), and potassium hydroxide (KOH), requires the water suppression method to ensure accuracy and reliability of liquid products [69,84–87]. Therefore, the need for optimization of water suppression method becomes crucial to enhance the signal-to-noise ratio and reduce the signal artifacts, leading to enhancing the sensitivity and resolution of the obtained NMR spectrum of the eCO₂RR mixture [64]. Moreover, the advanced pulse technique associated with solvent suppression and WATERGATE techniques, are commonly used to further enhance the sensitivity and specificity of ¹H NMR measurements in eCO₂RR aqueous complex reaction mixture [64,69,84–87].

4. Pulse experiments associated with water suppression method

The analysis of eCO₂RR products in carbonate or hydroxide electrolytes requires effective suppression of the water signal in ¹H NMR spectra, mitigating the interference of the water peak signal, otherwise, it will obscure the product peaks and distort the spectrum baseline [69,84–87]. Furthermore, the water suppression method is particularly vital especially for aqueous electrolytes, as they suffer from concentration disparities between water and liquid products [83]. Also, the water signal may compromise the reliability and accuracy of quantification of electrolyte products, resulting into dynamic range obstacles and baseline distortions [88,89]. In this regard, it is of utmost priority for researchers to develop and optimize water suppression techniques for advancing the quantification of eCO₂RR liquid products.

The suppression of the water peak in aqueous aliquots is pivotal due to two substantial reasons: the first one is dynamic range issues, and the second reason is baseline distortion and peaks overlapping [88,89]. The dynamic range issues arise when the NMR signal is being collected after the analog-to-digital conversion stage (ADC). This could lead to the substantial concentration disparities and several orders of magnitude (as the intensity of NMR signal is proportional to the concentration) [88]. This might be affected by the peak orders of magnitude of the water peaks and the liquid products' peak. The inability to suppress the water peak causes receiver saturation, leading to spectral distortion which manifests as spurious spectral lines and non-linear baseline oscillation [89]. In addition, it results into inaccurate quantification of eCO₂RR liquid products [64,88]. On the other hand, the failure to suppress the water peak has a great influence on the spectrum baseline, which also

complicates the precise quantification of peak integrals for the desired products. Some peaks can be hidden under the large water peak or overlapped by its tail [64,88,89]. This phenomenon can also impact the visible peaks by causing baseline distortion, which adversely affects the precise analysis of the products [90]. It is, therefore, very important to rectify these two problems by effective suppression of water so that accurate analysis of the product concerning the nearby chemical shifts can be obtained. It increases the reliability and accuracy of the analysis of liquid products by ¹H NMR spectroscopy and enables a deeper understanding of kinetic parameters and the elucidation of reaction mechanisms [88–90].

Various experimental techniques have been developed with the purpose of effectively suppressing water signal interference in NMR spectroscopy. This was reported by Giraudeau et al., where they illustrated some experimental techniques in NMR that can be used to suppress the water signal (Fig. 2, Table 1) [88,89]. Generally, these can be summarized into three general steps: preparation, excitation, and readout [88,91]. Fig. 2a depicts continuous wave saturation, one of a number of techniques that, though in common use, are sensitive to frequency shift. Fig. 2b depicts the DANTE block, an alternative which provides variable suppression of water signals over a spectral region. Fig. 2c depicts the WET (Water suppression Enhanced through T1 effects) pulse sequence, generally cited as efficient and fast for suppressing water signals. Fig. 2d Flip-back approach: a selective pulse flips the water magnetization back to the longitudinal axis to render it undetectable. Excitation blocks, Fig. 2e–i: in this scheme CP and Sat-180 are used to reduce the perturbation of the distant water signal on the metabolite signals of interest. Finally, Fig. 2j–l covers readout blocks

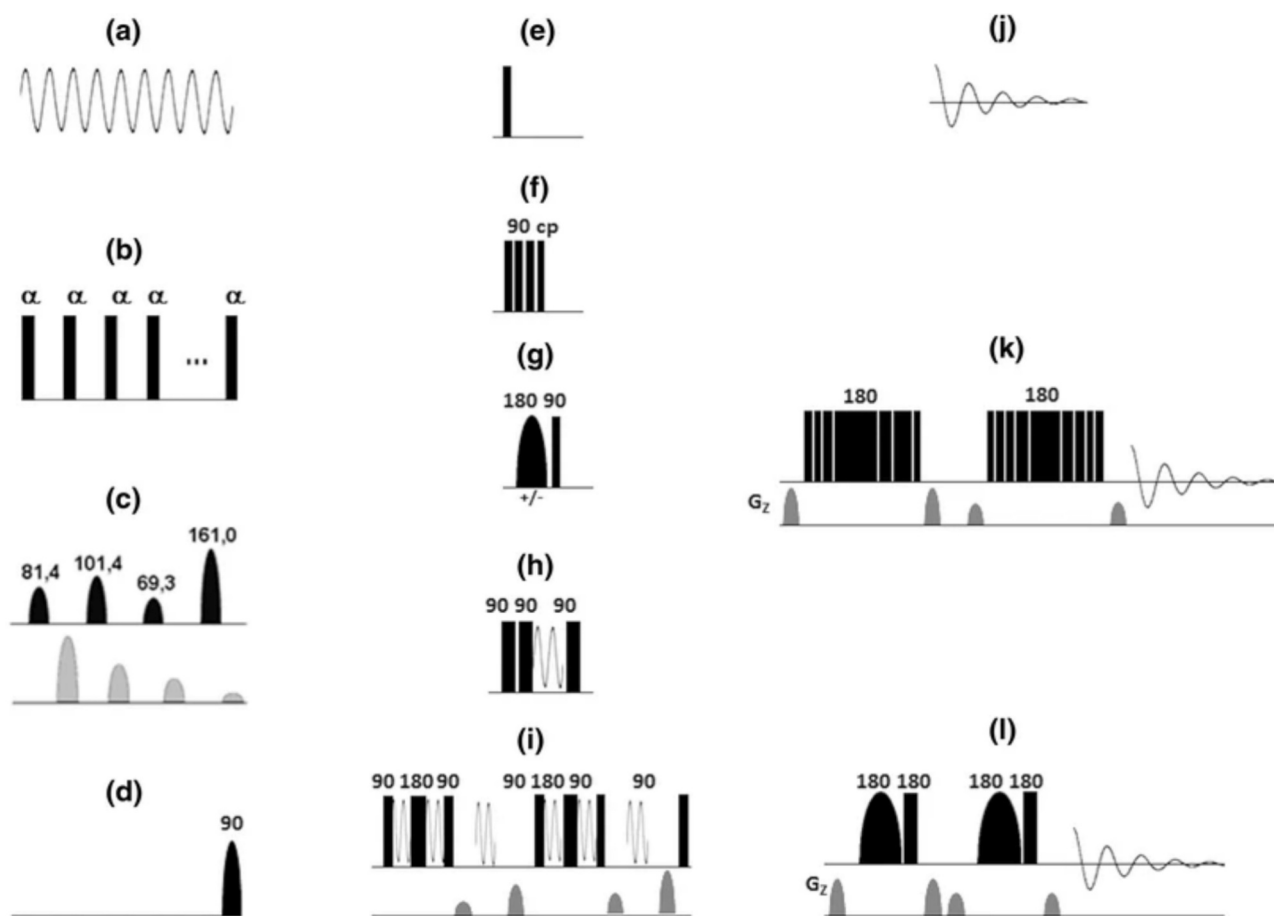


Fig. 2. Fundamental components forming the water suppression sequences. (a–c) Preparation blocks, (e–i) excitation blocks, and (j–l) readout blocks. Specifically, (a) Sat block, (b) DANTE block, (c) WET block, (d) Flip-back block, (e) standard 90° excitation, (f) CP block, (g) Sat-180 block, (h) NOESY-1D block, (i) PURGE block, (k) ES-W5 block, and (l) ES-Sel block. Reproduced with permission from Ref. [88]. Copyright 2015, Springer Nature.

Table 1
Comparison of Water Suppression Techniques in NMR [88,89].

Method	Best suited for	Advantages	Limitations
Presaturation	Samples with minimal exchangeable protons	- Availability - Simplicity	- Influences nearby signals - Sensitive to frequency shifts
WATERGATE	Metabolomics and biological samples	- Effective - Robust	- Requires careful tuning
WET (Water suppression Enhanced through T1 effects)	Hyphenated techniques (LC-NMR) and biomolecules	- Fast - Effective with inhomogeneous samples	- Requires precise calibration
NOESY-1D (Nuclear Overhauser Effect Spectroscopy 1D)	Metabolomics and small molecules	- Suppresses water while preserving signals	- Requires optimization of mixing time
CHESS (Chemical Shift Selective Suppression)	In vivo NMR and imaging applications	- Effective in live samples	- Needs careful tuning
PURGE (Presaturation Utilizing Relaxation Gradients and Echoes)	Quantitative NMR and biomolecules	- Reduces faraway water effects	- Requires multiple steps
Excitation Sculpting (ES)	Complex samples and strong water peaks	- Highly efficient	- Complex sequence

such as the WATERGATE and Excitation Sculpting experiments; these are particularly useful in protein NMR in order to detect exchangeable protons while effectively suppressing the water signal [88].

5. General tutorial for acquiring and analyzing a standard NMR spectrum

For the liquid products that obtained after CO₂ electroreduction, it is better to understand how to prepare the NMR sample and acquire and analyze the obtained NMR spectrum. First, after collecting the liquid product, a suitable amount of the electrolyte is dissolved in a deuterated solvent, such as D₂O, including an internal standard, e.g. dimethyl sulfoxide (DMSO), with a known concentration. Then a known volume of the resulting mixture is transferred into a fresh NMR (about 0.6 mL). The tube is placed within the spectrometer and calibrated to depth using a gauge; it is then accurately positioned within the machine. The spectrometer is set to deuterium resonance of the solvent such that the magnetic field is locked, and shimming is achieved to have maximum field homogeneity and increased spectral resolution.

Following the calibration of the instrument, an appropriate NMR experiment is selected—usually ¹H NMR to detect organic liquid products like formate, acetate, or ethanol, and ¹³C NMR to identify carbon-based compounds. Certain key parameters like spectral width, relaxation delay, and pulse sequences are optimized by setting them for improved detection of signals. The data are then captured and processed using Fourier Transform (FT) to convert the data into an interpretable spectrum. Phase and baseline corrections can be used to correct any distortion obtained in the spectrum. Peaks are ascertained by defining their chemical shifts (δ , in units of ppm), comparing them with known values for established CO₂ reduction products, and using integration to quantify concentration.

Finally, the resulting spectrum is then compared to reference spectra in terms of purifying and identifying the electroreduction products. In the case of observed interference caused by solvent or superposition signals, the resolution can be enhanced using solvent suppression techniques like WATERGATE or WET. By this technique, correct

identification and quantitation of CO₂ electroreduction liquid products are guaranteed, and this provides essential information on product selectivity and reaction efficiency.

6. Quantification of C₁ liquid products

C₁ products are a class of organic compounds that contain a single carbon atom in their chemical structure backbone. C₁ originates from the chemical nomenclature, as “C” represents the carbon and atom 1 relates to the number of carbon atoms in the molecule. Different chemical processes can produce C₁ products, including electrochemical reduction of CO₂, which is a potential pathway for sustainable production of fuels and chemicals. The electrochemical reduction of CO₂ reveals different C₁ products; gaseous products such as carbon monoxide (CO) and methane (CH₄); or liquid products such as formic acid/formate (HCOOH/HCOO⁻), methanol (CH₃OH), and formaldehyde (CH₂O) [92,93]. The liquid products can be analyzed using different analytical and spectroscopic techniques, such as HS-GC, LC-MS, HPLC, and NMR [12,13,31–36]. Recently, several reports have highlighted the importance of utilizing NMR as a powerful tool for identifying and analyzing C₁ products. This will be discussed in detail in the next sections.

6.1. NMR as a tool for characterizing and quantifying products with CO formation

The electrochemical reduction of carbon dioxide (CO₂) to carbon monoxide (CO) is one of the most promising ways to obtain a sustainable fuel, considering that CO is a key building block in many industrial processes [94,95]. As a rule, CO is present in the gaseous phase after the reaction; however, under proper conditions and using an appropriate catalyst, liquid products like formate/formic acid, methanol and/or ethanol may form [96–103]. On the other hand, NMR plays a critical role in confirming liquid products [96–99]. The ability of NMR to accurately detect and quantify any liquid phase products that may coexist with CO provides much-desired information which may be used in optimizing the reaction conditions for high CO selectivity [96–99].

For instance, oxide-derived nanostructured Ag catalysts (OD-Ag) showed a better catalytic activity than untreated polycrystalline Ag with a much lower overpotential and higher selectivity for CO with a Faradaic efficiency of approximately about 80 % [97]. ¹H NMR was used to analyze the liquid products by mixing 450 μ L of electrolyte with a known concentration of tert-butanol, as internal standard, in 50 μ L D₂O. The ¹H NMR experiments were conducted by recording 8 scans and after applying a hard-pulse solvent presaturation pulse sequence accompanied with a 2-s saturation delay, 2-s relaxation delay, 2.5-s acquisition time, and a spectral window of 6400 Hz [97]. Similarly Hatsukade et al. utilized ¹H NMR to investigate the possibility of liquid product formation [96]. They found that their metallic silver electrode could produce CO with high Faradaic efficiency, however, some liquid products were formed during electrolysis, such as formate, methanol and ethanol. ¹³C-labeling electrolysis experiment was conducted to confirm the origin of formed liquid products. As seen in Fig. 3, the peaks of methanol, ethanol and formate were split, which can be attributed to the well apparent coupling between ¹H to ¹³C, confirming that those products were originating from CO₂ [96].

Mun et al. reported that monodisperse Cu–Pd nanoparticles (NPs) with ratio 1:1 exhibited higher selectivity of CO production with Faradaic efficiency of 87 % at a potential of –0.9 V versus reversible hydrogen electrode (RHE) [98]. In the other hand, they investigated the formation of liquid products by quantifying the amount of produced ethanol and formate using a dual internal standards system of DMSO and phenol, respectively. The NMR sample was prepared by mixing 1.0 mL of the electrolyte with 50 μ L of internal standard solution (25 mM phenol with 5 mM DMSO). Finally, 150 μ L of the mixture was transferred to NMR tube containing 450 μ L of D₂O. As seen in Fig. 4, the concentration of obtained formate and ethanol were calculated in

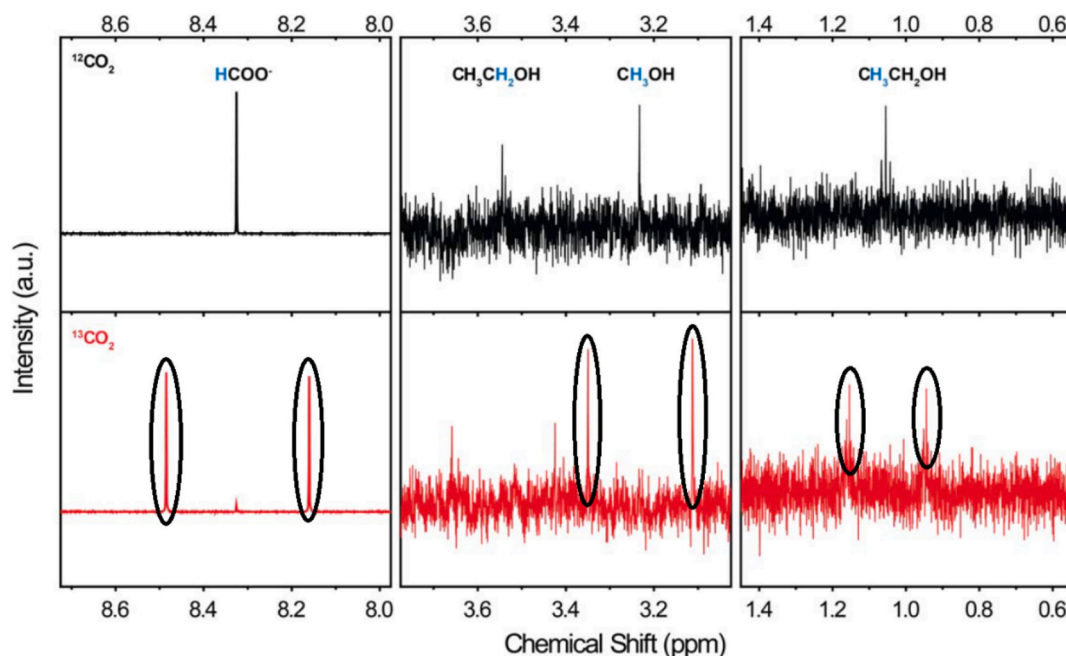


Fig. 3. ^1H NMR spectra of the liquid aliquot from $^{12}\text{CO}_2$ (black) and $^{13}\text{CO}_2$ (red) feeding experiments. Split peaks are in black ovals for each product. Reproduced with permission from Ref. [96]. Copyright 2014, Royal Society of Chemistry. (For interpretation of the references to colour in this figure legend, the reader is referred to the web version of this article.)

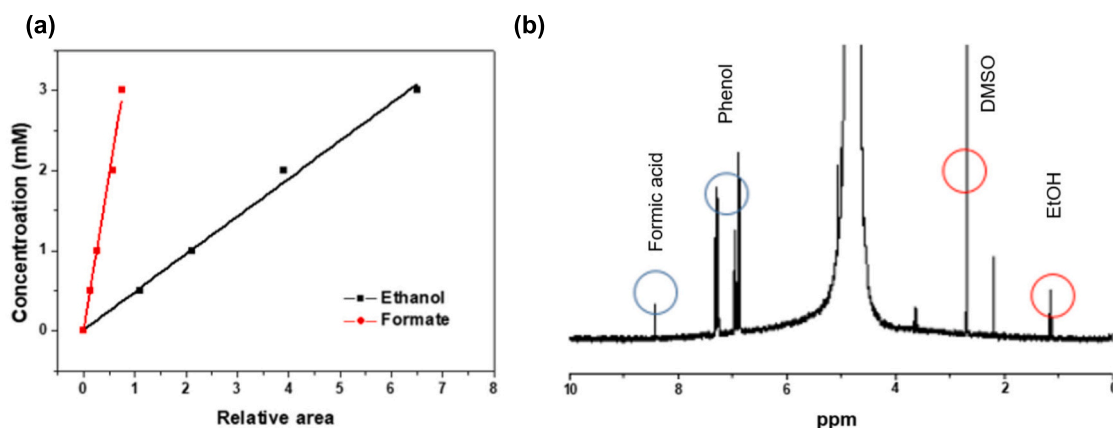


Fig. 4. Standard curves of formate and ethanol based on the relative peak area between the analyte and internal standard (a) and ^1H NMR spectrum after electrolysis showing the presence of formate and ethanol (b). Reproduced with permission from Ref. [98]. Copyright 2019, Elsevier.

reference to the calibration curves of each analyte [98].

Recently, higher selectivity of CO with higher Faradaic efficiencies were obtained by Mady's team of 93.2 % and nearly 100 % for silver-loaded boron-doped graphitic carbon nitride nanocomposite (Ag-B-g- C_3N_4) and sulfur-doped Ni-N-C catalyst (Ni-NS-C), respectively [11,104]. The higher selectivity in both studies was recorded at a potential of -0.8 V versus RHE, with no liquid products obtained as confirmed by ^1H NMR. For ^1H NMR analysis, a certain amount of the electrolyte was mixed with D_2O in the presence of one drop of DMSO for Ni-NS-C electrocatalyst (Fig. 5a) [11], while for (Ag-B-g- C_3N_4) no DMSO drop was added as no liquid products were formed (Fig. 5b) [104]. These two studies display the importance of using NMR to confirm the high selectivity toward the CO production [11,104].

6.2. NMR as a quantitative tool for formic acid/formate

The analysis of formic acid/formate that is produced during eCO_2RR

has been investigated extensively in the literature [12–17,76,105–116]. It can be analyzed through several techniques, such as HPLC and NMR [12,13,15,17,69,105]. For example, the formic acid concentrations were monitored during electrolysis at different current densities using a divided cell by zero-gap anode connected with an inline HPLC system (Fig. 6) [76]. Similarly, two recent studies by Arslan et al., showed the importance of HPLC as a powerful technique for analyzing formic acid in the catholyte compartment. The Faradaic efficiencies obtained were 61.3 % and 57 % using lead sulphate deposited on acid treated tin foil ($\text{PbSO}_4/\text{AtSn}$) and colloidal NiCo-based catalyst with rGO support (NiCo@rGO), respectively [12,13].

On the other hand, several reports have shown the employment of ^1H NMR as a spectacular analytical technique for the eCO_2RR liquid products. The NMR analysis of formic acid/formate in the liquid product relies on using an organic solvent with a known chemical shift to be used as an internal standard. For instance, most of the published reports have used DMSO as an internal standard [16,69,70,84,85,106–111]. While

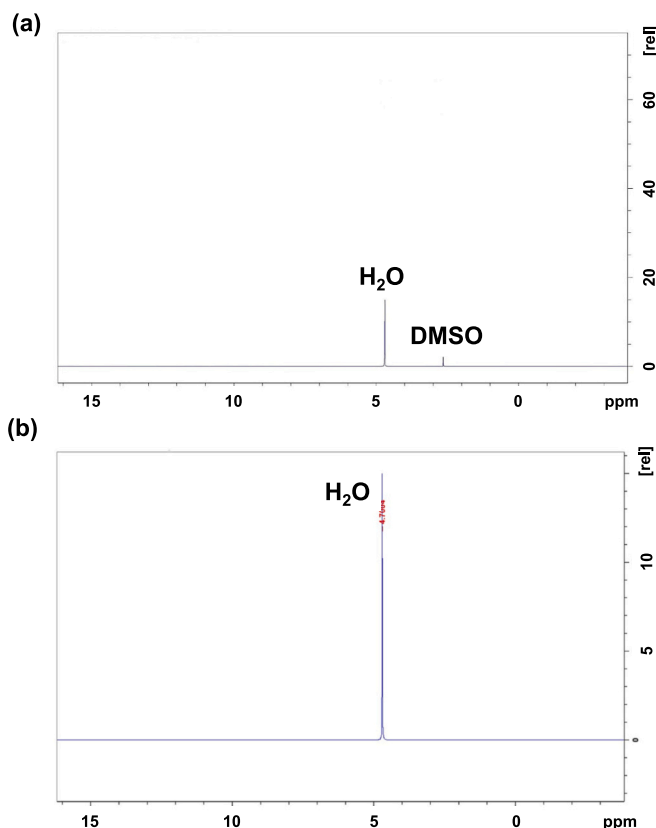


Fig. 5. ^1H NMR of the electrolyte after 1-h electrolysis at potential of -0.80 V vs RHE for Ni – NS – C catalyst (a). Reproduced with permission from Ref. [11]. Copyright 2022, John Wiley and Sons. Ag-B-g- C_3N_4 catalyst (b). Reproduced with permission from Ref. [104]. Copyright 2022, American Chemical Society.

fewer reports utilized dimethyl formamide (DMF) [105,112], phenol [113,114], maleic acid [115,116], and a mixture of phenol and DMSO as internal standards [14].

6.2.1. Dimethyl sulfoxide as internal standard for formic acid/formate quantification

Dimethyl sulfoxide is frequently utilized as an internal standard to accurately measure the amount of liquid products of eCO_2RR . This can be attributed to its chemical stability and non-overlapping spectral signals with formic acid/formate signals. This leads the researchers to precisely calculate the concentration of formic acid/formate by measuring the calibration curves. For instance, Yan et al., investigated a 3D porous electrode (TDPE) as potential electrocatalyst for eCO_2RR to formic acid/formate in acidic condition. They explored the reduction in two different electrolytes, neutral electrolyte and acidic electrolyte (pH 2.7). The collected samples after electrolysis were then transferred to NMR tube (600 μL) and mixed with 100 μL of deuterium oxide (D_2O) and 0.05 μL of DMSO as an internal standard. They confirmed the production of formic acid which has a peak with a chemical shift around δ 8.44 ppm in the neutral electrolyte, while this peak was shifted to δ 8.21 ppm at a pH of 2.7 (Fig. 7) [111]. This was consistent with a previous study by Hofsommer's team, where they studied the electrochemical performance of Lead (Pb) working electrode toward CO_2 reduction in dual methanol/water electrolyte to produce methyl formate that its concentration was measured by NMR [117]. As seen in Fig. 8, The dependence of the pH on the NMR chemical shift, indicates that the peak shifts are indeed behaving sigmoidally with the change of formic acid from its protonated to its deprotonated form [117]. Below pH 3.2, no detectable formate was present, while at higher pH values, a formate anion was formed. This shift reflects the relative balance between formic acid and

formate as influenced by the pH of the surrounding environment [111,117].

Wang et al., quantified the concentration of formic acid by mixing the 500 μL of the liquid phase with 100 μL of a mixture of D_2O :DMSO (1000:1, v:v). The formic acid concentration C_x was calculated based on integrals of formic acid and DMSO (standard) measured by NMR (I_x and I_{std} , respectively), number of protons in both formic acid and DMSO (N_x and N_{std} , respectively), and the known concentration of DMSO (C_{std}). The concentration of the formic acid was calculated based on eq. (1) [106]:

$$C_x = \frac{I_x}{I_{\text{std}}} \times \frac{N_{\text{std}}}{N_x} \times C_{\text{std}} \quad (1)$$

In another report by Jia et al., the formic acid and formate content in the liquid phase was quantified by NMR. The NMR sample was prepared by mixing 10 mL of the electrolyte solution with 50 μL of 100 mM DMSO solution to prepare the sample stock solution. Then 250 μL of the stock solution was diluted in 350 μL of D_2O . The Faradaic efficiency was calculated based on eq. (2) [16]:

$$\text{FE} = \frac{2FVC}{Q} \times 100\% \quad (2)$$

Where F is the Faradaic constant ($96,485\text{C mol}^{-1}$), V is the sample volume, C is the concentration of formic acid/formate in the electrolyte, and Q is the charge [16].

Water suppression methods have been developed to suppress the water peak in aqueous solutions. This method is widely used to eliminate the dominant water peak, which leads to a more precise and reliable analysis of the formic acid/formate peak [82,88]. For example, Nguyen et al., investigated the performance of a bismuth gas diffusion electrode on a polytetrafluoroethylene-based electrically conductive silver substrate (Ag@Bi) in both neutral and basic media. The analysis of the liquid products was performed using ^1H NMR. The authors employed the water suppression method (PRESAT) to accurately measure the concentration of formate or formic acid [84]. The FEs of formic acid/formate were calculated for the collected samples after electrolysis at a wide range of current densities (100–300 mA cm^{-2}). The values of the FEs were notably high ranging between 90 and 95 % (Fig. 9) and calculated based on eq. (3) [84]:

$$\text{FE} = \frac{nF\eta}{Jt} \times 100\% \quad (3)$$

Where n represents the number of electrons for formic acid/formate reduction, F is the Faradaic constant, η is the number of moles of the corresponding product, J is the current and finally t is the time of electrolysis [84].

Similarly, Tsujiguchi et al., evaluated the performance of Sn/reduced graphene oxide (Sn/rGO) composites toward eCO_2RR and calculated the Faradaic efficiencies of the produced formate using the standard curve method in both GC and NMR [69]. The samples were collected at 3 different potentials; -820 mV, -920 mV and -1020 mV versus reversible hydrogen electrode (RHE) and prepared for NMR analysis by diluting the liquid phase in D_2O as a solvent and DMSO as an internal standard. The NMR spectra were obtained through the water suppression method associated with the excitation sculpting method. The authors demonstrated that the obtained results by NMR were more accurate than those obtained by GC. This was assigned to the higher sensitivity of NMR than GC, see Table 2 [69].

In addition, Li et al., utilized the water suppression method to accurately analyze the concentration of formate using ^1H NMR. The NMR sample was prepared by mixing 1 mL of analyte or catholyte, 200 μL of D_2O and 100 μL of DMSO (1/1000 solution). The faradaic efficiency of formic acid/formate was calculated based on eq. (4) [85]:

$$\text{FE}_{\text{HCOO}^-} = \frac{n \times F \times V \times c}{1000 \times M \times Q} \quad (4)$$

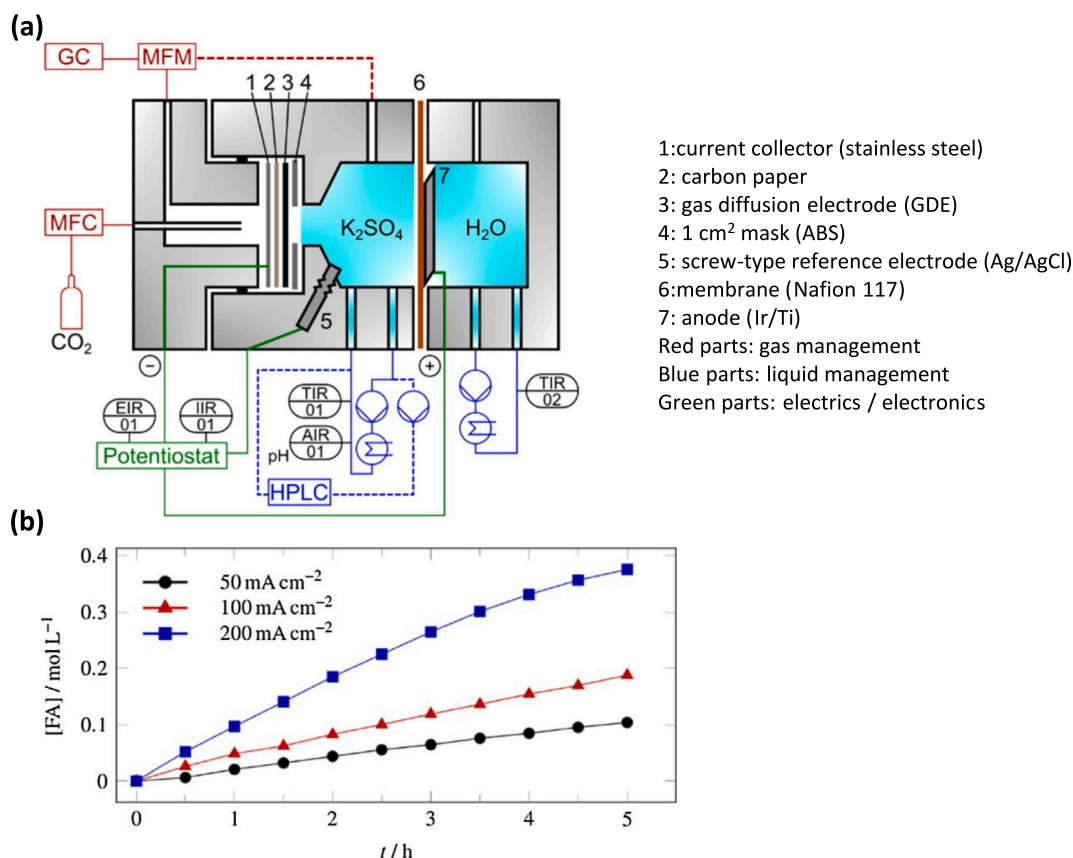


Fig. 6. A schematic overview of a divided cell with zero-gap anode (a) and the amount of the produced formic acid during 5-h electrolysis at different current densities (b). Reproduced with permission from Ref. [76]. Copyright 2022, Elsevier.

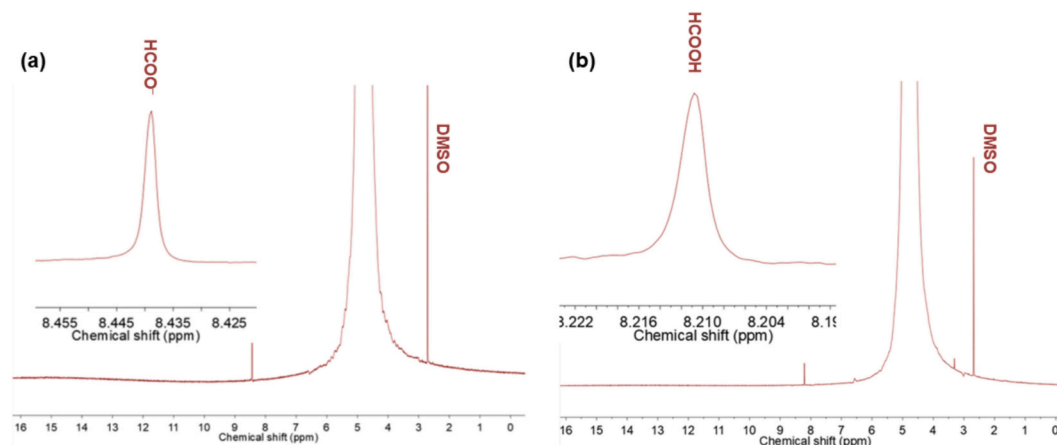


Fig. 7. The ¹H NMR spectra of the electrolyte show the generation of formate at neutral condition (a) and formic acid in acidic condition (pH 2.7) (b). Reproduced with permission from Ref. [111]. Copyright 2023, John Wiley and Sons.

Where n is the number of transferred electrons for formate, F is the Faradaic efficiency, V is the electrolyte volume, c is the concentration of formic acid/formate generated by the reaction (calculated by NMR), M is the molar mass of formic acid/formate, and Q is the total amount of charge consumed during the electrolysis [85].

6.2.2. Other solvents as internal standard for formic acid/formate quantification

On the other hand, several reports employed other organic solvents as internal standards for quantitative NMR analysis. *N,N*-dimethylformamide (DMF) has been used as an internal standard in NMR

quantification of formic acid resulting from the eCO₂RR. The main benefit of using DMF is that the signal of DMF in ¹H NMR does not interfere with the formic acid/formate signal [112]. For example, the NMR sample was prepared by mixing 630 μL of the liquid product of tin (Sn) nanosheets decorated with bismuth (Bi) nanoparticles on a porous carbon substrate (Bi-Sn/CF) with 70 μL of 4.61×10^{-3} of DMF standard solution. The concentration of formic acid (η) was calculated based on the calibration curves of sodium formate and the Faradaic efficiency was calculated based on eq. (5) [112]:

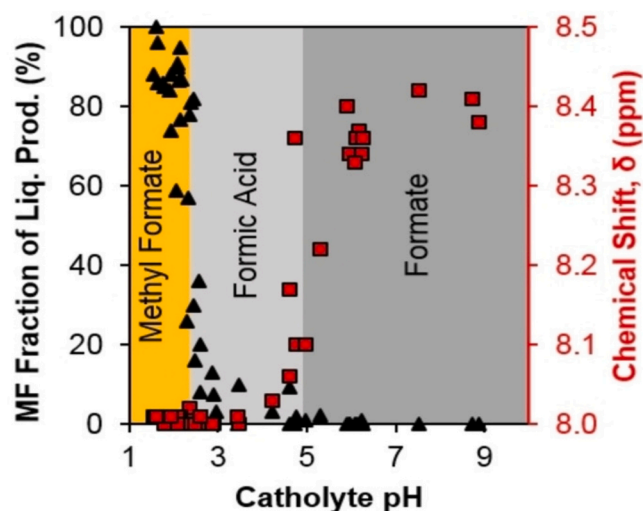


Fig. 8. The eCO₂RR liquid products conversions to methyl formate (black triangles) and the NMR signal chemical shift (red squares) in the KCl-saturated methanol catholyte. Shaded regions are related to the dominant liquid products: dark grey for formate; light grey for formic acid; and yellow for methyl formate. Reproduced with permission from Ref. [117]. Copyright 2022, John Wiley and Sons. (For interpretation of the references to colour in this figure legend, the reader is referred to the web version of this article.)

$$FE = \frac{2 \times F \times \eta}{Q} \quad (5)$$

Similarly, the liquid product of indium single atom dispersed on a nitrogen-doped carbon skeleton (In-N-C) was identified and quantified by ¹H NMR using the water suppression method [105]. The DMF was used as an internal standard and was diluted to obtain a 12.90 mM of DMF solution in D₂O. Then 50 μL of the standard stock solution was mixed with 550 μL of electrolyte for NMR quantification. For the calibration curve, the pure formate was used to prepare different concentrations of formate standards and to generate the calibration curve (Fig. 10) needed for calculation [105].

In addition, phenol has been used as an internal standard for formic acid quantification. It is known that phenol is considered one of the best internal standards for NMR quantification of eCO₂RR products as it does not interfere with any products, and it has the lowest relaxation time compared to the other common solvents [83,118]. Based on that, phenol was used as an internal standard to calculate the concentration and the Faradaic efficiency of the formic acid that is produced from the eCO₂RR

Table 2

The concentrations of formate obtained by GC and NMR. Reproduced with permission from Ref. [69]. Copyright 2021, American Chemical Society.

	Sample 1	Sample 2	Sample 3
NMR	34.3 ppm	34.5 ppm	46.5 ppm
GC	32.7 ppm	33.27 ppm	44.78 ppm

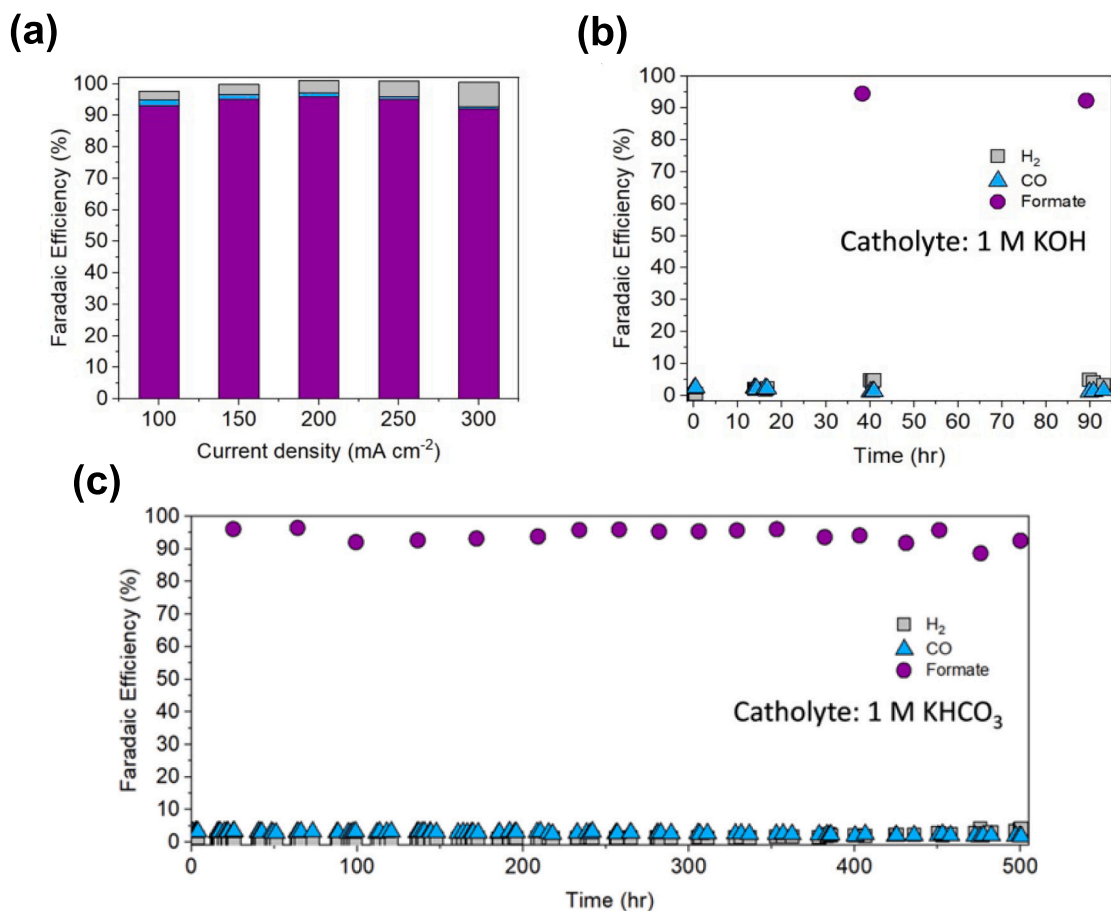


Fig. 9. Product distribution at current densities between 100 and 300 mA cm⁻² at neutral conditions (pH = 7) (a), the Faradaic efficiencies of formate (purple), CO (turquoise) and H₂ (grey) of continuous electrolysis for 90 h in the basic electrolyte (b) and 500 h in the neutral electrolyte (c). Reproduced with permission from Ref. [84]. Copyright 2024, John Wiley and Sons. (For interpretation of the references to colour in this figure legend, the reader is referred to the web version of this article.)

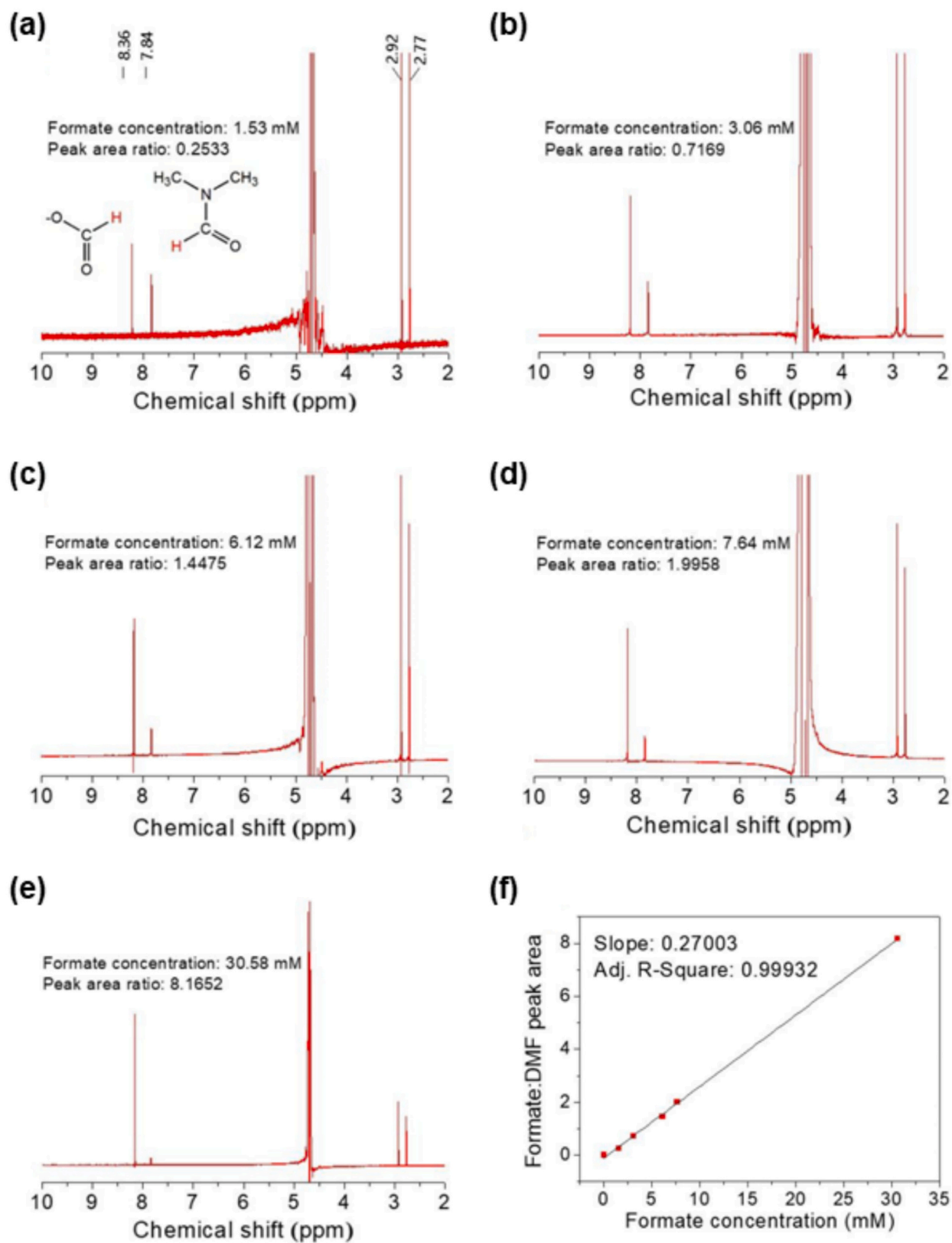


Fig. 10. Peak area ratio of different formate concentrations compared to 12.90 mM of DMF: (a) 1.53 mM, (b) 3.06 mM, (c) 6.12 mM, (d) 7.64 mM, and (e) 30.58 mM. c_{DMF} : 12.90 mM. (f) The proportional relationship between formate concentration and relative peak area vs. DMF. Reproduced with permission from Ref. [105]. Copyright 2021, American Chemical Society.

of potassium bicarbonate solution reduction by Pd and Pd–B electrodes [114]. In the same context, Jiang quantified the concentration of formic acid by NMR using phenol as an internal standard (Fig. 11) [113]. The NMR sample was prepared by mixing 35 μL of the standard stock solution of phenol (3 μL in 3 mL of D_2O) with 700 μL of the electrolyte. The Faradaic efficiency of formate was calculated according to eq. (6) [113]:

$$\text{FE} = \frac{N \times c \times V \times F}{Q} \quad (6)$$

Where N is the total number of transferred electrons, c is the concentration of formate content, V is the total volume of liquid, F is the Faradaic constant, and Q is the total charge of the electrolysis process [113].

Furthermore, using dual internal standard system to quantify the concentration of liquid products of eCO_2RR . This method has been reported by Chung et al., as they prepared a standard solution consisting of 10 mM phenol and 2 mM DMSO in D_2O [14]. For NMR quantification, 30 μL of the standard solution was mixed with 540 μL of the liquid product. The concentration of the formate was calculated by comparing the integral area of the formate signal with that of the phenol signal [14].

It is noteworthy that maleic acid has been used recently as internal standard for qualification and quantification the content of formic acid/formate. Garcia et al., reported the utilization of NMR to identify the peaks of several cathodic CO_2 electrochemical products [119]. As shown in Fig. 12, the maleic acid peak resonates at a chemical shift of δ 6.10 ppm and was used to identify the chemical shifts of several CO_2 reduction products, such as formate (δ 8.5 ppm), acetate (δ 1.9 ppm), acetone (δ 2.2 ppm) and ethanol (δ 1.2 and 3.2 ppm). The authors claimed that they were not able to calculate the Faradaic efficiencies, this was related to the lower concentration of CO_2 reduction products [119]. To avoid this problem, Hailu et al., represent the applied NMR method while analyzing the CO_2 reduction products [120]. This was performed by calibration of the pulse-width (pw90). This was accomplished by acquiring 1D spectra with incrementally increasing pulse widths to find the point of no signal or equal positive/negative signals, then relaxation times (T_1) for formate and maleic acid were determined using the inversion-recovery method by manipulating the time (D_7) between pulses. The D_7 values for formate and maleic acid in the electrolyte

media were found to be 4.5 and 3.8 μs respectively, with the longer D_7 for formate being used to calculate the relaxation delay (D_1). For sample preparation for NMR analysis, 250 μL of cathodic electrolyte was mixed with 225 μL of standard solution (5 mM maleic acid in D_2O), and the concentration of formic acid was calculated by comparing the ratio of area of formate signal with the area of maleic acid [120].

6.3. NMR as a quantitative tool for methanol

Recently, methanol has gained considerable attention as a versatile chemical that is used in fuel, solvents, and industrial feedstock [121,122]. One of the most environmentally friendly techniques to produce methanol is the electrochemical reduction of CO_2 [123,124]. The amount of produced methanol can be measured using several analytical techniques, such as HPLC [37,38], GC-FID [125,126], GC-MS [37,127], HS-GC [33,81], and NMR [128,129]. For example, The predominant quantity of methanol was analyzed by GC and HPLC after 2-h chronoamperometry experiment for CO_2 reduction over Cu-oxide electrodes [38]. Similarly, cuprite@polyaniline ($\text{Cu}_2\text{O}@PANI$) electrode produced methanol with a Faradaic efficiency of 45.21 %. The amount of produced methanol was measured by HPLC and GC-MS [37]. In addition, GC-FID was the main tool to analyze the content of methanol in the CO_2 catholyte [125,126]. For example, Cuprite (Cu_2O) was deposited on carbon cloth and evaluated as a potential electrode for producing methanol through electrochemical reduction of CO_2 approach. The CO_2 -saturated electrolyte was collected at a potential of -1.7 V (vs Ag/AgCl electrode) and analyzed by GC-FID [125]. Combination of head space to the GC-FID has been used to analyze the concentration of volatile organic solvents (such as methanol) that might be produced during the eCO_2RR process [33,81]. Boron phosphide nanoparticles on carbon paper (BP/CP) electrode was found to be a high effective eCO_2RR electrocatalyst to CH_3OH with high selectivity and faradaic efficiency of 92.0 % at -0.5 V and with a high electrochemical stability [81].

Recently, NMR as a powerful tool for liquid products quantification was extensively utilized to measure the concentration of produced methanol [86,87,128–134]. Methanol shows two peak groups in ^1H NMR: one due to the resonance of a methyl group $-\text{CH}_3$, usually between δ 3.3 and δ 3.5 ppm, and hydroxyl group $-\text{OH}$ between δ 4.5 and δ 5.5 ppm [135,136]. The hydroxyl group may appear at a different location because of factors such as hydrogen bonding and solvent effects. In ^{13}C NMR, methanol exhibits a single resonance for the methyl carbon at approximately δ 50 ppm [135,136]. Precise chemical shifts in both ^1H and ^{13}C NMR spectra can be affected by solvent interactions and by the experimental conditions, but these values provide a good reference for the characterization of methanol in different contexts of analysis [135,136].

Different organic solvents were used as internal standard to measure the concentration of methanol. DMSO was the most used solvent as internal standard for methanol quantification [71,81,129,130,132,133,137–139], whereas a mixture of DMSO and phenol [87,131,140–142], dimethyl formamide (DMF) [143], 4-nitrophenol [72], and tetramethylsilane (TMS) [144–147] were used less frequently.

6.4. Dimethyl sulfoxide as internal standard for methanol quantification

Highly selective boron phosphide nanoparticles (BP NPs) electrocatalyst was developed and investigated toward methanol production from eCO_2RR in CO_2 -saturated KHCO_3 solution [81]. ^1H NMR was used for quantification of liquid products (Fig. 13a), while IC was used to confirm the absence of formate ion (Fig. 13b). After 12 h of electrolysis at -0.6 V versus RHE, methanol was obtained as a predominant product. For ^1H NMR quantification purposes, DMSO was used as internal standard. While for Faradaic efficiency calculations, eq. (7) was utilized:

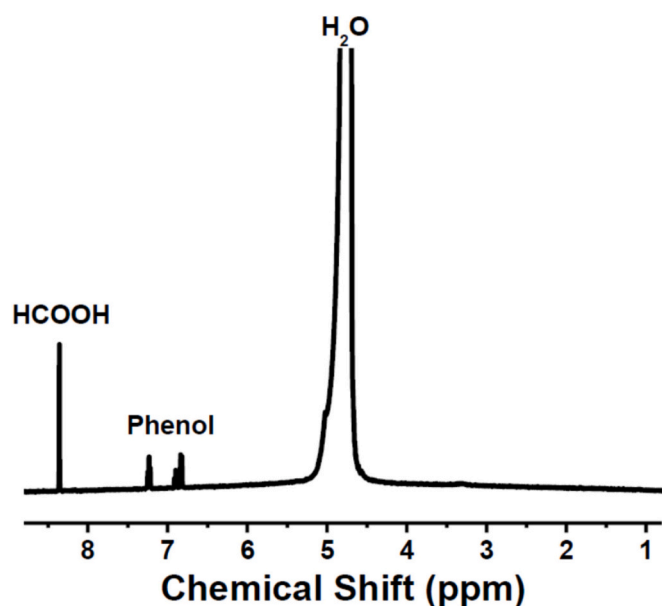


Fig. 11. ^1H NMR spectrum of formic acid and the internal standard (phenol). Reproduced with permission from Ref. [113]. Copyright 2018, American Chemical Society.

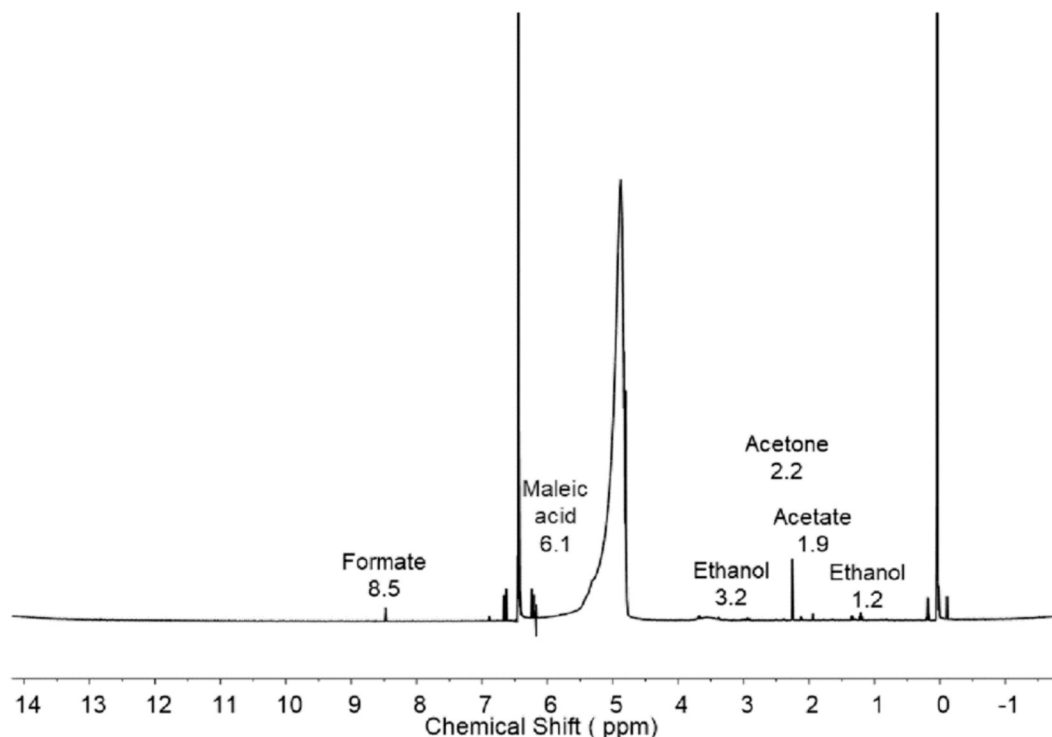


Fig. 12. ^1H NMR chemical shifts for CO_2 electrochemical reduction products. Reproduced with permission from Ref. [119]. Copyright 2024, Springer Nature.

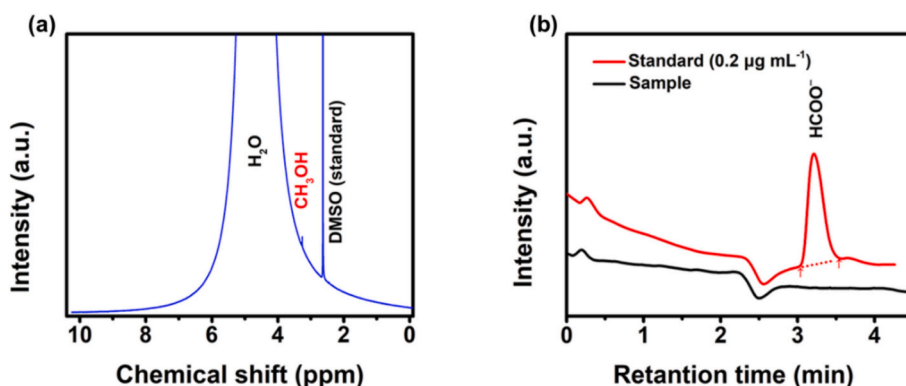


Fig. 13. ^1H NMR spectrum of the liquid product using BP NPs confirming the production of methanol (a) and IC chromatogram confirming the absence of formate ion production during electrolysis (b). Reproduced with permission from Ref. [81]. Copyright 2019, John Wiley and Sons.

$$\text{FE} = \frac{z n F}{Q} \quad (7)$$

Where Z is the amount of electrons transferred during electrolysis to produce methanol, n is the number of moles, and F is the Faraday constant [81].

Liang et al. investigated nickel salophen dispersed in a 2D nickel organic framework toward eCO_2RR to methanol [129]. After 1 h of electrolysis, 500 μL of the catholyte were mixed with 150 μL internal standard (2.5 mM DMSO in D_2O), then it was transferred to an NMR tube for analysis. The concentration of methanol was calculate based on calibration curve (Fig. 14), while the relative peak ration was calculated using eq. (8):

$$\text{Relative peak ratio of methanol} = \frac{\text{peak area of methanol at } \delta \text{ 3.23 ppm}}{\text{peak area of DMSO at } \delta \text{ 2.6 ppm}} \quad (8)$$

Based on that, the Faradaic efficiencies of methanol were calculated based on eq. (9):

$$\text{FE} = \frac{C_{\text{methanol}} \times V \times N_A \times 6e}{N_{\text{total}}} \quad (9)$$

Whereas C_{methanol} is the concentration of methanol, V is the catholyte volume, N_A represents the Avogadro's number, and N_{total} is the total charge that measured during electrolysis [129]. Also, the concentration of methanol was calculated based on the peak ratio of DMSO, whereas a single atom Co catalyst was explored for the process of CO/CO_2 electroreduction (CO_xRR) by Ren's et al. [130]. As seen in Fig. 15, the predominant product was methanol with minor production of H_2 as a gaseous product. The concentration of methanol was measured by ^1H NMR using water suppression method, and the analysis sample was prepared by mixing 1 mL of the electrolyte with 0.1 mL of D_2O containing 2.5 μL of DMSO as internal standard [130]. The Faradaic efficiencies of methanol were calculated based on eq. (10):

$$\text{FE}_i = \frac{Q_i}{Q_{\text{total}}} = \frac{N_i \times n \times F}{Q_{\text{total}}} \quad (10)$$

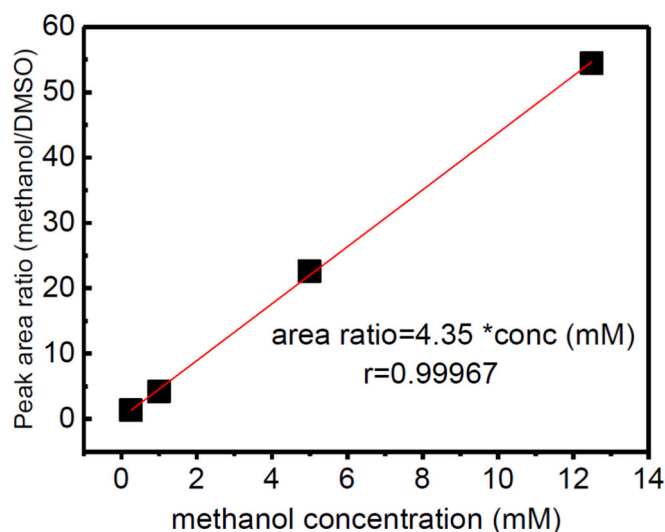


Fig. 14. Methanol calibration curve in 0.2 mM DMSO. Reproduced with permission from Ref. [129]. Copyright 2022, Elsevier.

Where Q_i is the charge needed for the production of methanol, Q_{total} is the total amount of charge obtained during electrolysis, N_i is the number of moles, n is the number of electrons consumed during electrolysis and F is the Faradaic constant [130].

Recently, cobalt phthalocyanine (CoPc) was explored for the electroreduction of CO_2 in CO/CO_2 co-feeding experiments [132]. The methanol (main product) was quantified by ^1H NMR using water suppression method (Fig. 16). This was accomplished by mixing 500 μL of the catholyte with 100 μL of internal standard solution (1.37 mM DMSO in D_2O). The Faradaic efficiency of methanol was calculated according to eq. (11):

$$\text{FE} = \frac{C_{\text{Me}} \times V_{\text{liq}} \times n \times F}{Q} \quad (11)$$

Where C_{Me} is the calculated concentration of methanol, V_{liq} is the volume of catholyte and n is the number of electrons consumed to produce methanol (4 in CO and 6 in CO_2), F is the Faradaic efficiency, and Q is the total charge [132].

Cu-BTC (1,3,5-benzene tricarboxylic acid) MOF derived materials were also investigated as a potential catalyst to produce methanol [139]. Different Cu/Cu₂O materials were synthesized by calcination of Cu-BTC at different temperatures (300 °C, 400 °C, or 500 °C). Among them, Cu/Cu₂O-400 °C exhibited the best performance in terms of methanol production. After 2-h electrolysis, 0.4 mL of the catholyte was collected and mixed with 0.1 mL DMSO (internal standard) for ^1H NMR quantification. The results revealed that Cu/Cu₂O-400 °C exhibited the highest Faradaic efficiency (45 %) at a potential of -0.7 V versus RHE [139].

^{13}C -labeling CO_2 experiments would provide insights about the source of methanol in the electrochemical reduction of CO_2 [71,133]. For example, Song's team utilized ^1H NMR for quantitative and qualitative analysis for eCO_2RR of iminium covalent organic nanosheets (iminium-CONs) [133]. For quantitative purposes, an NMR sample was prepared by mixing 450 μL of catholyte with 50 μL of internal standard solution (10 mM DMSO in D_2O). For qualitative analysis, ^1H NMR was utilized to confirm the source of methanol through ^{13}C -labeling CO_2 isotope. Two characteristic doublets for $^{13}\text{CH}_3\text{OH}$ were observed in the ^1H NMR spectrum at δ 3.16 and δ 3.4 ppm (Fig. 17a), which demonstrates that methanol was originally produced from the CO_2 reduction. This result was consistent with the chronoamperometry experiments under argon atmosphere which confirmed that the only produced product is methanol other than any impurities (Fig. 17b) [133].

Similarly, Boutin et al. investigated cobalt phthalocyanine complex with multi-wall carbon nanotubes (CoPc-MWCNT), a well-known to

reduce CO_2 electrochemically to CO , as electrocatalyst to catalyze CO_2 or CO to methanol [71]. ^{13}C -labeling experiment was conducted in a $\text{KH}^{13}\text{CO}_3$ electrolyte which was previously saturated with $^{13}\text{CO}_2$. The NMR samples were prepared by mixing 392 μL of the electrolyte with 40 μL of 4 mM DMSO and 48 μL of D_2O . The NMR experiments were done after accumulating of 128 scans with a water presaturation method with a relaxation time of 25 s. As seen in Fig. 18, the NMR spectrum reveals a clean split of CH_3 proton peak around δ 3.35 ppm into a doublet with methanol with a coupling constant of $J = 142$ Hz, confirming that the $^{13}\text{CO}_2$ is the main source of produced methanol [71].

Hierarchical Pd/SnO₂ nanosheets with abundant Pd–O–Sn interfaces were investigated toward electroreduction of CO_2 [134]. After electrolysis, 500 μL of the catholyte were collected and mixed with 100 μL internal standard (0.05 μL DMSO in 100 μL D_2O) then analyzed by ^1H NMR for quantification. Fig. 19a and Fig. 19b display the NMR spectra of different concentration of methanol and their calibration curve plot with regression of 0.99983. This was used to determine the concentration of produced methanol at different potential. The results exhibit that methanol was the predominant product for Pd/SnO₂ at potential of -0.24 V vs RHE NSs at different electrolysis time with Faradaic efficiencies around 55 % (Fig. 19c and Fig. 19d) [134].

Huang and his coworkers demonstrated that the production of methanol with a Faradaic efficiency of 97.0 % is obtained at potential of -0.98 V versus saturated calomel electrode (SCE) through the electroreduction of CO_2 in a solution of NaHCO_3 [137]. First, they studied the effect of bare glassy carbon electrode, where it revealed no activity toward the electroreduction of CO_2 (Fig. 20a) and no signal of methanol in the ^1H NMR spectrum (Fig. 20b). The same result was obtained when Nafion film was applied (Fig. 20c and d). After that, they ran the electrolysis experiment in both N_2 and CO_2 environments using the hollow urchin-like $\text{Co}(\text{CO}_3)_{0.5}(\text{OH}) \cdot 0.11\text{H}_2\text{O}$ electrocatalyst. In N_2 -saturated NaHCO_3 solution, no reduction peak was observed and no signal of methanol in the ^1H NMR spectrum (Fig. 20e and f), while in CO_2 -saturated catholyte a significant reduction peak was obtained and a CH_3 signal at about δ 3.32 ppm and δ 49.1 ppm for ^1H NMR and ^{13}C NMR, respectively (Fig. 20e, g, and h). The ^{13}C NMR was used for qualitative analysis and ^1H NMR for quantitative analysis. The method for preparation sample for NMR qualitative and quantitative analysis was as follows: 0.5 mL of catholyte was mixed with 0.1 mL D_2O and 0.5 μL DMSO (as internal standard). The Faradaic efficiency was calculated based on the following equation: Faradaic efficiency = $6F \times n_{\text{methanol}}/Q$, where 6 is the number of electrons needed to produce methanol from CO_2 reduction, F is the Faraday constant, n is the number of moles, and Q is the total charge [137].

6.4.1. Other solvents as internal standards for methanol quantification

Many reports used dual internal standard system to quantify the eCO_2RR products. Phenol and DMSO were widely utilized for this purpose as both are considered non-volatile solvents, which is important for using their stock standard solutions for all measurements [87,131,140–142]. In ^1H NMR, DMSO and phenol signals do not interfere with any product peak ($\delta \sim 2.6$ ppm and $\delta \sim 7.45$, respectively), allowing to accurately calculate the concentration of the products signals that resonate before (with reference to DMSO) and after (with reference to phenol) the water peak [141,142]. For example, Zhang et al. constructed a molybdenum-based metal carbide catalyst loaded onto nitrogen-doped carbon nanotubes ($\text{Mo}_2\text{C}/\text{N-CNT}$) and utilize it as potential catalyst toward high selectively methanol production through eCO_2RR with a Faradaic efficiency of 80.4 % at -1.1 V versus standard hydrogen electrode (SHE) [141]. After electrolysis, a sample of catholyte and anolyte were withdrawn and quantified by ^1H NMR and HS-GC. For ^1H NMR, 400 μL of electrolyte was mixed with 100 μL of the internal standard solution (50 mM phenol and 10 mM DMSO in D_2O). The concentration of produced methanol was calculated based on eq. (12) [141]:

$$\frac{M_X}{M_Y} = \frac{I_X}{I_Y} \times \frac{N_Y}{N_X} \quad (12)$$

Where X refers to methanol and Y refers to DMSO, M is the concentration of both compounds, I is the area of resonance peak for methanol or DMSO, and N is the total number of protons that resonates

for methanol ($N = 3$) and DMSO ($N = 6$) [141].

In addition to utilizing DMSO as internal standard, dual solvent system including DMSO and phenol were used to analyze the concentrations of methanol [87,131,140–142]. For example, NMR can be used as a powerful tool to investigate and quantify the crossover volatile liquids through gas diffusion electrode (GDE) and anion exchange

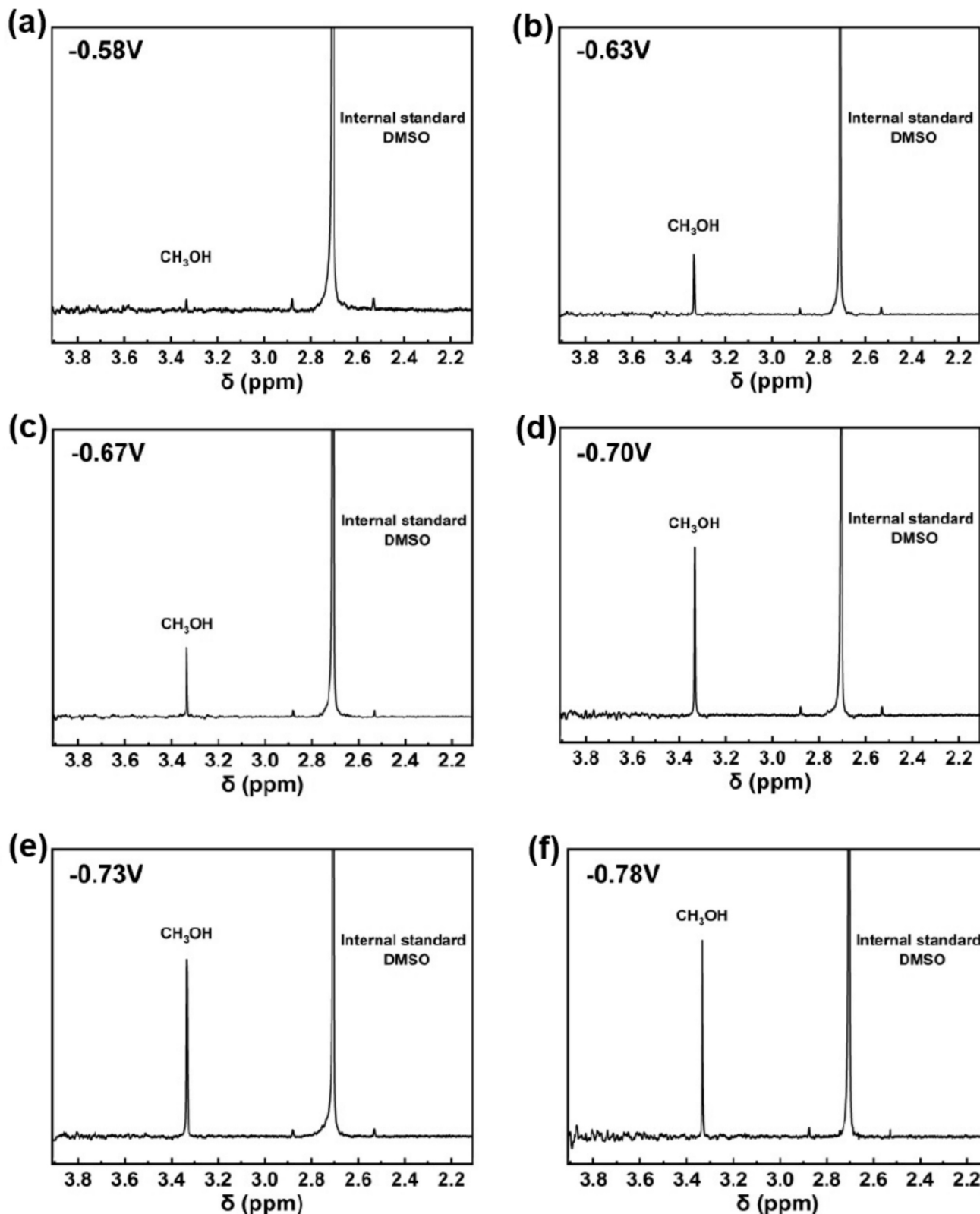


Fig. 15. ^1H NMR spectra of the electrolyte after CO reduction electrolysis at -0.58 V (a), -0.64 V (b), -0.67 V (c), -0.70 V (d), -0.73 V (e), and -0.78 V (f). The potential was measured against RHE electrode. Reproduced with permission from Ref. [130]. Copyright 2023, Springer Nature.

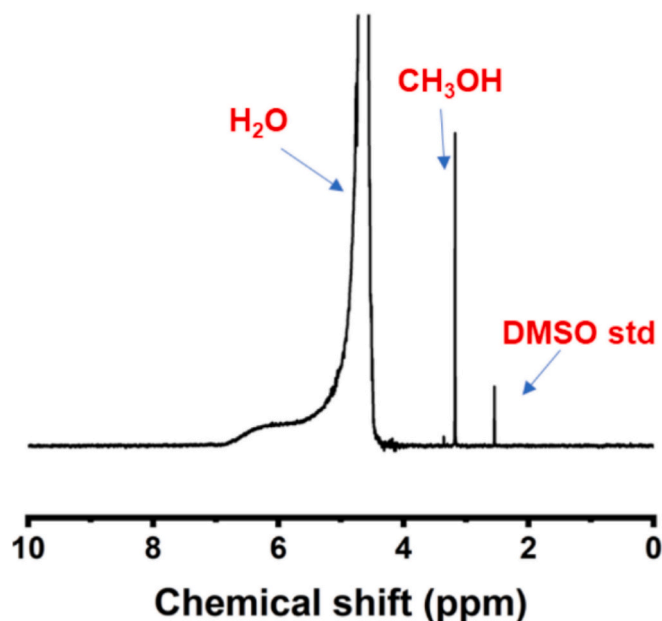


Fig. 16. A typical ^1H NMR spectrum for the liquid product after CO/CO_2 electrolysis. Reproduced with permission from Ref. [132]. Copyright 2024, American Chemical Society.

membrane (AEM) in a three-chamber flow cell setup. This was done by Zhang's team, where they explored the crossover of volatile liquid products using copper- and tin-based GDEs in a flow cell setup [142]. ^1H NMR was used to quantify the possible liquid products that might migrate through the chambers. A sample of catholyte, anolyte and washing liquid used to wash the CO_2 -off (Fig. 21a) were taken and analyzed. As seen in Fig. 21b, many volatile materials and other organic compounds were found in the 3 chambers including: n-propanol, propionaldehyde, ethanol, acetate and formate were found in the catholyte and anolyte chamber. While in the CO_2 -off gas chamber, methanol was found in addition to the previous mentioned products. The quantification of the produced products was performed based on DMSO and phenol internal standard (Fig. 21c), where the signals appeared before the water peak were quantified based in DMSO peak (Fig. 21d) and the signals appeared after the water signal were calculated based on phenol standard (Fig. 21e). The faradaic efficiency of the liquid products was calculated based on eq. (13):

$$FE = \frac{nFC_iV}{Q} \quad (13)$$

Where n is the number of electrons that transferred for each product i , F is the Faraday's constant, C is the concentration for the product i , V is the volume of electrolyte, and Q is the total charge consumed during the electrolysis [142].

CoPc on multiwalled carbon nanotubes (MWCNTs) integrated onto Au electrodes by using a poly(3,4-ethylenedioxythiophene) polystyrenesulfonate (PEDOT:PSS) adhesion layer (CoPc/MWCNT on PEDOT:PSS on Au) was examined toward eCO_2RR [131]. ^1H NMR was used to quantify methanol and identify the source of methanol. A dual internal standard system was used for this purpose, where 50 mM of DMSO and 50 mM of phenol were prepared using deionized water, then 50 μL of the internal standard was mixed with 400 μL from the catholyte and 50 μL of D_2O . The NMR experiment was performed after obtaining the 90-pulse width for each solvent and the center of water peak followed by water suppression method using 25-s delay time. The concentration of methanol was calculated based on the integration ratio between methanol and DMSO after performing the calibration curve of the internal standard and different concentration of methanol and potassium formate. The Faradaic efficiency was calculated based on concentration of reference (C_{ref}), integrations of the reference and the product (I_R and I_P , respectively), the number of proton for each reference and product (H_R and H_P , respectively), which are 6 for DMSO and 3 for methanol, the number of electrons to reduce the CO_2 to methanol ($n = 6$), Faraday's constant, volume of catholyte (V), and dilution factor ($5/4$), as 400 μL of catholyte was diluted to 500 μL , using eq. (14) [131]:

$$FE = C_{ref} \cdot \frac{I_P}{I_R} \cdot \frac{H_R}{H_P} \cdot \frac{nFV}{Q} \cdot \frac{5}{4} \times 100 \quad (14)$$

For qualitative analysis, ^{13}C -labeling experiment of CO_2 was used to confirm that the source of methanol. The ^1H NMR spectrum displays exhibits two peaks for methanol with a j coupling value of 142.3 Hz [131].

Similarly, copper gallium intermetallic compound (CuGa_2) was found to be an excellent candidate for eCO_2RR [87]. After electrolysis, 500 μL of electrolyte was mixed with 30 μL of internal standard (50 mM phenol and 10 mM DMSO in D_2O) and then applied in NMR analysis using water suppression method to minimize the intensity of water peak. The NMR experiment display the formation of methanol, formate and acetate after reducing CO_2 electrochemically Fig. 22a. ^{13}C -labeling experiment was conducted to elucidate the source of produced methanol and explored by ^{13}C NMR and GC-MS tools. Fig. 22b displays the ^{13}C

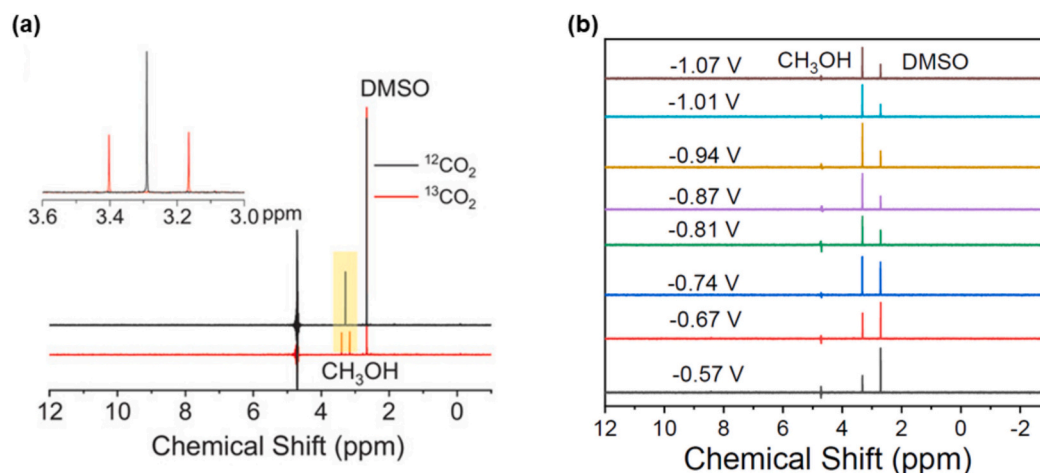


Fig. 17. ^1H NMR spectra of methanol in $^{12}\text{CO}_2$ (black signal) and $^{13}\text{CO}_2$ (red signal) saturated electrolytes (a) and Chronoamperometry experiments at different potentials (b) for iminium-CONs catalyst. Reproduced with permission from Ref. [133]. Copyright 2024, John Wiley and Sons. (For interpretation of the references to colour in this figure legend, the reader is referred to the web version of this article.)

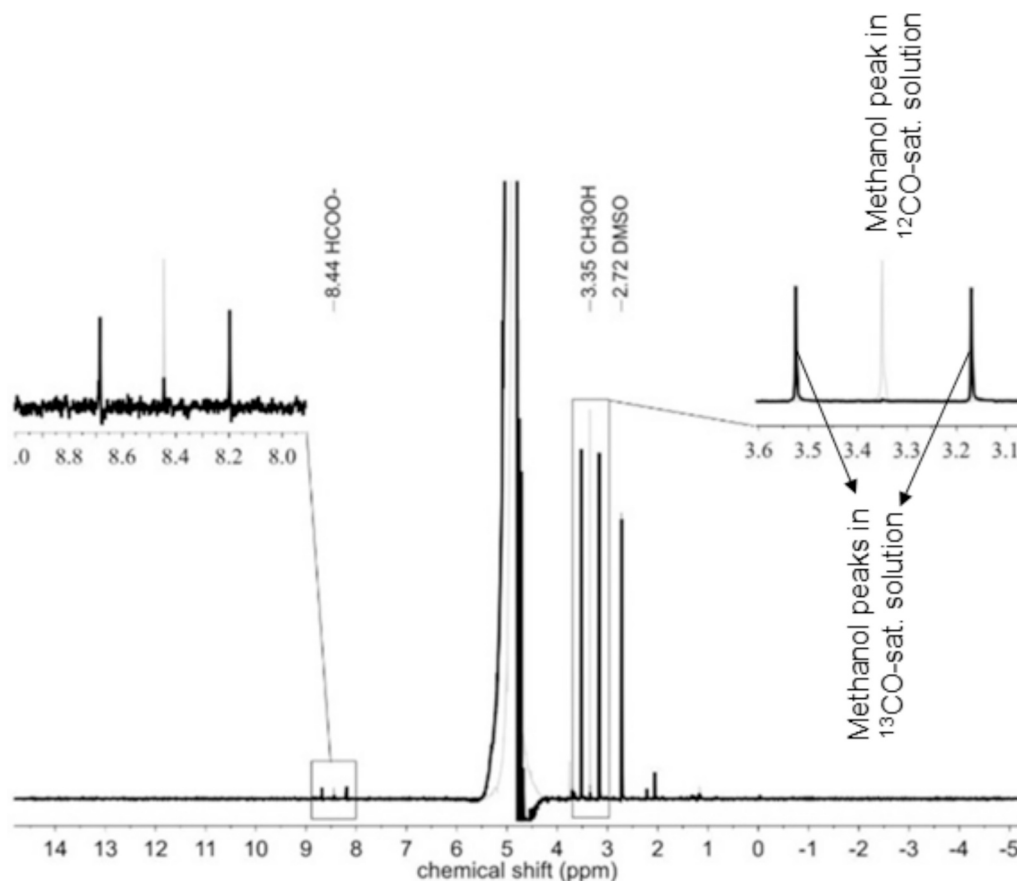


Fig. 18. ^1H NMR spectra of catholyte after 2-h electrolysis at -0.64 V vs. RHE in ^{12}CO - and ^{13}CO -saturated electrolytes. Reproduced with permission from Ref. [71]. Copyright 2019, John Wiley and Sons.

NMR spectrum of liquid aliquot after purging with $^{13}\text{CO}_2$, it displays the peak of $^{13}\text{CH}_3\text{OH}$ at 49.5 ppm which is related to C in the $^{13}\text{CO}_2$ atmosphere, which cannot be detected when $^{12}\text{CO}_2$ RR was carried. For further confirmation, GC-MS displays only ^{13}C enriched methanol, with a higher m/z value of $^{13}\text{CH}_3\text{OH}$ compared to $^{12}\text{CH}_3\text{OH}$ (Fig. 22c) [87].

Dimethylformamide (DMF), as internal standard, was used to quantify the methanol concentration in the electrolyte. Copper promoted molybdenum sulfide cluster ($\text{Cu}_2\text{Mo}_6\text{S}_8$) was found to be selective to methanol over formate at a potential of -0.4 V versus RHE [143]. The ^1H NMR analysis was done by utilizing DMF as internal standard which displays a signal at δ 7.92 ppm for the liquid products collected at the potential window between -0.4 V to -1.0 V versus RHE. At a potential of -1.0 V, it was clearly seen that methanol was the dominant product over formate. However, when the feeding gas was changed from CO_2 to CO , the formate signal disappeared with maintaining the methanol peak, suggesting that the formate pathway was suppressed by removing the CO_2 gas from the electrochemical cell. This can be attributed to the fact that switching adsorbate-electrode coordination from carbon to oxygen and the insertion of addition of oxygen atom which is required to formate formation [25,143].

Furthermore, 4-nitrophenol was used as internal standard to analyze the concentration of methanol. Carbon-supported PtZn nano-alloys (Pt_xZn) exhibit a higher selectivity toward methanol production [72]. After 4-h electrolysis, 0.1 mL of the electrolyte was collected and mixed with 0.1 mL D_2O and 5 mg of 4-nitrophenol, then it was transferred to an NMR tube. The NMR analysis was done for 256 scans, revealing two signals which are corresponding to methanol at δ 3.26 ppm and acetate at δ 1.96 ppm, and other two signals for 4-nitrophenol at around δ 8.00 ppm and δ 6.60 ppm (Fig. 23). For methanol concentration calculation, the peak area ratio between methanol and 4-nitrophenol (S) was

calculated according to eq. (15):

$$S = \frac{\text{Peak area of methanol at } \delta 3.26 \text{ ppm}}{\text{Peak area of 4-nitrophenol at } \delta 8.00 \text{ ppm}} \quad (15)$$

Then, the concentration of methanol was calculated after plotting the calibration curve using eq. (16):

$$\text{Concentration of methanol} = \frac{S}{\text{Slope}} \quad (16)$$

Finally, the Faradaic efficiency was calculated using eq. (17):

$$\text{FE} = \frac{n_j F C_i V}{Q_t} \quad (17)$$

Where, n_j is the number electrons to reduce CO_2 to methanol, F is the Faradaic constant, C_i is the calculated methanol concentration, V is the catholyte volume, and Q_t is the total charge that obtained after electrolysis [107].

Tetramethylsilane (TMS) has been employed as a qualitative and quantitative reference standard in NMR analysis [144–147]. TMS provides a constant reference point from which the chemical shifts are measured in varied solvents and sample conditions [82,148]. In qualitative analysis, TMS enables the identification of unknown compounds by offering their chemical environment through special peak patterns in the NMR spectrum [82]. Quantitatively, TMS allows for correct concentration determinations by comparing integration of its peaks to those of the analyte and thus enables the quantification of species in complex mixtures with reliability [82,148]. Second, its well-defined chemical shift, generally referenced to 0 ppm, increases the reproducibility and comparability of the NMR data from one study to another [82,148]. For example, Hossain et al. utilized the thermal-assisted synthesis route to

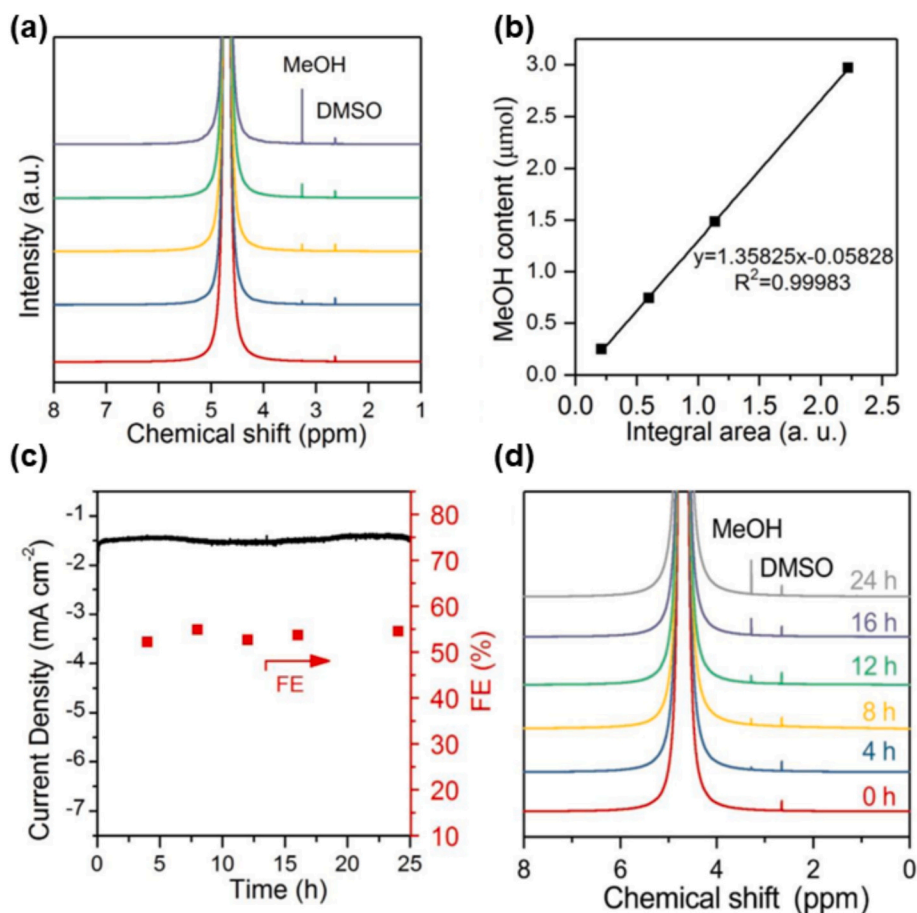


Fig. 19. ¹H NMR spectra of different concentration of methanol (a), The calibration curve of different concentration of methanol (b), chronoamperometry experiment at 24 h at -0.24 V vs RHE (c) and ¹H NMR spectra at the potentials of -0.24 V versus RHE for Pd/SnO₂ NSs (Pd:Sn = 1:1) (d). Reproduced with permission from Ref. [134]. Copyright 2018, John Wiley and Sons.

synthesize copper nanodendrites on titanium substrate to reduce CO₂ electrochemically to valuable products, such as CO, CH₄, formate, acetate, and methanol. After two-hour electrolysis at -0.6 V versus RHE, a 0.05 μL of TMS as internal standard was mixed with a solution of catholyte and 20 % D₂O. The electrolysis reveals that the total faradaic efficiency of copper nanodendrites is 68.18 [144].

It worth mentioning that ionic liquids (ILs) have recently emerged as electrolytes in CO₂ electroreduction [145–147]. This can be attributed to their high CO₂ solubility, low volatility, and tunable ionic interactions. These properties provide a means for IL-based electrolytes to enhance efficiency and selectivity toward the conversion of CO₂ into added-value products by offering a stable and versatile environment for the electrochemical reaction [145–147]. For example, copper selenide nanocatalysts exhibited outstanding performance toward the electroreduction of CO₂ using [Bmim]PF₆ (30 wt%)/CH₃CN/H₂O (5 wt%) electrolyte [145]. After electrolysis at -2.1 versus Ag/AgCl electrode, the NMR solution was prepared by mixing the electrolyte with acetonitrile-*d*₃ (CD₃CN) with TMS as internal standard. The NMR analysis revealed that methanol was the predominant product with a Faradaic efficiency of 77.6 % over other produced products. As seen in Fig. 24, ¹³C-labeling experiments were conducted, confirming that the CO₂ was the source of methanol production [145].

In the same context, the ionic liquid [Bmim]BF₆ was found to be a stable electrolyte for CO₂ electroreduction [146]. Palladium-copper bimetallic aerogel (Pd₈₃Cu₁₇) is considered a powerful candidate to convert CO₂ into methanol electrochemically at a very low overpotential (0.24 V) with a high Faradaic efficiency 80.0 % [146]. Because of the high stability of the IL [Bmim]BF₆, it was used as internal standard for

the quantification of methanol. This was done by mixing the electrolyte with CD₃CN and TMS (as internal standard for peak positions). As the concentration of the IL is known, the relative peak area ratio can be calculated in reference to the C(2)-H signal of the IL's cation. The required number of electrons to produce product can be calculated according to eq. (18) [146]:

$$N = C \times V \times N_A \times ne \quad (18)$$

Where *C* is concentration of methanol, *V* is the catholyte volume, *N_A* is the Avogadro's constant, and *ne* is the number of electrons to convert CO₂ to methanol.

The total number of electrons can be measured based on the charge the obtained from the chronoamperogram and the elementary charge ($e = 1.602 \times 10^{-19}$ C) as follows [146]:

$$N_{\text{Total}} = \frac{Q_{\text{Total}}}{e} \quad (19)$$

Finally the Faradaic efficiency is calculated based on eq. (20) [146]:

$$FE = \frac{N}{N_{\text{Total}}} \times 100\% \quad (20)$$

6.5. NMR as a quantitative tool for formaldehyde

Formaldehyde (HCHO) is considered one of the simplest organic compounds [149,150]. This substance finds major application in the manufacture of numerous types of resins, plastics, textiles, disinfectants, and even in the tanning of leather [151–153]. It is a very reactive aldehyde and has a key place in most industrial and chemical processes

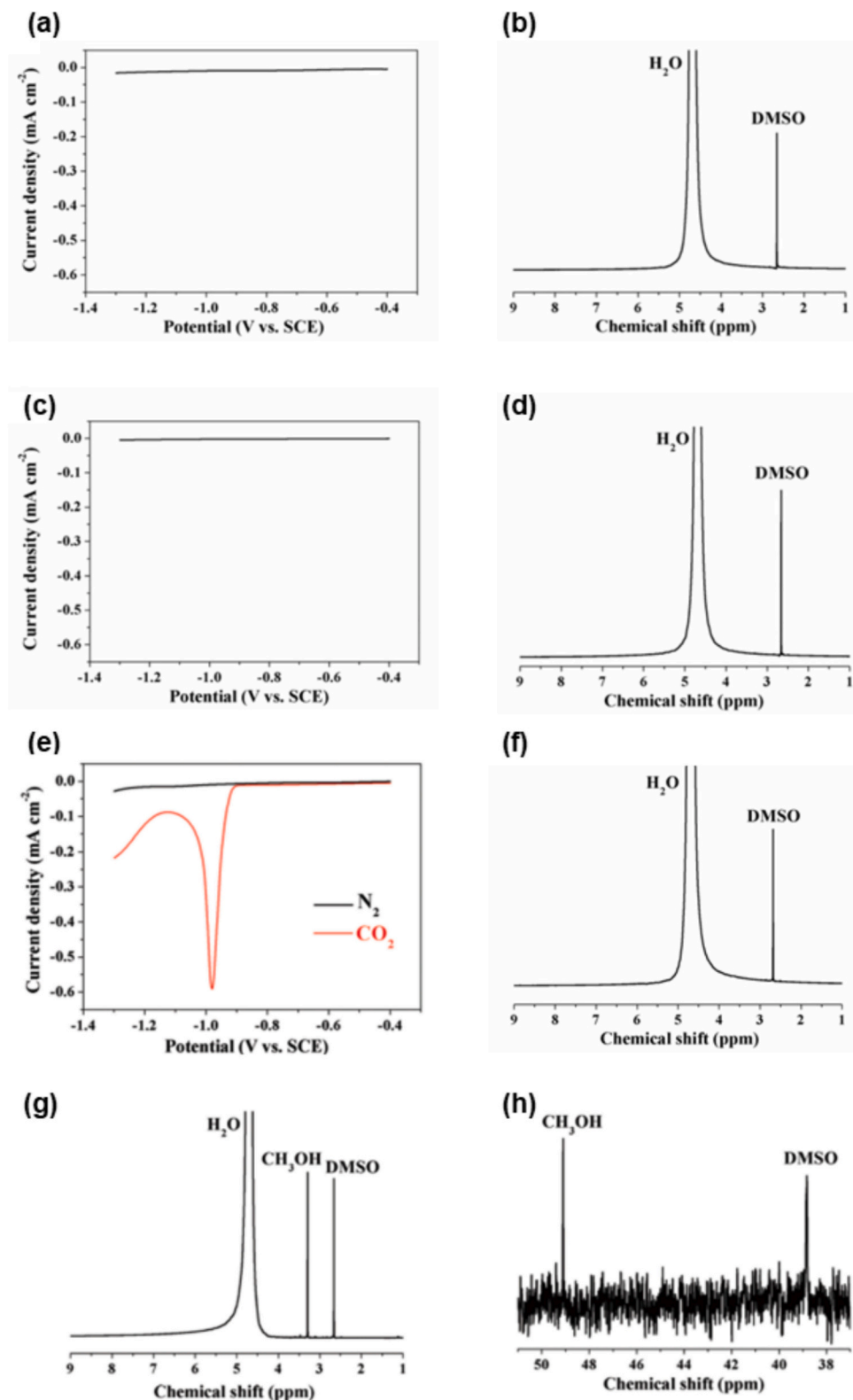


Fig. 20. LSV (a) and ^1H NMR spectrum of the catholyte after electrolysis (b) of bare glassy carbon electrode in CO_2 -saturated NaHCO_3 solution, LSV (c) and ^1H NMR spectrum of the catholyte after electrolysis (d) of bare glassy carbon with Nafion film in CO_2 -saturated NaHCO_3 solution, LSV of hollow urchin-like $\text{Co}(\text{CO}_3)_{0.5}(\text{OH}) \cdot 0.11\text{H}_2\text{O}$ in N_2 -saturated (black) and CO_2 -saturated (red) NaHCO_3 solution (e), ^1H NMR spectrum of the catholyte after electrolysis in N_2 -saturated electrolyte (f), and ^1H NMR and ^{13}C NMR spectra after electrolysis in CO_2 saturated electrolyte (g) and (h), respectively. Reproduced with permission from Ref. [137]. Copyright 2018, Royal Society of Chemistry. (For interpretation of the references to colour in this figure legend, the reader is referred to the web version of this article.)

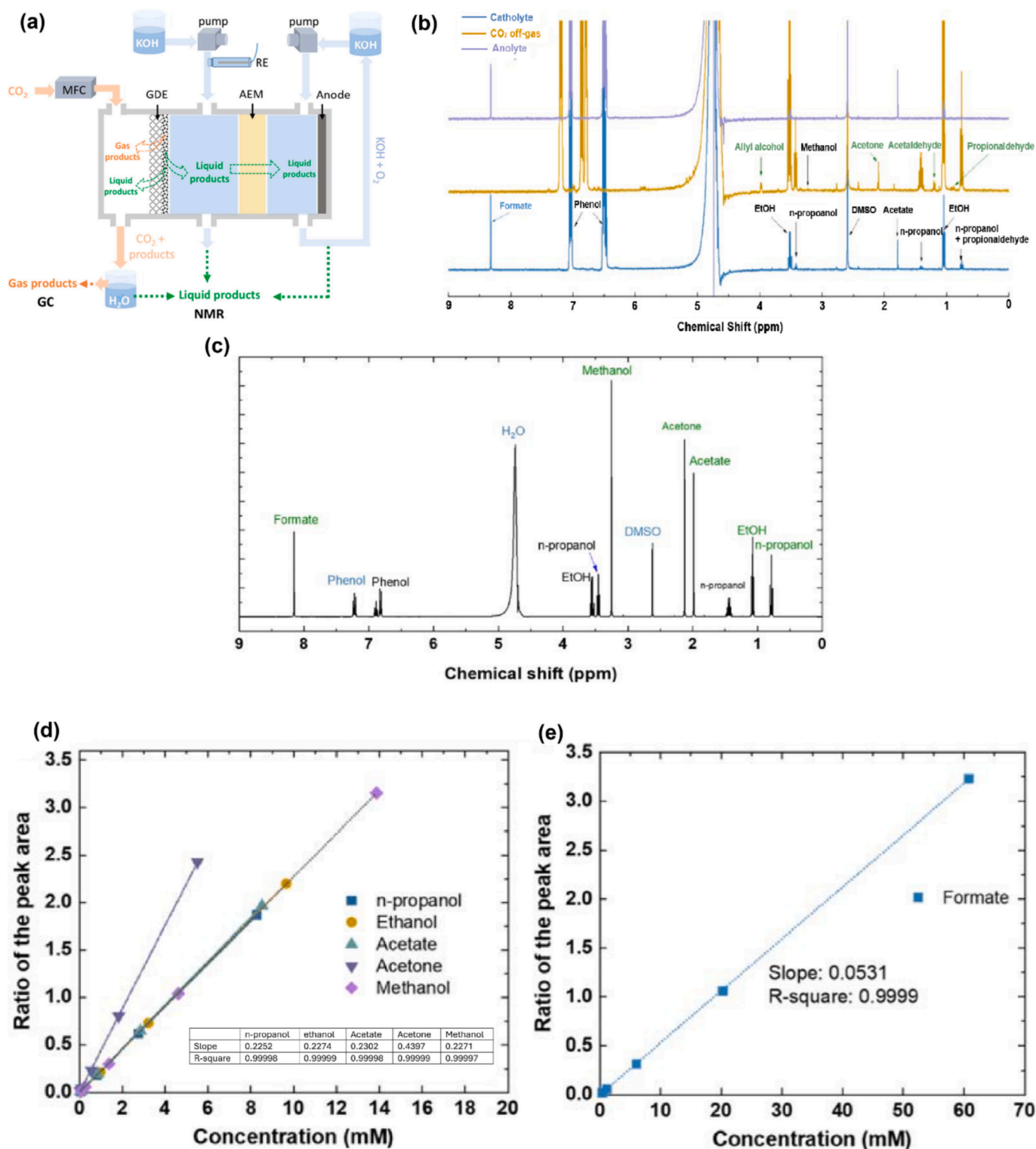


Fig. 21. Schematic presentation of the 3-chamber flow cell setup for eCO₂RR (a), ¹H NMR spectra of the liquid products collected from the 3 chambers (b), ¹H NMR spectrum of standard solution used for calculation (c), calibration curve for products resonate before the water signal with reference to DMSO (d), and calibration curve for products resonate after the water signal with reference to phenol (e). Reproduced with permission from Ref. [142]. Copyright 2020, Elsevier.

[154]. Traditionally, formaldehyde is produced by the oxidation of methanol in the presence of metal catalysts, such as silver or iron oxide, at high temperatures [155,156]. One of the best current alternatives in development involves electrochemical carbon dioxide reduction reaction (eCO₂RR) and electrochemical carbon monoxide reduction reaction (eCORR), a considerably greener production means for formaldehyde

through the electrochemical reduction of CO₂/CO, generally in the presence of catalysts such as copper and other metals, nanodiamonds [157–163]. However, only a limited number of reports exist on HCHO, due to its successive reduction pathways once formed. Often, HCHO is identified as a minor product in eCO₂RR [131,140,163,164].

The detection or analysis of produced formaldehyde through

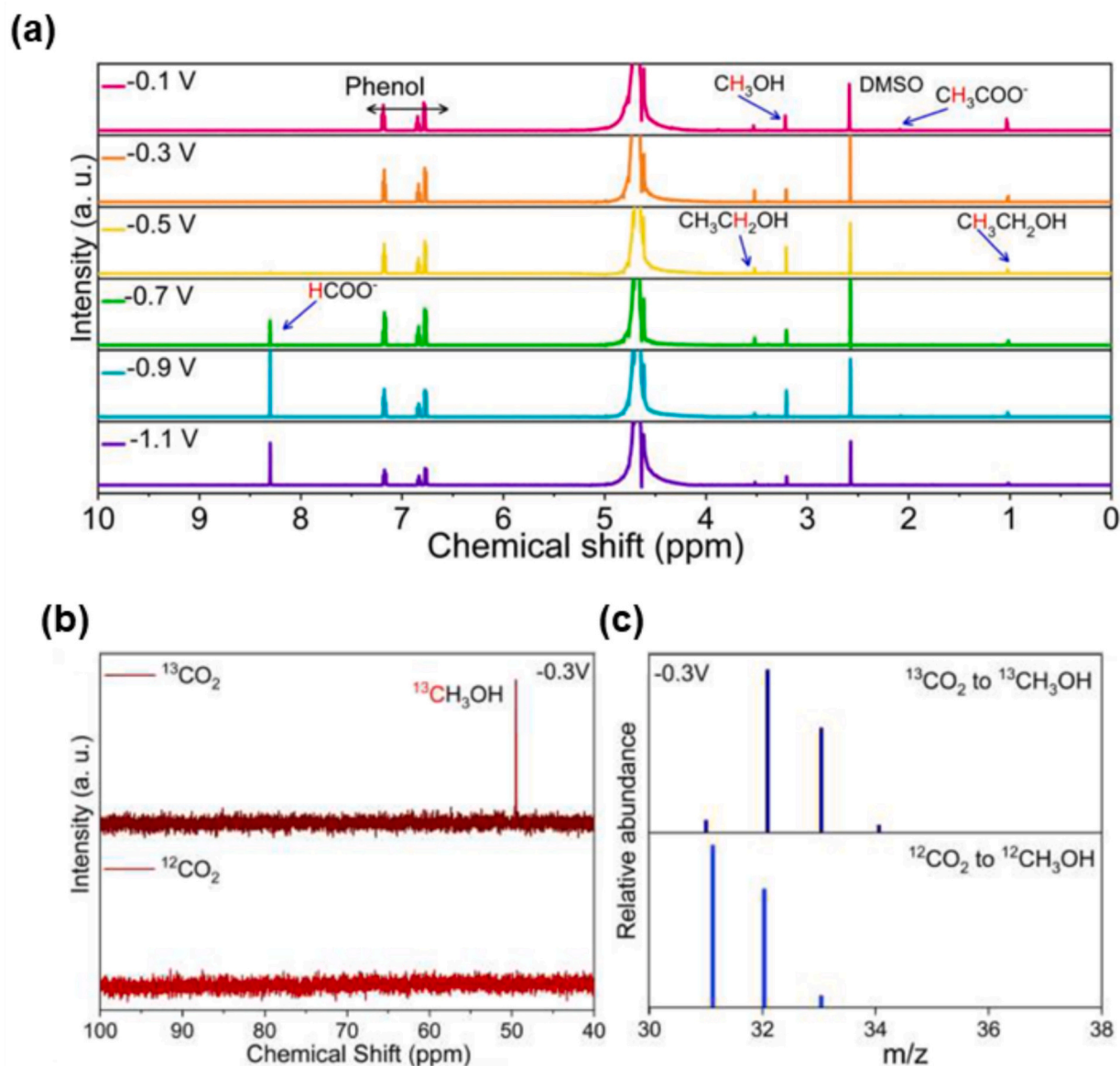


Fig. 22. NMR Spectrum of electrolyte at different potentials (a), ^{13}C NMR spectra (b) and GC-MS spectra (c) after $^{12}\text{CO}_2$ and $^{13}\text{CO}_2$ electrolysis at -0.3 V on CuGa_2 catalyst. Reproduced with permission from Ref. [87]. Copyright 2022, John Wiley and Sons.

eCO_2RR has been reported by utilizing different techniques [159,161]. For instance, Fourier transform infrared spectroscopy (FTIR) and ^{13}C NMR have been utilized to detect the presence of formaldehyde in the liquid aliquot after electrochemical reduction using a pterin electrocatalyst, 6,7-dimethyl-4-hydroxy-2-mercaptopteridine (PTE) [161]. Methanol as a liquid product was quantified using the GC method with a Faradaic efficiency of 10–23 %. However, formate and formaldehyde were unable to analyze by this method and they were only detected by FTIR and ^{13}C NMR [161]. In the same context, Girardi et al., investigated the polyoxometalate catalyst $(\text{TOA})_6[\alpha\text{-SiW}_{11}\text{O}_{39}\text{Co}(\text{O})]$, where TAO is tetraoctyl ammonium and (O) refers to the vacant position in the coordination sphere of Co, toward the electrochemical reduction CO_2 [159]. The electrolysis was performed in a CO_2 saturated electrolyte containing dichloromethane (CH_2Cl_2) and 0.1 M of tetrabutylammonium tetrafluoroborate (TBABF_4) as supporting electrolyte. Upon electrolysis at -1.5 V versus saturated calomel electrode ($\text{Hg}_2\text{Cl}_2/\text{Hg}$) for 4.5 h, the formation of CO was detected accompanied by detection of formaldehyde through the colorimetric Nash test [159].

In the other hand, formaldehyde, as a minor product in eCO_2RR , was

quantified by GC-MS and HPLC [71,131,157,163]. Cobalt(III) triphenylphosphine corrole complexes, as eCO_2RR electrocatalyst, produced variety of C_1 and C_2 products, such as methanol, formate, formaldehyde, ethanol, and acetate [163]. The content of formaldehyde was quantified by GC-MS by mixing the electrolyte with ethanol and then acidified with *p*-toluenesulfonic acid. The peak at m/z 104 represents the dimerization of HCHO into dimethoxymethane which displays the formation of formaldehyde. The highest content of formaldehyde was observed at -0.65 V versus RHE with a value of 5 % and its dimer with 2 % (Fig. 25). Representing its low content and Faradaic efficiency compared to the total Faradaic efficiency for other products [163]. Similarly, the low content of formaldehyde obtained by cobalt phthalocyanine on multi-walled carbon nanotubes (Co-MWCNTs) was also quantified through GC-MS by derivatization using the derivatizing agent pentafluorobenzylhydroxylamine (PFBHA) [131].

Alternatively, Boutin's team identified in their study that formaldehyde is a key intermediate toward the production of methanol [71]. The low concentration of formaldehyde was quantified by HPLC after 2-h electrolysis at -0.54 V versus RHE. After derivatization using 2,4-

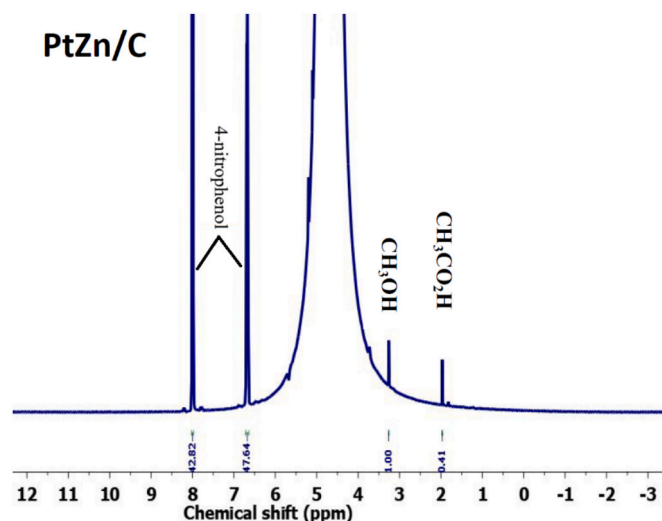


Fig. 23. The ^1H NMR spectrum of catholyte after 4-h electrolysis at -0.9 V vs RHE. Reproduced with permission from Ref. [72]. Copyright 2020, American Chemical Society.

dinitrophenylhydrazine (DNPH), the formaldehyde exhibited a Faradaic efficiency of 3.3 % [71]. Higher faradaic efficiencies were obtained in different electrolytes by exploring the activity of the boron-doped

diamond (BDD) toward as eCO_2RR electrocatalyst [157]. After electrolysis at different potential, the liquid aliquot was analyzed by HPLC to quantify the concentration of formed formaldehyde and formic acid. After 1 h electrolysis at a potential of -1.5 V versus Ag/AgCl electrode, the highest Faradaic efficiency was obtained in methanol based tetrabutylammonium perchlorate solution (0.1 TBAP) with a value of 65 %, while the electrolysis in 0.1 M NaCl solution and seawater displayed lower efficiencies of 62 % and 36 %, respectively (Table 3) [157].

The quantification of formaldehyde produced from electrochemical reduction of CO_2 is somewhat in its infancy, and reports remain comparatively rare [160,165]. One of the significant challenges facing CO_2 reduction to value-added chemicals, such as formaldehyde, is the difficulty of the selective reduction of CO_2 under mild conditions [2,93]. It is, therefore, quite interesting to note that there have been works recently that involve the use of carbon monoxide as an electrochemical reduction alternative for CO_2 with much higher selectivity and efficiency [158,162,166]. These results would thus hint that direct CO_2 reduction is a field that is still developing, while an indirect process involving CO as an intermediate may be a promising route toward formaldehyde and other products [158,162,166].

Yao et al. utilized NMR to identify the formation of formaldehyde as the only produced liquid product [158,162]. This was accomplished by mixing 500 μL of the collected catholyte with 100 μL of D_2O . The formaldehyde concentration was then calculated using the acetylacetone method and measured by UV-Vis. They identified the formaldehyde peak to resonate at δ 4.17 ppm as the formaldehyde undergoes

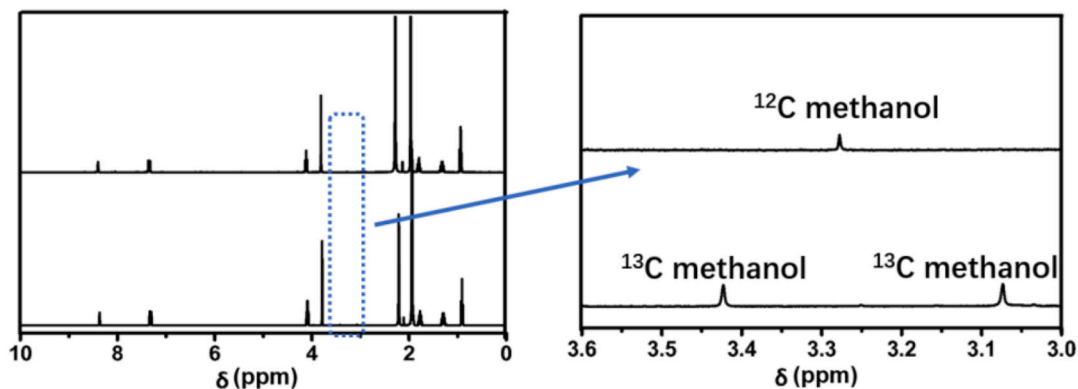


Fig. 24. ^1H NMR spectrum of $^{12}\text{CO}_2$ - and $^{13}\text{CO}_2$ -saturated [Bmim] PF_6 (30 wt%)/ $\text{CH}_3\text{CN}/\text{H}_2\text{O}$ (5 wt%) electrolyte after 5-h electrolysis. Reproduced with permission from Ref. [145]. Copyright 2019, Springer Nature.

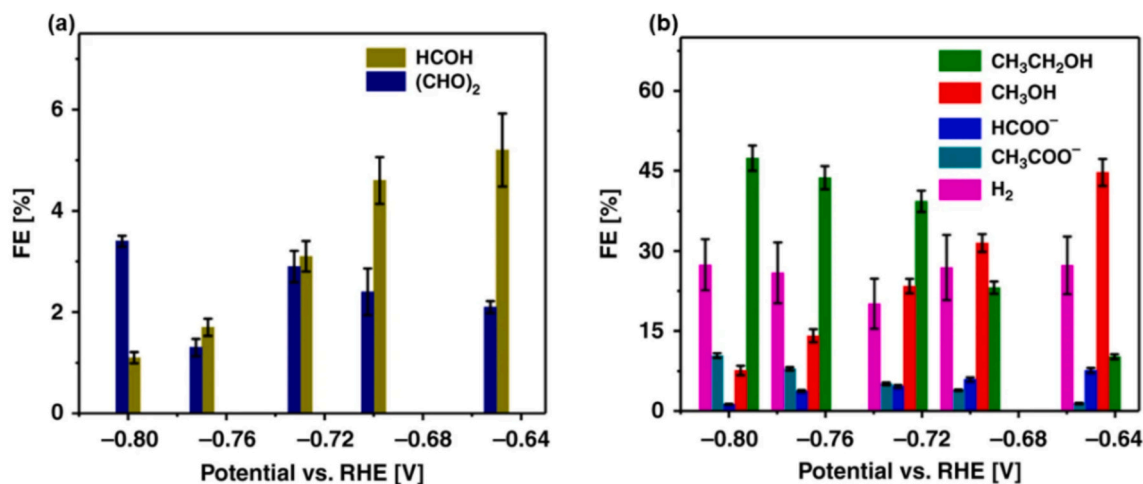


Fig. 25. The Faradaic efficiencies for minor formed formaldehyde and its solvated dimer of at different potentials (a) and for methanol, formic acid, ethanol and acetic acid (b). Reproduced with permission from Ref. [163]. Copyright 2019, Springer Nature.

Table 3

Faradaic efficiencies of liquid and gaseous products of eCO₂RR using BDD at −1.5 V vs Ag/AgCl. Reproduced with permission from Ref. [157]. Copyright 2014, John Wiley and Sons.

Electrolyte	Formaldehyde	Formic acid	Hydrogen
0.1 M TBAP in methanol	65 %	14 %	5.2 %
0.1 M NaCl in water	62 %	3.2 %	22 %
Seawater	36 %	1.5 %	58 %

hydration reaction to form methanediol (CH₂(OH)₂). While they ignored the signal at δ 8.34 ppm as they claimed that this peak appears in every NMR signal (Fig. 26) [158,162].

Based on the above-mentioned analysis method, and due to the high reactivity of formaldehyde, it is worth mentioning that these methods have some drawbacks as they require organic solvents, and the UV–vis detector cannot distinguish between isotopes H¹²CHO and H¹³CHO, which is important for identifying the carbon source. Therefore, a method must be established to overcome the obstacles that might face the researcher during the quantification process of formaldehyde [66,166]. This was accomplished by developing a simple quantitative approach to formaldehyde through routine ¹H NMR analysis, by means of detection of the HCHO-bisulfite adduct (A) formed under the reaction of sodium bisulfite (NaHSO₃) with formaldehyde in water (Fig. 27) [66,166]. The reaction is strongly exergonic, and the adduct is stable for several days. This procedure represents the first quantitative approach using ¹H NMR for formaldehyde determination and identification of H¹³CHO [66,166]. In a typical experiment, 5 mM formaldehyde was mixed with an equimolar amount of 1 M NaHSO₃ at a mixing ratio of 50:50 v/v and exhibited a well-shifted peak from water at δ 4.79 ppm to around δ 4.39 ppm. The quantitative results of the ¹H NMR method for formaldehyde was obtained based on the relative area of adduct A to an internal standard. DMSO was not considered as internal standard as it reacts with the bisulfate. Alternatively, dimethylsulfone (DMSO₂) was adopted and it demonstrated stable at least for two days [66].

This protocol was applied to determine the formaldehyde content in the liquid products. Benefiting from this, Singh et al. quantified the formaldehyde that is formed after the electroreduction of CO using cobalt phthalocyanine immobilized on multiwalled carbon nanotubes (CoPc-MWCNTs) [166]. After electrolysis, 392 μL of the HCHO-bisulfate adduct (equivalent volume of the catholyte and 1.0 M NaHSO₃) was mixed with 48 μL of D₂O and 40 μL of 4 mM DMSO₂ (internal standard). Presaturation method with water suppression was used, with a relaxation time of 2 s, to obtain the NMR spectrum after accumulating 64 ¹H NMR scans. The Faradaic efficiency of formaldehyde was then calculated and found to be 17.5 % with a total Faradaic efficiency of 61.2 % for liquid products [166].

7. NMR as a quantitative tool for C₂ Products

C₂ products refer to a class of organic compounds with two carbon atoms in the backbone of their chemical structure. C₂ refers to the naming convention in chemistry, where the letter C identifies carbon and the number “2” the number of carbon atoms contained within the molecule. These compounds can be obtained using different types of chemical route processes, among them electrochemical CO₂ reduction—one of the promising ways of sustainable fuel and chemicals productions. The common commodities of C₂ products include gaseous products such as ethylene (C₂H₄) and ethane (C₂H₆), while the liquid products could be ethanol (C₂H₅OH), and acetic acid (CH₃COOH) [167–169]. The liquid C₂ products can be measured by a wide variety of analytical techniques, such as HS-GC, HPLC, and NMR [33,74,83,167,168,170]. In this regard, recent reports have emphasized the use of NMR as a powerful tool in the identification and analysis of C₂ products. Further detail about this will be given in the next sections.

7.1. NMR as a quantitative tool for ethanol

Ethanol is a versatile chemical which, during the last couple of decades, has emerged as one of the major building blocks in fuels, beverages, and industrial feedstock [171,172]. Its production methods vary from biomass fermentation, where microorganisms convert the sugars of crops like corn or sugarcane into ethanol, to the catalytic hydration of ethylene in the petrochemical industry [173,174]. Among them, the electrochemical reduction of CO₂ has been considered one of the cleanest approaches owing to the use of feedstock CO₂, hence decreasing greenhouse gas emissions while producing ethanol in a green manner. Quantification of the produced ethanol can be calculated using several analytical techniques such as HPLC [170,175], HS-GC [176,177], and NMR [73,74,83]. For example, different compositions of CuO-ZnO_x catalyst were explored toward the production of ethanol through eCO₂RR. The content of produced ethanol in the liquid aliquot was determined by HPLC. The highest production rate of ethanol (121 μmol h^{−1} L^{−1}) was obtained by CuO-ZnO₁₀ as electrocatalyst at −0.80 V (vs RHE), revealing a Faradaic efficiency of 22.27 % [175]. Also, HPLC was utilized to quantify the content of formed multi-carbon (C₂₊) products including ethanol through the electrochemical reduction by a boron, nitrogen-doped graphitic frustrated Lewis pair catalyst (BN-GDLP). The obtained total Faradaic efficiency for the multi-carbon products was 87.9 % at a partial current density of −6.0 mA/cm² [170]. Additionally, HS-GC was used to measure the concentration of ethanol produced by silver, copper bimetallic catalyst. The content of copper played a significant role toward producing ethanol through eCO₂RR, where the relation between of copper content and the Faradaic efficiency is

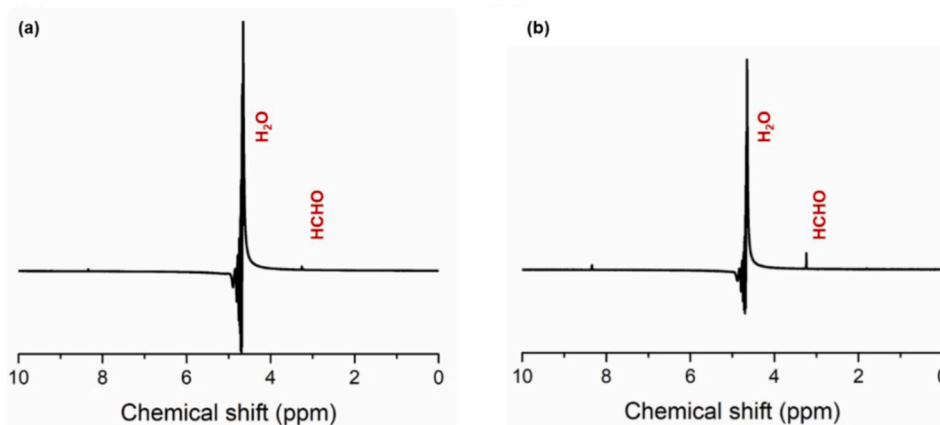


Fig. 26. ¹H NMR spectrum of liquid product obtained after electrolysis (a) and the ¹H NMR spectrum of HCHO standard solution (b). Reproduced with permission from Ref. [162]. Copyright 2020, Royal Society of Chemistry.

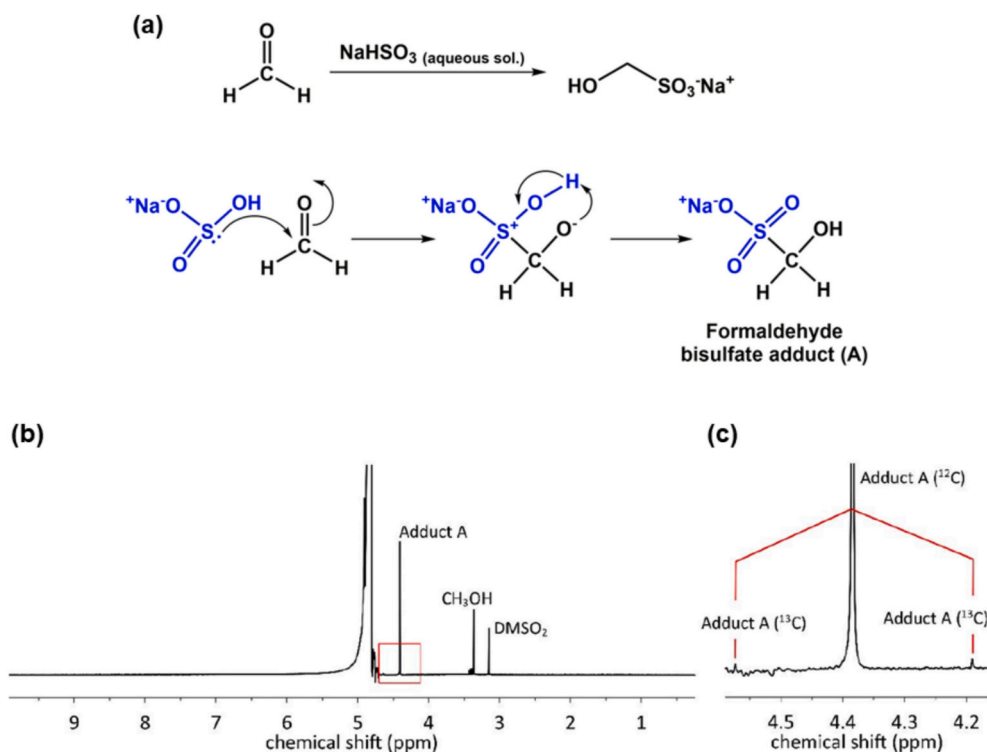


Fig. 27. Reaction mechanism pathway of formaldehyde with sodium bisulfate (a), full ^1H NMR spectrum of the reaction mixture of formaldehyde and NaHSO_3 solutions in the presence of DMSO_2 as internal reference (b), and enlarged spectrum representing the peaks corresponding to adduct (A) (c). Reproduced with permission from Ref. [66]. Copyright 2020, Royal Society of Chemistry.

inversely proportional. The highest Faradaic efficiency (23 %) was obtained at a current density of -20 mA cm^{-2} for the copper content of 45 % [176]. Similarly, Zhao et al. employed HS-GC to quantify the concentration of the electrochemically produced ethanol through reducing CO_2 by Cu octahedra modified with low-coordinated Cu nanoclusters (Cu oct @Cu₂NCs). After electrolysis at -1.17 V vs. RHE, ethanol was formed with a high Faradaic efficiency of 48.15 % [177].

Nowadays, NMR has gained wide acceptance as one of the key methods for the quantification of liquid products, including ethanol. Ethanol usually shows two typical peak groups in the ^1H NMR spectrum: A triplet signal representing the methyl group ($-\text{CH}_3$) that resonates between $\delta 1.0$ and $\delta 1.3 \text{ ppm}$, and a quartet peak related to the methylene group ($-\text{CH}_2$) that appears between $\delta 3.3$ and $\delta 3.8 \text{ ppm}$ [135,136]. In general, the proton of the hydroxyl group ($-\text{OH}$) appears as a broad singlet, although its chemical shift may vary from $\delta 4.5$ to $\delta 5.5 \text{ ppm}$, depending on hydrogen bonding and solvent effects [135,136]. Major resonances in the ^{13}C NMR of ethanol are two: one for the methyl carbon at approximately $\delta 18 \text{ ppm}$, and one for the methylene carbon around $\delta 58 \text{ ppm}$ [135,136].

The quantification of the formed ethanol after the electrochemical reduction of CO_2 has been done extensively by NMR. This can be done through using several internal standards to quantify the concentration of ethanol accurately [73,74,83,163,175,178–194]. DMSO has been considered the predominant solvent used for this purpose [73,74,175,178–189]. However, some researchers reported the use of a mixture of phenol and DMSO as dual internal standard system [163,190–193]. While few reports displayed the employing of phenol [83], and TMS [194] as internal standards.

7.1.1. Dimethyl sulfoxide as internal standard for ethanol quantification

Carbon nanospire (CNS) electrode with electro-nucleated Cu nanoparticles (Cu/CNS) showed considerable activity toward the direct electrochemical conversion of CO_2 to ethanol with a Faradaic efficiency of 63 % and selectivity of 86 % [178]. The content of ethanol was

measured by ethanol in the collected liquid aliquot after electrolysis at ambient conditions, where 700 μL of the electrolyte was mixed with 35 μL of 10 mM DMSO in D_2O and transferred to an NMR station. The analysis was performed using the presaturation method (PRESAT) accompanied with the following acquisition parameters: spectral width (SW) = 8012.8 Hz; Pulse Width (pw) = 45° ; delay 1 (d1) = 5 s, delay 2 (d2) = 0 s; presaturation (presat) = 5 s; acquisition time (at) = 4 s, steady state scans (ss) = 2, number of transients (nt) = 64 [178]. Two-step CO_2 -to-ethanol cascade electrolysis system (Fig. 28a), silver nanocoral (Ag-NC) in 0.1 M KHCO_3 (electrolyzer 1) and oxide-derived Copper (OD-Cu) in 0.1 M KOH (electrolyzer 2), was used to produce ethanol electrochemically exhibiting a total Faradaic efficiency of 11 % at an average applied potential -0.52 V versus RHE [74]. After electrolysis, equal volumes of the catholyte from the second electrolyzer and D_2O were mixed with a known low concentration of DMSO for internal calibration using NMR analysis. As shown in Fig. 28b, a sample was withdrawn for analysis by ^1H NMR, which displayed the production of ethanol, as evidenced by its characteristic peaks at $\delta 1.0 \text{ ppm}$ and $\delta 3.5 \text{ ppm}$. However, the analysis after 1-h electrolysis revealed the absence of ethanol, 4 new signals appeared at $\delta 1.4$, $\delta 2.2$, $\delta 7.0$ and $\delta 7.8 \text{ ppm}$, which can be assigned to propionaldehyde (first two peaks), while the signals at $\delta 7.0$ and $\delta 7.8 \text{ ppm}$ are ambiguous and may be assigned to aromatics [74].

Introducing different binding sites to a Cu catalyst, promotes the ethanol formation through the eCO_2RR [185]. After the electrolysis using bimetallic Ag/Cu electrocatalyst, the liquid aliquot was mixed with a mixture of DMSO and D_2O as an internal standard and a lock solvent, respectively. The Faradaic efficiency was recorded as 41 % at a current density of 250 mA cm^{-2} and a potential of -0.67 V versus RHE [185]. Ethanol was found to be the predominant product when CO_2 electrochemically reduced using AuCu alloy nanoparticle embedded Cu submicrocone arrays (AuCu/Cu-SCA) with a Faradaic efficiency of 20 % [189]. The amount of ethanol was quantified as follows: 0.5 mL of the catholyte after electrolysis was mixed with 0.1 mL D_2O and 0.03 μL

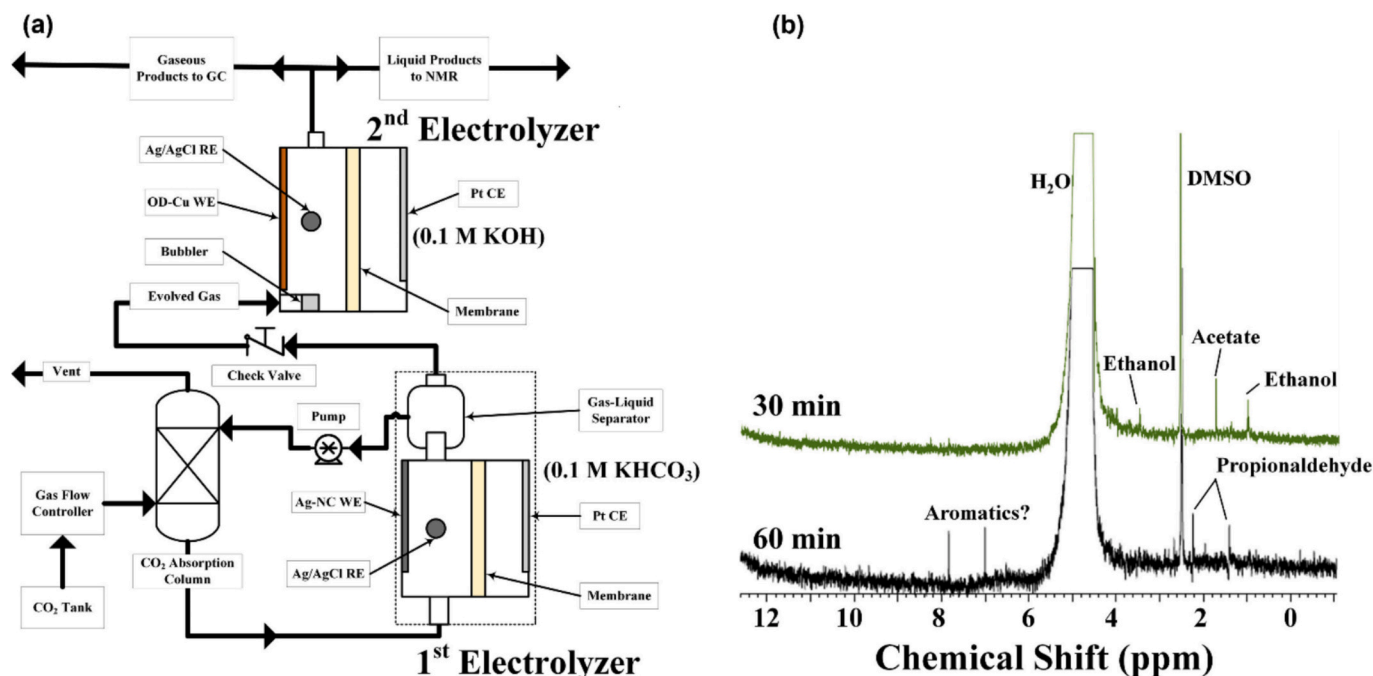


Fig. 28. Illustrative scheme of the two-step CO_2 -to-ethanol cascade electrolysis system (a) and ^1H NMR analysis of electrolyte after 30-min and 60-min electrolysis (b). Reproduced with permission from Ref. [74]. Copyright 2018, Elsevier.

DMSO. The analysis was conducted with water suppression by a pre-saturation method. After measurement the faradaic efficiency was calculated as follows:

$$\text{FE} = \frac{n \times F \times N}{Q} \quad (21)$$

Where n is the number of moles of ethanol, F is the Faraday constant, N is the number of transferred electrons for ethanol ($12 e^-$) and Q is the quantity of charge [189].

Xu et al., investigated the catalytic performance of carbon-supported copper catalysts (Cu/C) as potential catalyst for producing ethanol [182]. The liquid products collected at constant potentials were quantified by ^1H NMR spectroscopy (Fig. 29). The measurement was carried

out using DMSO as internal standard. Acquisition of all spectra was done under the same conditions: time domain data size (TD) = 65,536; dummy scans (DS) = 2, Number of scans (NS) = 16; spectral width (SW) = 19.99 ppm (in Hertz = 10,000 Hz); filter width (FW) = 125,000 Hz; pause width (pw) = 45°; delay 1 (d1) = 5 s; and delay 2 (d2) = seconds. For the sample preparation, 700 μL of electrolyte was added to 35 μL of a DMSO solution (10 mM in D_2O), and standard curves were made from relative peak areas. As seen in Fig. 29, ^1H NMR revealed the formation of ethanol with a high Faradaic efficiency of 91 % at a low potential of -0.6 V and -0.7 V versus RHE [182].

Similarly, Ma et al. investigated fluorine-modified copper electrode as powerful candidate for C_{2+} products [187]. Faradaic efficiency of 80 % was obtained mainly for ethylene and ethanol at a current density of

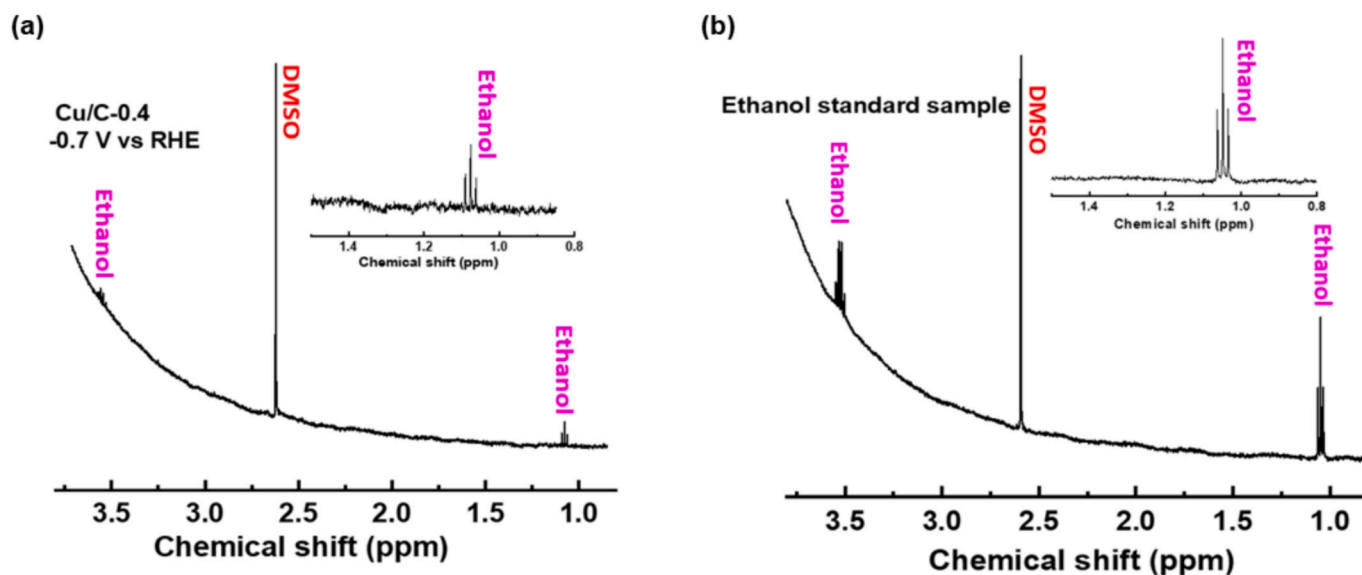


Fig. 29. ^1H NMR spectrum of the electrolyte after electrolysis using Cu/C-0.4 at -0.7 V versus RHE (a) and 0.2 mM ethanol standard in 0.1 M KHCO_3 solution (b); The insets of (a and b) are the zoomed region of the ethanol's signal at $\delta 1.09 \text{ ppm}$. Reproduced with permission from Ref. [182]. Copyright 2020, Springer Nature.

1.6 A cm⁻² with high selectivity (85.8 %) and single-pass yield (16.5 %) toward C₂₋₄. After electrolysis, the liquid products (acetate, ethanol, formate, and *n*-propanol) were analyzed by ¹H NMR as follows: 0.5 mL of the electrolyte was mixed with 0.1 mL of 100 ppm DMSO in D₂O (internal standard). After analysis, the concentration of liquid products (C_l) was quantified through internal standard method and then implied in eq. (22) to obtain the Faradaic efficiency:

$$FE_l = \frac{q_l}{q_{total}} = \frac{96485 \times C_l \times V \times z_l}{q_{total}} \quad (22)$$

Where 96,485 is the value of Faraday constant, *V* is the electrolyte volume, *z_l* is the electrons passed during electrolysis and *q_{total}* is the total charge produced during electrolysis [187].

In 2022, Su et al. reported their high-performance CuO clusters supported on N-doped carbon nanosheets (Cu₂-CuN₃) catalyst toward

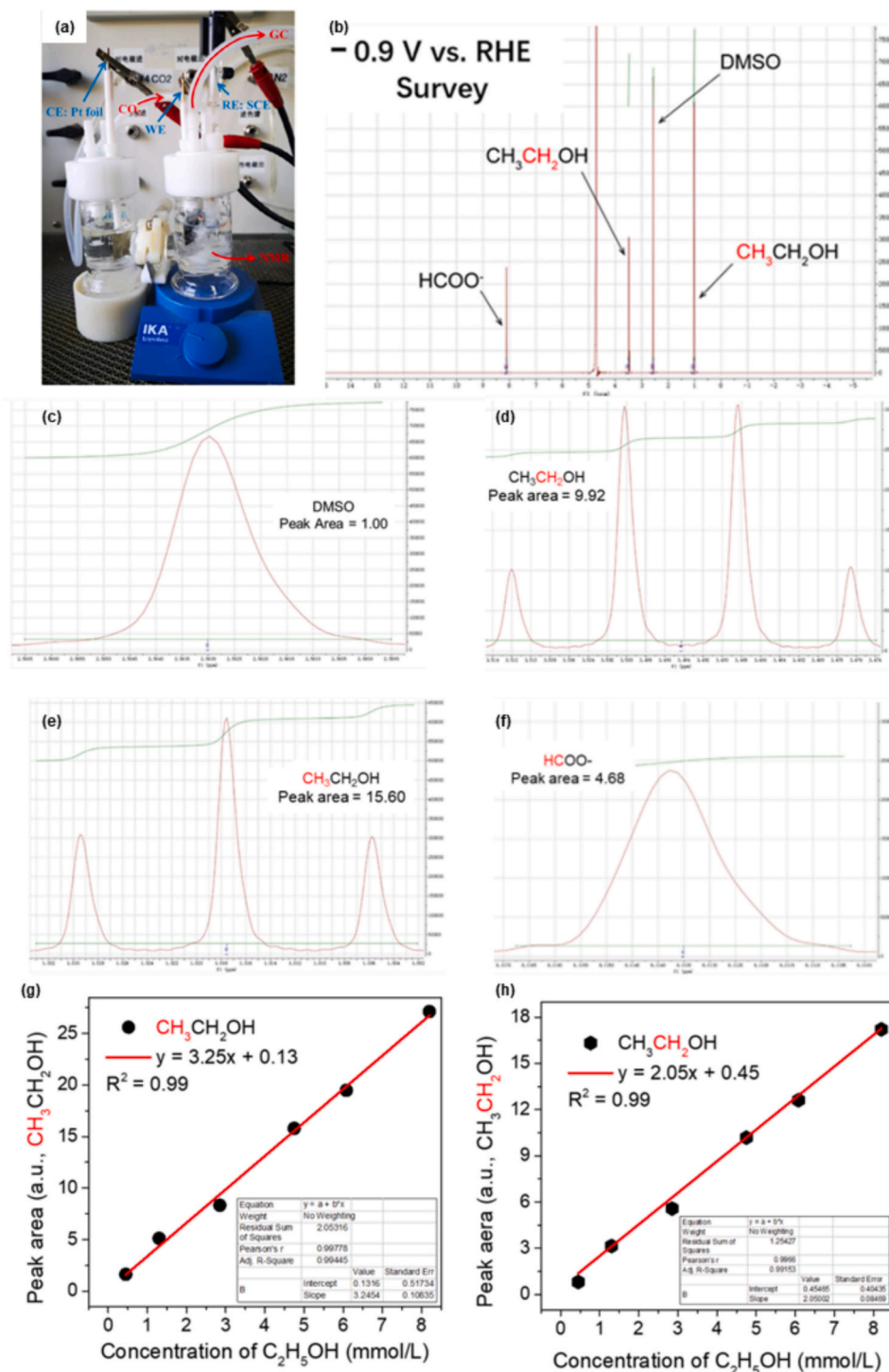


Fig. 30. The electrochemical eCO₂RR setup represented by the H-type electrochemical cell, where WE is the working electrode, CE is the counter electrode, and RE is the reference electrode (a). The NMR spectrum of 0.45 mM ethanol (b), the enlarged region of DMSO (c), CH₃ (d), CH₂ (e), and formate (f) with baseline and integrated peak area indicated, and the Calibration curves based on the integrated area of the CH₃ (g) and CH₂ (h) peaks in the NMR spectra. Reproduced with permission from Ref. [181]. Copyright 2023, Springer Nature.

eCO₂RR. Higher selectivity (51 %) and Faradaic efficiency (73 %) for ethanol production at a potential of -1.1 V vs. RHE and a current density of 14.4 mA cm^{-2} [188]. They selected NMR as a powerful machine for ethanol quantification with 2 s pre-saturation delay and 2 s relaxation delay for analyzing the NMR sample containing 300 μL of the catholyte and 300 μL of 5 mM DMSO (internal standard) in D₂O [188]. A year later, a tin-based tandem electrocatalyst exhibited higher Faradaic efficiency (82.5 %) and selectivity (80 %) toward ethanol production at a lower potential (-0.9 V vs. RHE) using H-type cell configuration (Fig. 30a) [181]. The ¹H NMR was utilized to detect and quantify the liquid products without the need for KHCO₃ removal (Fig. 30b). Solvent suppression method was used to remove the water peak with constant spectral acquisition parameter. The authors demonstrated that ¹H NMR is capable of precisely measuring product concentrations (Fig. 30c, d, e, and f). After phase and baseline correction, peaks were integrated, ethanol concentration from CO₂RR was determined with calibration curves (Fig. 30 g and h) [181].

The validation of eCO₂RR products' source is a crucial route to confirm whether the feeding CO₂ gas is the source of the formed products. In relation to this, validation of the selectivity and efficiency of the catalysts in the production of certain target molecules will be very important for better understanding and optimization of the process. This was done Li et al. as they employed Cu–Sn bimetallic catalysts for electrochemically reduction of CO₂ to ethanol. It was found that at higher negative potentials, the Faradaic efficiency of ethanol increased but for ethylene decreased, that displays high selectivity toward ethanol production [180]. For example, at a potential of -1.4 V (RHE), CuSn_{0.025} exhibited the highest FE of ethanol (25.93 %) with a large partial current density of 15.05 mA cm^{-2} . This confirms the high stability of the CuSn_x catalysts, which was demonstrated by the stability of the current at such high potential. The validation of C₂ product formation from eCO₂RR was then carried out by the electrolysis at -1.3 V versus RHE and under Ar and CO₂ environments using CuSn_{0.025}, which revealed that ethanol was produced from CO₂ reduction not from the bicarbonate in the electrolyte solution [180].

Another way to confirm the source of ethanol is the well-known isotope labeling experiment, which including the gas feeding of ¹³CO₂ during electrolysis and analyze the liquid products using different techniques such as NMR [73,175,179,183,184], GC–MS [179], GC–FID [183], and/or HPLC [175]. For example, Li et al. investigated the cooperative catalyst design of molecule–metal catalyst interfaces (FeTPP [Cl]/Cu; where TPP: 5,10,15,20-tetraphenyl-21H,23H-porphine) as a good catalyst for CO₂ electroreduction [184]. The ethanol was produced at -0.82 V vs. RHE with a partial current density of 124 mA cm^{-2} and a Faradaic efficiency of 41 %. NMR was used to quantify the liquid products with reference to DMSO as an internal standard (Fig. 31a). To confirm the source of ethanol, isotope labeling experiments were conducted, and the liquid products were analyzed by ¹H NMR and ¹³C NMR (Fig. 31b and d, respectively). The ¹³CO₂-labeling experiment exhibited signal splitting of the ethanol's protons [184]. Similarly, CoO-anchored N-doped carbon material (MC–CNT/Co) was reported as eCO₂RR catalyst [73]. Ethanol was the predominant product with a Faradaic efficiency of 60.1 % and current density of 5.1 mA cm^{-2} . The origin of ethanol was confirmed first by 6-h electrolysis at a potential of -0.3 V vs. RHE using Ar instead of CO₂, which confirmed the absence of ethanol and other products as a result of electrolysis under Ar atmosphere. Furthermore, isotope-labeling experiments were conducted using ¹³CO₂ and ¹²CO₂ saturated 0.5 M KHCO₃ electrolyte. The formed liquid products at a potential of -0.32 V (RHE) were analyzed by ¹H NMR, which revealed the signal splitting of the ethanol's protons. This confirms that the source of produced ethanol is from CO₂ not from any other C-source in the reaction system [73].

Along with the analysis of liquid products by NMR for quantification and source confirmation, other techniques were also used in parallel to identify ethanol as a product of eCO₂RR. In 2019, Cu nanoparticles decorated on pyridoxine modification graphene oxide sheets (GO-VB₆-

Cu) was investigated toward electroreduction of CO₂ [179]. The product formation in the liquid phase was monitored by ¹H NMR, wherein ethanol was quantified from its peak versus DMSO peak (internal standard) and its concentration interpolated from a standard curve. The highest Faradaic efficiency of ethanol production using GO-VB₆-Cu was obtained at -0.250 V vs. RHE with a value of 56.3 %. To confirm the origin of ethanol, an ¹H NMR analysis was performed for the liquid products after electrolysis in CO₂, and N₂ environments revealing the presence of ethanol in CO₂ experiment and its absence in N₂ experiment. Followed by the isotopic labeling experiment using ¹³CO₂, which confirmed that ethanol was the only detected liquid product. Further GC–MS was used to identify the source of ethanol, which revealed that ethanol is mainly produced from the electroreduction of CO₂, since the distinctive isotopic signals for ¹³CH₃¹³CH₂OH ($m/z = 47, 48$) and ¹²CH₃¹³CH₂OH ($m/z = 45, 46$) are found in the mass spectra [179]. In addition, GC–FID was used by Liu's team to confirm the amount of produced ethanol by reducing CO₂ electrochemically using Ru(II) polypyridyl carbene complex/N-doped porous carbon (RuPC/NPC) electrode [183]. Ethanol, acetate, methanol and formate, as liquid products were analyzed by ¹H NMR. To confirm that the liquid products were reduced mainly from CO₂, bulk electrolysis was carried out at -0.97 and -1.07 V versus normal hydrogen electrode (NHE) in Ar-saturated 0.5 M KHCO₃ solutions, which was further confirmed by the ¹³CO₂-labeling experiment. The ¹H NMR spectrum displays explicit H–¹³C signals for all liquid products, where each product signal has been split into two peaks by the coupling to ¹³C atoms [183].

On the other hand, HPLC was used to confirm the amount of produced ethanol (Fig. 32c and d), which had been initially analyzed by NMR, using oxide-based Cu and Zn bimetallic (CuO–ZnO_x) catalyst [175]. After electrolysis, 0.5 mL of the catholyte was mixed with 0.2 mL of D₂O and 0.1 mL of 1 mM DMSO in 0.1 M KHCO₃ and transferred to NMR tube for analysis. The analysis was performed using water suppression method, to enhance the sensitivity of products that appear near to water peak (Fig. 32a and b). The Faradaic was then calculated based on the concentration of ethanol obtained with reference to the calibration curves and calculated based on the results obtained by NMR and HPLC [175].

7.1.2. Other solvents as internal standards for ethanol quantification

Alkoshab and coworkers employed phenol as an internal standard to quantify the produced ethanol by eCO₂RR using Cu/Cu_xO nanoparticles into nitrogenous porous carbon cuboids Cu/Cu_xO–PCC [83]. Phenol was chosen due to its structural unrelatedness with the target analytes. Its chemical shifts are also not overlapping with those analytes, and it has not shown excessively long T1 relaxation times. The NMR sample was prepared by taking 630 μL of the electrolyte solution which was then mixed with 70 μL of D₂O and 30 μL of 50 mM phenol (in highly pure deionized water). The NMR analysis was carried out using the water peak suppression method with the mean of the presaturation technique, considering the following acquisition parameters: 128 scans, pulse width 90°, spectral width 27.76 ppm, time-domain size of 32,000, dummy scans of 8, and delay 1 of 10 s. The phenol's chemical shift at δ 7.2 ppm was chosen for calculation and the product quantification was done based on the signal integrals (*I*) of the analyte and internal standard and the number of nuclei (*N*) giving rise to signal through a simple molar ratio analysis using eq. (23) [83]:

$$\frac{M_x}{M_y} = \frac{I_x}{I_y} \times \frac{N_y}{N_x} \quad (23)$$

In addition to utilizing phenol as an internal standard, the dual internal standard system of phenol and DMSO has been also used to quantify the content of produced ethanol and other product that may formed electrochemically [163,190–193]. In 2018, Ag nanoparticles anchored onto a 3D graphene wrapped nitrogen-doped carbon foam (Ag–G–NCF) reduced CO₂ electrochemically to ethanol with a high Faradaic efficiency of 82.1–85.2 % at -0.6 – -0.7 V vs. RHE [191]. After

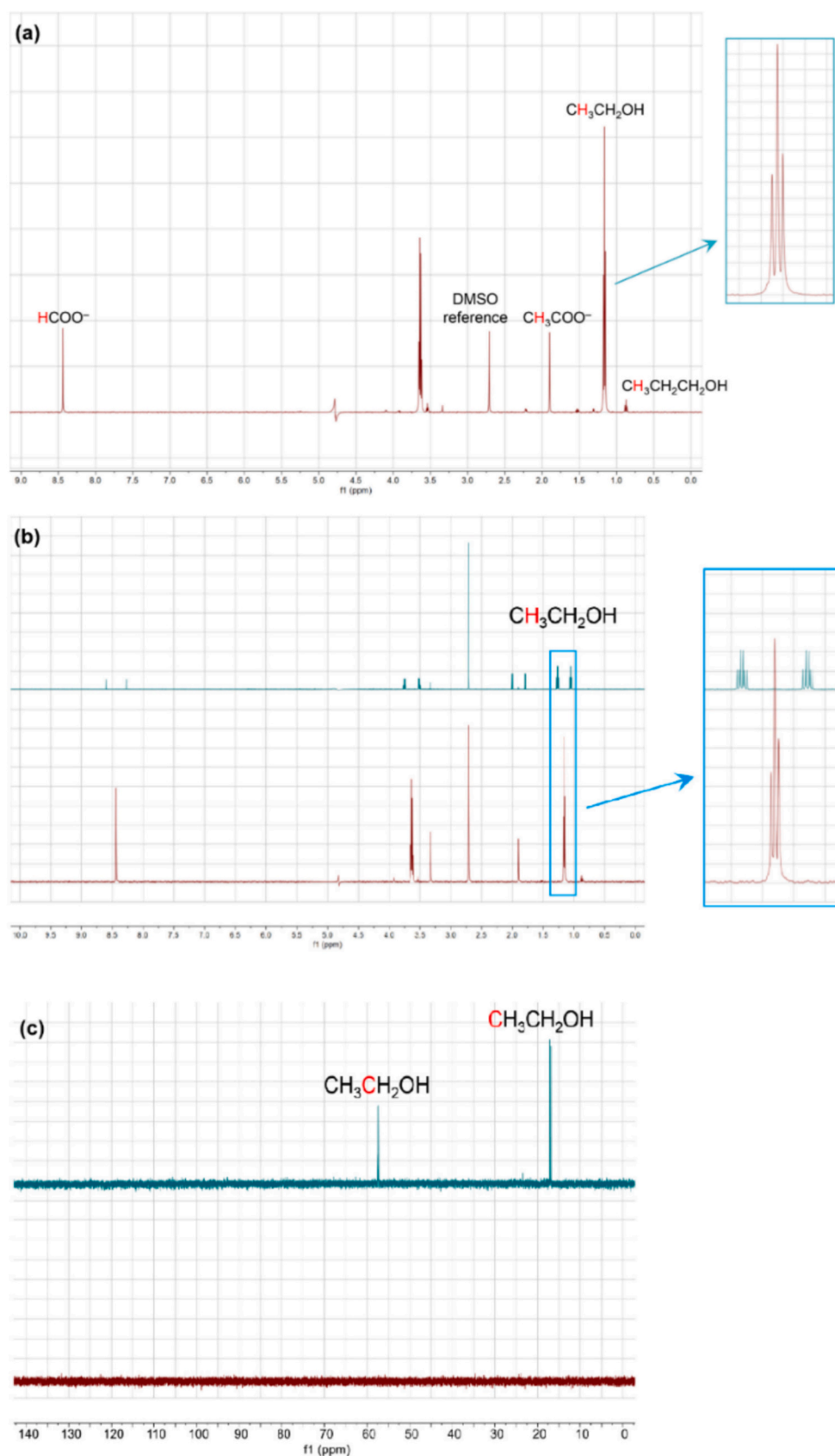


Fig. 31. ^1H NMR spectrum of liquid products of FeTPP[Cl]/Cu catalyst after electrolysis (a) and ^1H NMR (b) and ^{13}C NMR (c) spectra of the liquid products in $^{13}\text{CO}_2$ atmosphere (teal) and $^{12}\text{CO}_2$ atmosphere (red). Reproduced with permission from Ref. [184]. Copyright 2020, Springer Nature. (For interpretation of the references to colour in this figure legend, the reader is referred to the web version of this article.)

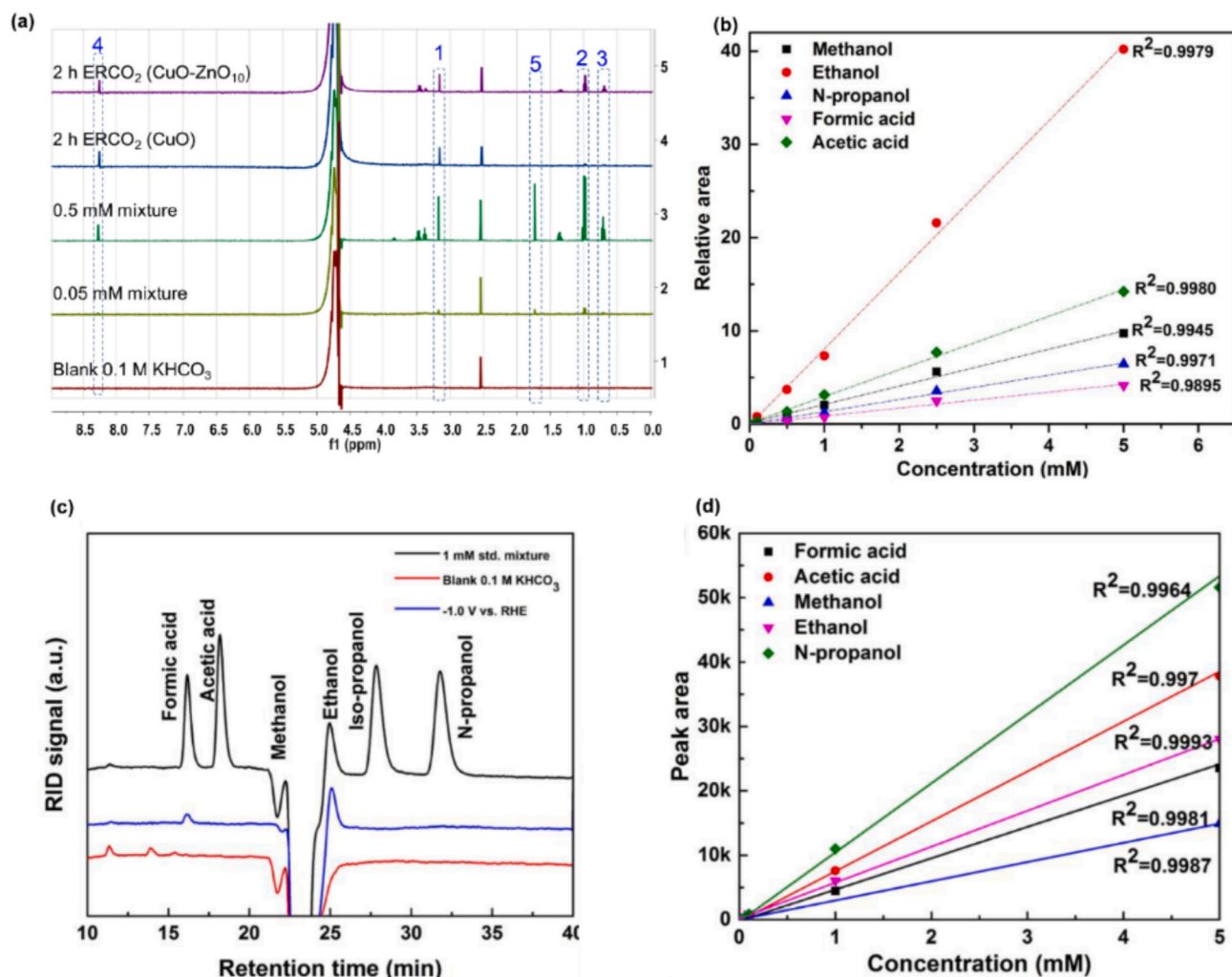


Fig. 32. ^1H NMR spectra of CuO-ZnO_{10} (purple), CuO (blue), 0.5 mM mixture (green), 0.05 mM mixture (olive) and blank electrolyte solution (red), The numbers are as follows: 1 is methanol, 2 is ethanol, 3 is *n*-propanol, 4 is formic acid and 5 is acetic acid (a) and the calibration curves calculated based on ^1H NMR (b). HPLC chromatograms of standard solution (black), blank electrolyte (red) and liquid products at -0.1 V vs. RHE (blue) (c) and the calibration curves calculated based on HPLC (d). Reproduced with permission from Ref. [175]. Copyright 2021, Elsevier. (For interpretation of the references to colour in this figure legend, the reader is referred to the web version of this article.)

two-hour electrolysis, the produced ethanol was quantified by mixing 665 μL of the catholyte and mixed with 70 μL of internal standard (5 mM DMSO and 25 mM phenol in D_2O) and analyzed by ^1H NMR using water suppression method (Fig. 33). Eq. (24) was used to measure the concentration of ethanol [191]:

$$\text{Relative peak area ratio of ethanol} = \frac{\text{Area of Ethanol triplet signal at } \delta 1.1 \text{ ppm}}{\text{Area of DMSO signal at } \delta 2.6 \text{ ppm}} \quad (24)$$

A year later, Gonglach et al. succeeded to produce ethanol in parallel to other products such as methanol, formate, formaldehyde, and acetate, using cobalt(III) triphenylphosphine corrole complexes [163]. Ethanol was the predominant species with the highest Faradaic efficiency of 48 %. The NMR sample was prepared by mixing 350 μL of the catholyte with 50 μL of internal standard solution (20 mM phenol and 10 mM of DMSO in 20 mL H_2O) and 200 μL D_2O . During the measurement, water

suppression method was adopted to enhance the signal-to-noise ratio of the analytes. The content of ethanol and was quantified by ^1H NMR and calculated based with reference to phenol peak at $\delta 7.3$ ppm (Fig. 34a). As depicted in Fig. 34a and b, the ^1H and ^{13}C NMR, respectively, demonstrated the formation of ethanol and other products. The isotope

labeling electrolysis was conducted at -0.8 V versus RHE. The ^{13}C NMR spectrum revealed two doublet characteristic signals for ethanol with at $\delta 17.6$ ppm ($J = 37.5$ Hz) and $\delta 58.3$ ppm ($J = 37.5$ Hz), indicating the formation of C—C bond as a result of reduction of $^{13}\text{CO}_2$ [163].

Furthermore, Cu_xAu_y nanowire arrays (NWAs) has demonstrated powerful catalytic activity toward ethanol production with a Faradaic efficiency of 48 % at a potential of -0.5 V vs. RHE [192]. The content of ethanol and other liquid products (Table 4) were determined by ^1H NMR using the water suppression method through noesygppr1d pulse

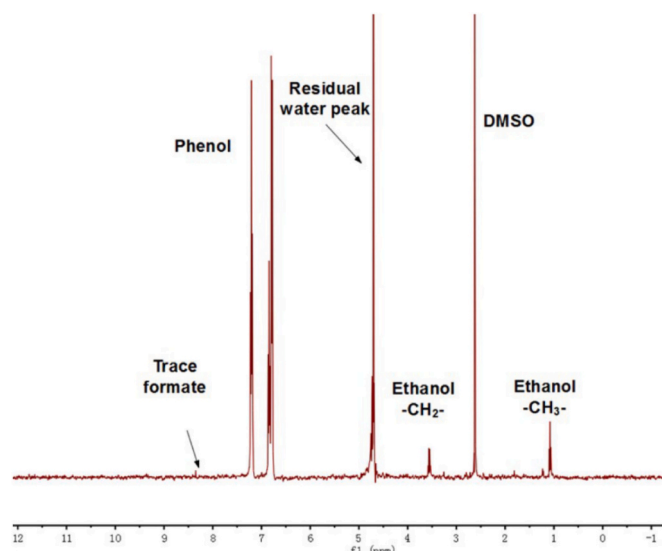


Fig. 33. The ^1H NMR spectrum of the liquid products after 2-h electrolysis at -0.6 V (RHE) using Ag-G-NCF. Reproduced with permission from Ref. [191]. Copyright 2018, Royal Society of Chemistry.

sequence with a presaturation power of 10^{-5} , a relaxation time of 7 s, and a sweep width of 8000 Hz. The NMR sample was prepared by mixing 1 mL of the electrolyte with 0.2 mL of D_2O and 50 μL of internal standard solution (25 mM DMSO and 5 mM phenol) [192]. Table 4 displays the chemical shifts with J coupling values (where applicable) obtained after acquiring the NMR analysis of the sample collected from the electrolyte and the prepared standards solution.

Similarly, a novel porous Cu/Cu $_2\text{O}$ aerogel network showed considerable activity toward ethanol production via eCO_2RR [193]. After electrolysis at -1.1 V, the liquid products were quantified by ^1H NMR through mixing 630 μL of the electrolyte with a 35 μL dual mixed internal reference (10 mM DMSO and 50 mM phenol) and 70 μL of D_2O . The Faradaic efficiency calculations (eq. (25)) of liquid products revealed the higher selectivity of ethanol with a Faradaic efficiency of 41.2 % and a high partial current density of 32.55 mA cm^{-2} [193].

$$\text{FE} = n \times F \times V \times 100 \times \text{j}^{-1} \quad (25)$$

Recently, the developing of copper single atom catalysts (SACs) on thin-walled N-doped carbon nanotubes (TWN) which were then fabricated on a silica-mediated hydrogen-bonded organic framework (HOF)-template results into superior active catalysts toward ethanol production electrochemically [190]. TWN-Cu $_{13.35}$ -600-SACs displayed the highest Faradaic efficiency of 81.9 % and a current density of 35.6 mA cm^{-2} at a potential of -1.1 V vs. RHE. As seen in Fig. 35a, the amount of ethanol and other liquid products were measured by ^1H NMR spectra by dissolving 1 mL of the catholyte with the internal standard (100 μL of each DMSO and phenol). 400 μL of this solution was then mixed with the 200 μL of the lock solution (D_2O). To confirm that CO_2 was the carbon source of ethanol, catalytic tests of ^{13}C -labeled CO_2 were conducted at -1.1 V vs. RHE (Fig. 35b) [190].

7.2. NMR as a quantitative tool for acetic acid/acetate

The analysis of the produced acetic acid/acetate by electrochemical reduction of CO and CO_2 (eCORR and eCO_2RR , respectively) can be performed by several analytical tools, such as IC [78–80], HPLC [77,195], and NMR [169,196–217]. In 2014, Grace et al. utilized IC to quantify acetic acid and formic acid that were produced using Cu $_2\text{O}$ nanoparticle decorated polyaniline matrix (PANI/Cu $_2\text{O}$) as electrode in 0.1 M tetrabutylammonium perchlorate (TBAP) and methanol electrolyte. At a potential of -0.3 V vs SCE, the Faradaic efficiencies of acetic

acid and formic acid were 63.0 % and 30.4 %, respectively [79]. A year later, Acetic acid was produced electrochemically using N-doped nanodiamond/Si rod array (NDD/Si RA) [80]. This was accomplished by reducing CO_2 in 0.5 M NaHCO_3 electrolyte at a range of potentials -0.55 to -1.3 V using a sealed two compartment cell. The liquid products were analyzed by IC revealing acetate with Faradaic efficiencies of 91.2–91.8 % at potentials of -0.8 to -1.0 V [80]. HPLC was further used as analysis tool to quantify the content of the electrochemically produced acetate. This was done by Ivandini by utilizing copper modified boron-doped diamond (Cu-modified BDD) to convert CO_2 electrochemically in 0.1 M NaCl electrolyte to acetate [195]. The content of formaldehyde and acetate was quantified using HPLC with a concentration of 3.81 ppm and 22.5 ppm [195]. Recently, spectroelectrochemical study of acetate formation was conducted using HPLC [77]. Commercial bismuth oxide nanoparticles (Bi_2O_3 NP) used to reduce CO_2 in amine-based capture solution as electrolyte. The acetate production was investigated in the absence and presence of a surfactant (cetrimonium bromide - CTAB). HPLC was used to quantify the amount of acetate at different current densities (-50 mA cm^{-2} , -100 mA cm^{-2} , and -150 mA cm^{-2}). It was found that surfactant was able to reduce CO_2 to acetate at lower current density (-50 mA cm^{-2}) with a Faradaic efficiency of 14.47 %, while without surfactant there was no formed acetate. At higher current densities, acetate was formed in the absence of surfactant at current densities of -100 mA cm^{-2} , and -150 mA cm^{-2} with Faradaic efficiencies of 4.06 % and 8.14 %, respectively [77].

NMR spectroscopy is one of the most accepted techniques for the identification and quantification of organic compounds, including carboxylic acids such as acetic acid. The ^1H NMR spectrum of acetic acid includes a singlet peak for the methyl group ($-\text{CH}_3$), which normally resonates between δ 1.9 and δ 2.2 ppm, while the proton of the carboxylic acid ($-\text{COOH}$) is a broad singlet in the range of δ 10.5 to δ 12.0 ppm, depending on hydrogen bonding and solvent effects [218–220]. In the other hand, the ^{13}C NMR spectrum of acetic acid, displays two signals due to the methyl carbon and the carbonyl carbon of the carboxylic acid group at around δ 20 to δ 22 ppm and δ 170 to δ 180 ppm, respectively [220].

The quantification acetate/acetic acid that is produced by eCO_2RR has been performed by NMR in the last years. DMSO has been used widely as internal standard to quantify the concentration of produced acetate through eCO_2RR [169,197,198,201,204,206–208,210,214,217]. While phenol [211] and a mixture of phenol/DMSO [199], were rarely reported as internal standards for acetate quantification. Further details will be provided in the next subsections.

7.2.1. Dimethyl sulfoxide as internal standard for acetate/acetic acid quantification

In 2019, DMSO- d_6 was used as a solvent with tetramethylsilane (TMS) as internal standard to quantify the amount of formate and acetate that were produced electrochemically using copper paddle wheel cluster-based porphyrinic metal-organic framework (MOF) nanosheets Cu $_2$ (CuTCPP) [208]. Acetate as a C–C coupling product was generated together with formate in the same catalyst within a wider voltage range (-1.40 V to -1.65 V) with a FE's ranging between 38.8 % and 85.2 %. This was attributed to the transformation of Cu(II) carboxylate nodes to CuO, Cu $_2\text{O}$, and Cu $_4\text{O}_3$ is supported by the porphyrin-Cu(II) complex which significantly convert CO_2 into formate and acetate from the porphyrin-Cu(II) MOFs [208]. Recently, Yang et al. reported the preparation of a hydrophilic amine-tailed, dendrimer-functionalized copper catalyst ($\text{G}_3\text{-NH}_2/\text{Cu}$) as a highly potential electrocatalyst toward acetate production [169]. The liquid products were collected and analyzed by dissolving a fresh sample in DMSO solution in D_2O (10 % v/v) using ^1H NMR. The data were collected after applying water suppression method. At a potential of -0.97 V (RHE), $\text{G}_3\text{-NH}_2/\text{Cu}$ displayed a partial current density of 202 mA cm^{-2} with a Faradaic efficiency of 47.0 %, which they claimed as one of the highest Faradaic efficiencies for CO_2 -to-acetate electrochemical conversion [169].

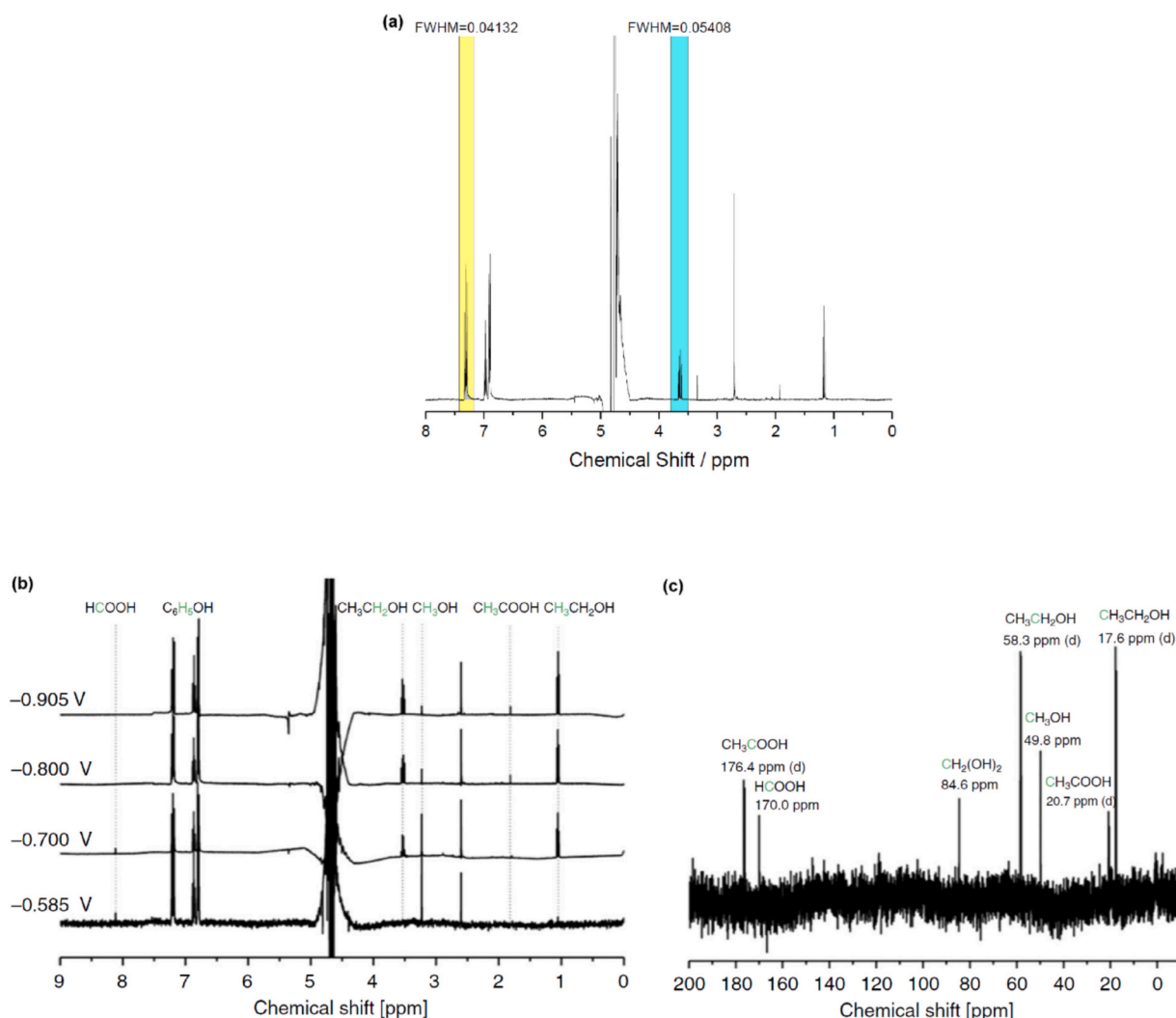


Fig. 34. Quantification of ethanol (sky blue) in reference to phenol peak (yellow) by the mean of ^1H NMR spectrum (a), The ^1H NMR spectrum of the liquid product after electrolysis at different potentials (b) and ^{13}C NMR of the liquid product after $^{13}\text{CO}_2$ -labeling electrolysis at -0.8 V vs. RHE (c). Reproduced with permission from Ref. [163]. Copyright 2019, Springer Nature. (For interpretation of the references to colour in this figure legend, the reader is referred to the web version of this article.)

Table 4

Peak position of the eCO_2RR liquid products compared to the standards solution. Reproduced with permission from Ref. [192]. Copyright 2019, Elsevier.

eCO_2RR liquid products	Assignment	Known standards
Chemical shift (δ , ppm)	Probed nucleus	Chemical shift (δ , ppm)
2.50	DMSO – (CH_3)	2.60
1.06 ($J = 7.5$ Hz)	Ethanol – (CH_3)	1.06 ($J = 7.32$ Hz)
3.53	Ethanol – (CH_2)	3.53
3.22	Methanol – (CH_3)	3.23
1.78	Acetate – (CH_3)	1.79
8.32	Formate – (HCO)	8.33

$\text{Mo}_8\text{@Cu/TNA}$ containing the Cu-O-Mo interface as an active site was explored as an electrocatalyst candidate for CO_2 reduction [201]. Electrolysis at relatively low applied potentials of -1.13 V versus RHE showed the generation of acetate with unusually high current density at ~ 110 mA cm^{-2} , faradaic efficiency at 48.68 %, and selectivity at 46.59 %. The liquid products were quantified by NMR by dissolving 540 μL of the working solution after 2-h electrolysis with 60 μL of 100 mM DMSO in D_2O (internal standard). The ^1H NMR spectrum was measured with water peak suppression using a presaturation technique. The Faradaic

efficiency of the liquid products is calculated using eq. (26) [201]:

$$\text{FE}\% = \frac{n\text{MVF}}{0.9J_{\text{tot}}} \times 100 \quad (26)$$

Where n denotes the number of electrons transferred, M is the product concentration quantified in the NMR sample, V is the liquid volume in the cathodic chamber (40 mL), 0.9 is the dilution factor, t is the time of analysis, and J_{tot} is the average current during the analysis [201].

To verify the carbon source, a series of control experiments can be conducted to confirm the carbon source. The most common experiment is ^{13}C -labeling experiments where the electrochemical reduction is performed in $^{13}\text{CO}_2$ environment. For example, two-dimensional phthalocyanine-based covalent-organic framework (COF), donated as PcCu-TFPN was investigated toward CO_2 electroreduction [204]. After electrolysis at -0.8 V vs. RHE in 0.1 M KHCO_3 solution, PcCu-TFPN showed high selectivity toward acetate with $\text{FE} = 90.3$ % and current density of 12.5 mA cm^{-2} . Trace amounts of methanol and ethanol were detected in liquid product while hydrogen was measured as a minor gas-phase product. 400 μL of the catholyte was mixed with 50 μL of 6 mM DMSO, was added as an internal standard, along with 50 μL of D_2O . The Faradaic efficiency was calculated based on the mass concentration (m),

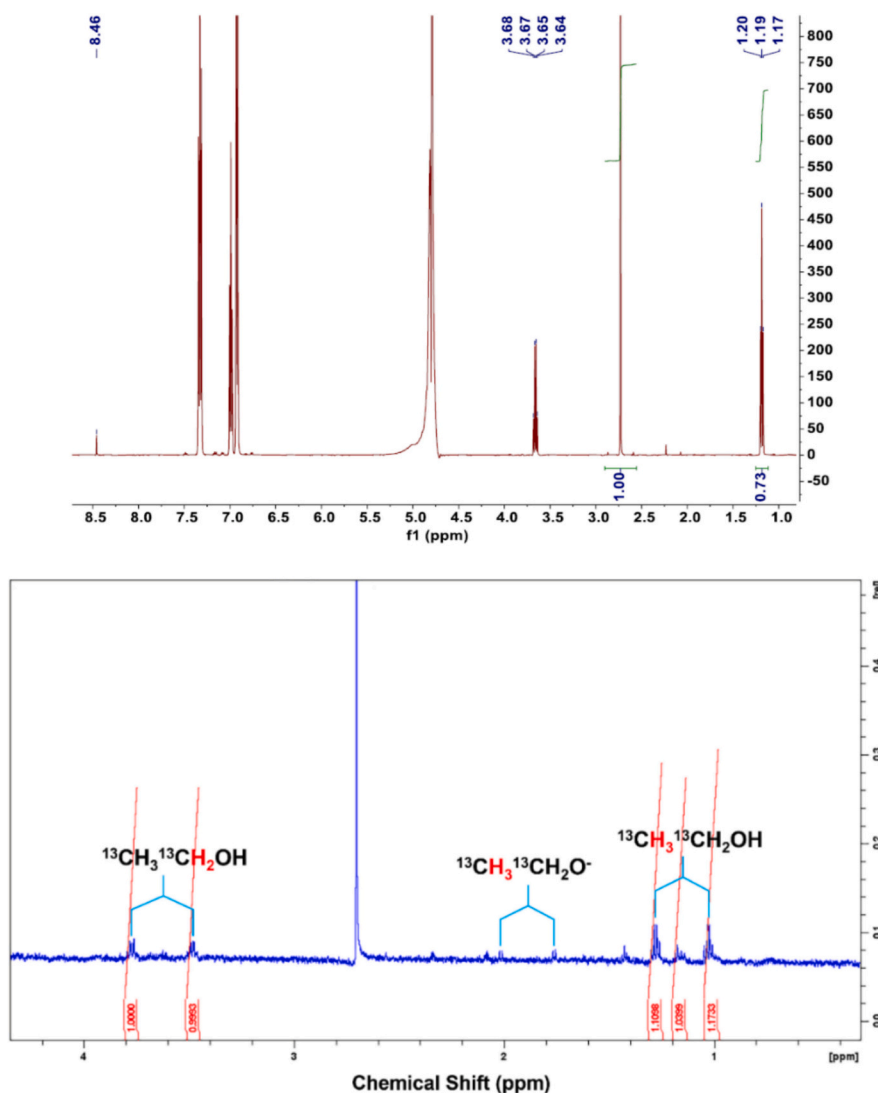


Fig. 35. The ^1H NMR spectrum of the catholyte after 1-h electrolysis at -1.1 V vs. RHE displaying the calculation of ethanol ($\delta = 1.19$ and 3.65 ppm) and formic acid ($\delta = 8.46$ ppm) (a). The ^1H NMR spectrum of the solution after 10-min electrolysis using ^{13}C isotope labeling experiment. Reproduced with permission from Ref. [190]. Copyright 2023, American Chemical Society.

anolyte volume (V), molecular mass (M) of the product, the number of electrons transferred (n) and the total charge passed (Q), using eq. (27) [204]:

$$\text{FE} = \frac{mV}{M} \times \frac{nF}{Q} \quad (27)$$

Isotopic labeling with $^{13}\text{CO}_2$ was performed to confirm the carbon source in acetate. As depicted in Fig. 36, substitution of CO_2 by $^{13}\text{CO}_2$ in the electrocatalytic test resulted in the splitting of one peak at $\delta 1.78$ ppm in the ^1H NMR spectrum of the methyl group of acetate into two peaks at $\delta 1.62$ and $\delta 1.94$ ppm, respectively, originating from the coupling between ^{13}C and H, thus confirming that CO_2 as the carbon source of acetate production [204].

Abdinejad et al. investigated functionalized, earth-abundant Mn-TPP-based molecular electrocatalysts via electro-grafting onto glassy carbon electrodes [207]. These catalysts indeed exhibit a remarkable FE of 94 % for CO_2 conversion, out of which 62 % for acetate production. They found that introducing sulfonate groups in Mn-TPPS (as electron withdrawing group) significantly enhanced the catalytic performance, which is attributed to enhancing the surface coverage, thus allowing electrostatic interactions of sulfonate groups with water molecules toward higher rates compared to unmodified Mn-TPP. The

electrochemically produced acetate and formate were investigated using GC, HPLC, and NMR spectroscopy. Among the gaseous products, only H_2 and CO were detected, whereas formate and acetate were observed as liquid products. The NMR samples were prepared by mixing 400 μL of the catholyte with 50 μL of 6 mM DMSO (internal standard). The analysis by ^{13}C NMR revealed signals corresponding to fully ^{13}C -labeled acetate ($\delta 23$ ppm and $\delta 181$ ppm) and formate ($\delta 170$ ppm). The ^1H NMR under $^{13}\text{CO}_2$ environment led to a couple of ^{13}C coupling of the methyl proton peak of acetate ($\delta 1.74$ ppm to $\delta 1.59$ and $\delta 1.91$ ppm) [207].

Recently, ultrasmall Cu_2O nanoparticles on a copper-based metal-organic framework (Cu-THQ) support (denoted as $\text{Cu}_2\text{O}@\text{Cu-THQ}$) showed excellent activity toward eCO_2RR [197]. The liquid products were characterized by ^1H NMR spectroscopy by adding 250 μL catholyte, 250 μL deionized water, 100 μL D_2O , and 100 μL DMSO as the internal standard. The analysis displayed the formation of acetate with a FE of 65 % at the low potential of -0.3 V vs. RHE with a current density of 10.5 mA cm^{-2} . No other liquid-phase product, like formate, methanol, or ethanol, was observed, which gave 100 % purity for the produced acetate. Isotope-labeling experiment was also performed to confirm the source of carbon and the purity of produced acetate [197].

Other control experiment is done besides the ^{13}C -labeling

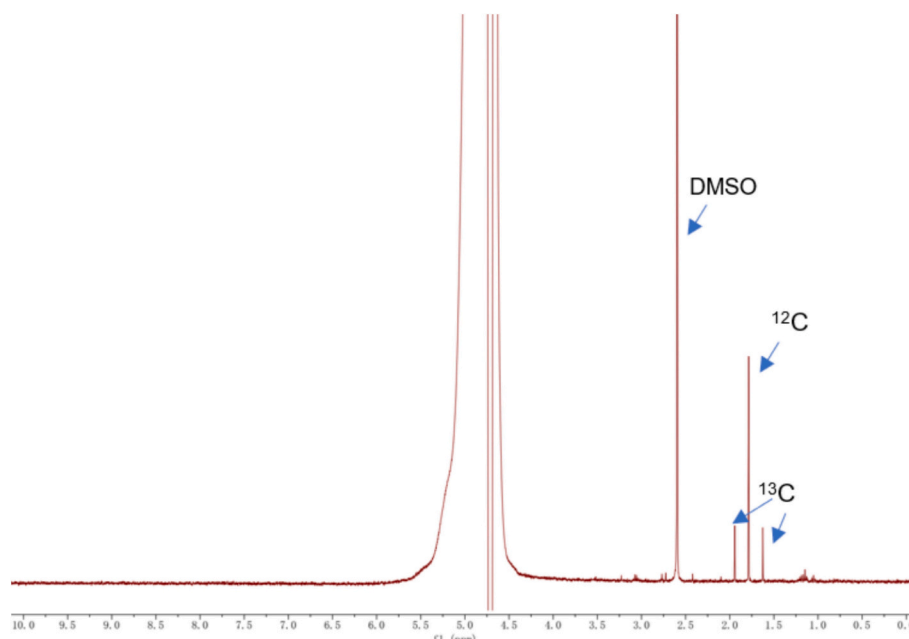


Fig. 36. ^1H NMR spectrum of the liquid products form electrocatalytic after electroreduction in $^{13}\text{CO}_2$ environment at -0.8 V vs. RHE in 0.1 M KHCO_3 solution. Reproduced with permission from Ref. [204]. Copyright 2022, John Wiley and Sons.

experiment, is the electrolysis without CO_2 or under inert atmosphere. In 2018, Wang et al. utilized copper-silver bimetallic nanoparticles to produce acetate through the electroreduction of CO_2 [206]. The liquid-phase products of CO_2 reduction were analyzed by ^1H NMR after mixing 0.5 mL of electrolyte after electrolysis was mixed with 0.1 mL of D_2O and 35 μL of 10 mM DMSO as an internal standard. The ^1H NMR analysis was performed using water suppression method. At a potential of -1.33 V (vs RHE), the faradaic efficiency of acetate was found to be 21.2% and it was determined using eq. (28), which relies on product amount (N), Faraday's constant (F), number of transferred electrons (n), and total charge passed during the electrolysis (Q):

$$\text{FE} = n \cdot N \cdot \frac{F}{Q} \times 100\% \quad (28)$$

$^{13}\text{CO}_2$ gas was used as an isotopic labeling reagent to trace the origin of acetate in 0.5 M KHCO_3 electrolyte. The analysis using ^{13}C NMR and

2D heteronuclear single-quantum coherence (HSQC) confirmed the production of acetate and formate at different selected potentials. Which demonstrates that formate and acetate were produced mainly through the electroreduction of CO_2 . Further controlled experiment was done by using N_2 instead of CO_2 . No product peaks were observed except that hydrogen was a major background product resulting from the reduction of the solvent as revealed by HS-GC [206].

In addition, polyoxometalate (POMs) have been proposed as powerful candidates to suppress the hydrogen evolution reaction (HER), one of the usual side reactions in eCO_2RR , by facilitating proton coupling through their reversible, stepwise multi-electron transfer processes. This was achieved by Sun's team where they investigated the synergistic catalytic activities of indium along with a prepared POM, $(n\text{-Bu}_4\text{N})_3\text{SVW}_{11}\text{O}_{40}$, for eCO_2RR [210]. Their catalyst exhibited Faradaic efficiencies as high as 67.4% for acetic acid and 19.4% for ethanol. The activity can be attributed to the electron transfer to the vanadium center

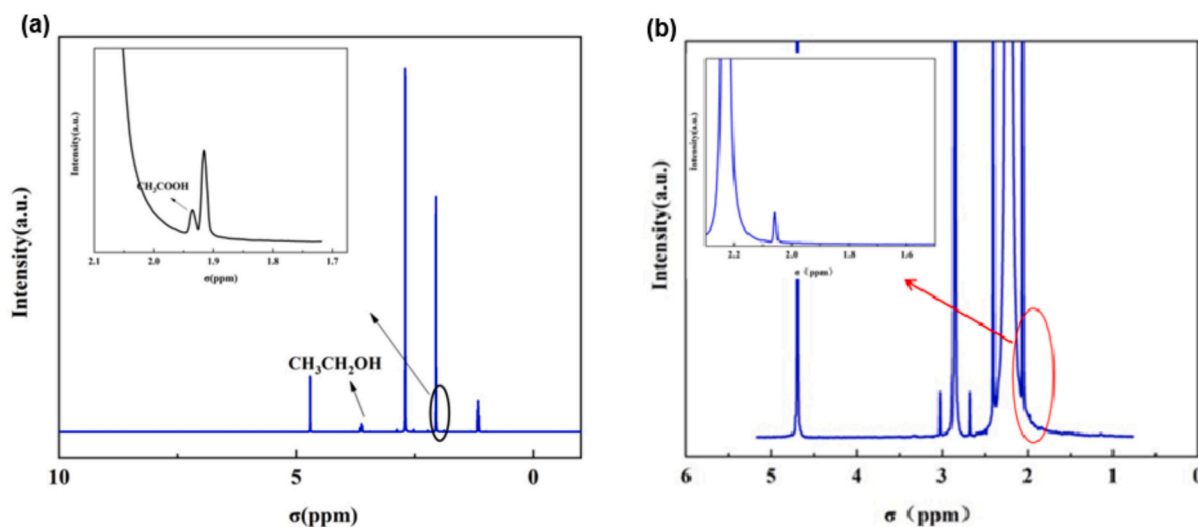


Fig. 37. ^1H NMR spectrum of the liquid products after electrolysis at -0.5 V (vs Ag/Ag^+), in CO_2 environment (a) and without CO_2 environment (b). Reproduced with permission from Ref. [210]. Copyright 2022, Elsevier.

in the SVW₁₁ and to the In³⁺, thereby recovering the activity of indium, leading to HSV^{IV}W₁₁O₄₀³⁻. This coupled electron transfer with proton in the V⁴⁺/V⁵⁺ redox system promotes eCO₂RR and diminishes the reaction overpotential, hence enhancing product selectivity. After 1-h electrolysis at −0.5 V (vs Ag/Ag⁺), the liquid products were analyzed by ¹H NMR (Fig. 37a), using DMSO as an internal reference and D₂O as a solvent. The control experiment was done by replacing CO₂ by N₂, which confirms that acetic acid and ethanol generated from eCO₂RR (Fig. 37b) [210].

Other control experiments have been conducted to confirm the source of carbon in acetate. In addition to ¹³C-labeling experiment and performing the electrolysis under Ar atmosphere, Zhu et al. utilized atomic emission spectrometry (ICP-AES) spectroscopy in corporation with ¹H NMR to investigate trinuclear copper(I) complexes [Cu₃(HBTz)₃(Btz)Cl₂] and introduced a stable π - π stacking framework electrocatalyst CuBtz for highly efficient eCO₂RR [217]. In a flow cell system (Fig. 38a), CuBtz achieved an FE of about 61.6 % for C₂⁺ products, with a current density of ~1 A cm^{−2} and value of 5639 μ mol m^{−2} s^{−1} at applied potential of −1.6 V vs. RHE. While in H-type cell, it revealed FE of 73.7 % for C₂⁺ products with ethylene of 44 %, ethanol of 21 %, acetate of 4.7 %, and propanol of 4 % at the applied potential of −1.3 V vs. RHE (Fig. 38b) [217].

The NMR sample was prepared by mixing 500 μ L of the electrolyte with 100 μ L D₂O and 100 μ L of 6 mM DMSO. In ¹³C-labeling experiment, the ¹H NMR spectra of the catholyte exhibit the spin splitting signals of ethanol and acetate assigned to ¹³CO₂, confirming it as the carbon source (Fig. 38c). The same conclusion was further confirmed by

electrolysis in an Ar atmosphere where no carbon-based product was observed, suggesting that only feeding CO₂ is the carbon source (Fig. 38d). On the other hand, ICP-AES analysis confirmed that no Cu²⁺ or Btz[−] ions from the CuBtz catalyst were detected in the catholyte, further confirming that CuBtz does not degrade under the electrochemical conditions [217].

The NMR sample was prepared by mixing 500 μ L of the electrolyte with 100 μ L D₂O and 100 μ L of 6 mM DMSO. In ¹³C-labeling experiment, the ¹H NMR spectra of the catholyte exhibit the spin splitting signals of ethanol and acetate assigned to ¹³CO₂, confirming it as the carbon source (Fig. 38c). The same conclusion was further confirmed by electrolysis in an Ar atmosphere where no carbon-based product was observed, suggesting that only feeding CO₂ is the carbon source (Fig. 38d). On the other hand, ICP-AES analysis confirmed that no Cu²⁺ or Btz[−] ions from the CuBtz catalyst were detected in the catholyte, further confirming that CuBtz does not degrade under the electrochemical conditions [217].

Similarly, tin(II) monosulfide (SnS) nanobelt piezocatalyst was investigated recently as a potential candidate for electrochemical conversion CO₂ to acetate [214]. The liquid aliquot was analyzed by NMR by mixing 400 μ L of the liquid aliquot mixture with 65 μ L of D₂O and 35 μ L of DMSO (internal standard). The NMR analysis revealed characteristic peaks for acetate only at δ 2.01 ppm (¹H NMR) and at δ 19.35 ppm and δ 186.66 ppm (¹³C NMR). These results confirmed the high selectivity toward acetate with 100 % and the highest production rate of 2.21 mMh^{−1} ever measured as claimed by the authors. IC and GC also confirmed the high selectivity of acetate. IC revealed the detection of

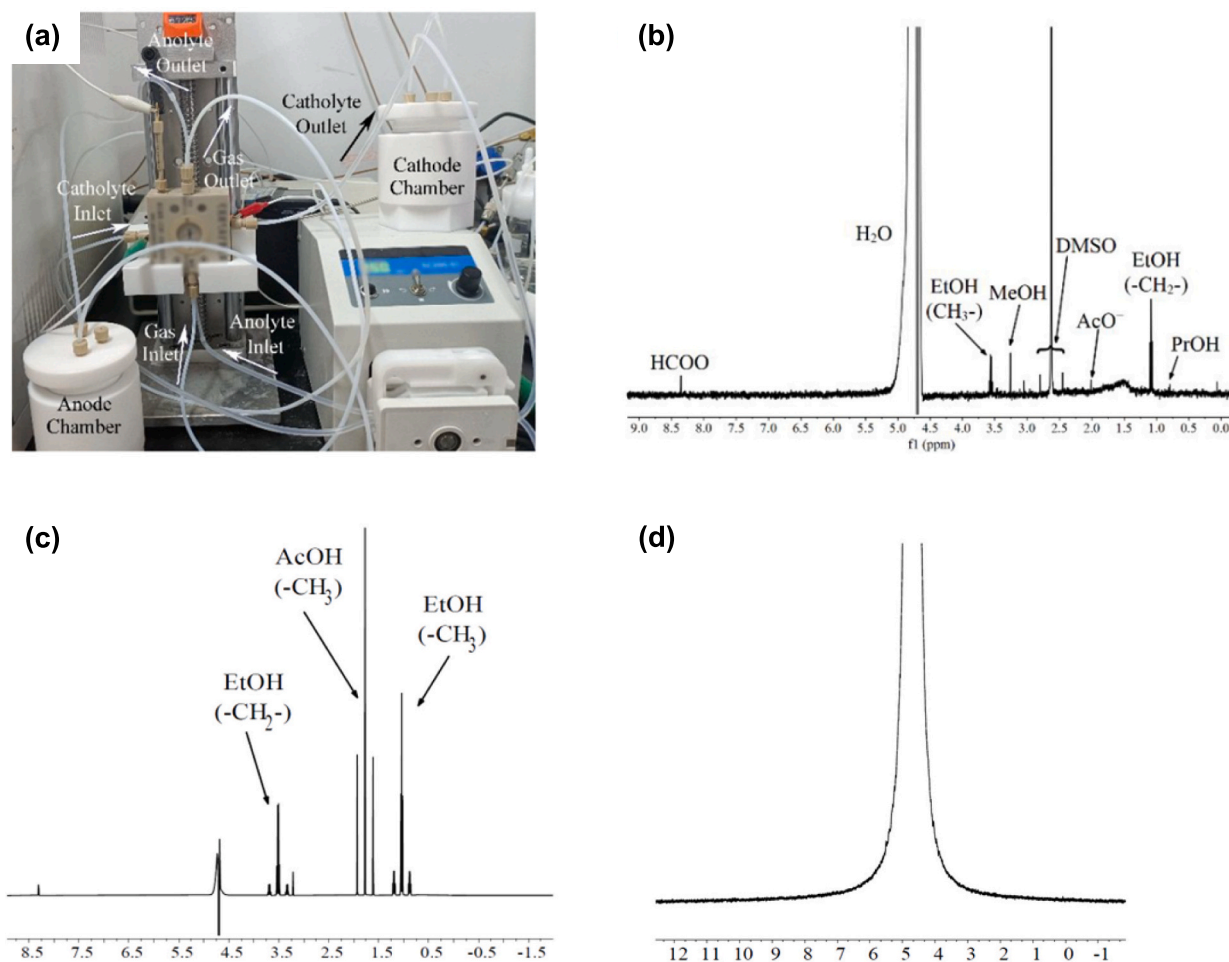


Fig. 38. Flow cell system (a), ¹H NMR spectra of the liquid products at the potentials of −1.3 V versus RHE (b), isotope-labeled liquid products (c) and the electrolyte in Ar atmosphere (d). Reproduced with permission from Ref. [217]. Copyright 2022, American Chemical Society.

acetate ion only while GC showed no gaseous product obtained after electrolysis [214].

A series of control experiments further confirmed that the catalyst and the specific conditions are responsible for the observed formation of acetate. No acetate was detected when the electrolysis was conducted without CO₂, with no ultrasound, or even in the presence of the inorganic sacrificial agent (Na₂SO₃). Similarly, the production of acetate was found to be negligible in the absence of catalysts. Under argon atmosphere, piezocatalytic measurements revealed no acetate formation and only a trace amount of H₂ production which could be ascribed to sonochemistry effects rather than catalytic activity. Further proof that the acetate indeed came from CO₂ reduction was provided by the ¹³C labeling experiment which displayed splitting in the ¹H NMR methyl proton resonance of acetate at δ 2.01 ppm into two peaks [214].

7.2.2. Other solvents as internal standard for acetate/acetic acid quantification

Based on our knowledge, only one study has been reported to use phenol as an internal standard for quantification of acetate using NMR. Serafini et al. investigated a series of CuMgAl layered double hydroxides as highly efficient catalysts toward the electrochemical reduction of CO₂ to acetate. Accordingly, the optimum composition of the CuMgAl LDH (2:1:1) expressed a productivity of 2.0 mmol_{CH₃COOH} g_{cat}⁻¹ h⁻¹ at -0.4 V (RHE). The liquid products were analyzed by ¹H NMR, using phenol as an internal standard and D₂O for the lock signal. A characteristic peak of acetate at round δ 2.0 ppm was obtained by ¹H NMR analysis, which proves a high selectivity and productive formation of acetate.

8. NMR chemical shifts of main liquid products in eCO₂RR

Accurate identification and quantitation of liquid product in electrochemical CO₂ reduction (eCO₂RR) is critical to understand reaction mechanisms and catalyst activities. Table 5 displays the ¹H and ¹³C NMR chemical shifts of the five liquid products discussed in this review, namely, formate, methanol, formaldehyde, ethanol, and acetate. The ¹H NMR are expressed as peak position and multiplicities (i.e., singlet, doublet, triplet), while the ¹³C NMR provide carbon environments of the product. The data are essential in the confirmation of product formation and measurement in eCO₂RR.

9. Faradaic Efficiency Equations for Electrochemical Synthesis

Table 6 compiles notable Faradaic Efficiency equations utilized to measure the utilization of charges in electrochemical CO₂ reduction. It provides formulas for the products of formic acid, methanol, ethanol, and acetate with parameters extending from Faraday's constant, concentration of product, electrolysis condition, to internal standard systems (e.g., DMSO, phenol). Referred to the foundational papers, it is an efficient model of comparison between conditions in experiments consistent with manuscript focus on the maximization of electrochemical reactions.

10. Future perspectives

NMR spectroscopy is a continually growing field, unveiling its

versatility and value in analyzing electrochemical CO₂ reduction processes. However, this field still remains wide open to more growth and innovation. Efforts in the near future should focus on surmounting these impediments, working also toward expanding the scope and application of the NMR technique to achieve unbiased insight into mechanisms and selectivities in CO₂ reduction.

The highest need and opportunity in methods development concern the enhancement of NMR sensitivity and resolution. Among others, one of the most important analytical challenges that remain to be faced is the detection and quantification of trace amounts of CO₂ reduction products. The signal-to-noise ratios of high-field NMR instruments with cryogenically cooled probes and novel pulse sequences can be improved considerably, affording more precise analysis [221]. Another very important aspect will be the optimization of water suppression techniques with the intent to decrease the problems related to interference associated with aqueous electrolytes, assuring clean and stable baselines in spectra [222].

From this viewpoint, one of the prospective directions of research could be the extension of NMR analysis toward more complex reaction intermediates and transient species involved in the pathways of CO₂ reduction. Recent *operando* ¹³C NMR studies have demonstrated the ability to track dynamic equilibria, such as CO₂/HCO₃⁻ exchange rates, and identify ion-pairing effects under applied potentials, offering molecular-level insights into electrolyte restructuring during electrolysis [223]. Thus, for instance, two-dimensional correlation spectroscopy (2D COSY) or HSQC multidimensional NMR techniques will give valuable information about structural intermediates, while ¹³C- and ²H-isotopic labeling will enable the tracing of carbon and hydrogen atoms during electrolysis. These will contribute significantly to our knowledge about reaction mechanisms and enable, in turn, the reasonable design of more active catalysts.

On the other hand, combining NMR with other techniques, such as GC and MS, it might be possible to understand reaction products better. While NMR is far more effective in the analysis of liquid-phase products, GC and MS become much more effective in the detection of gaseous species. Such a combination enables the selectivity and efficiency of various processes pertaining to CO₂ reduction to be judged in a holistic manner, having strong implications in reaction condition optimization.

Another trend in future research refers to the establishment of universal internal standards for quantitative NMR analysis. Up to now, only a few works have adopted phenol, whose limited relevant applications require the further screening of more versatile and stable standards applicable in different reaction systems. This will surely unify the methods of NMR and improve the comparability among different studies.

Particularly, the research on sustainable catalysts and electrolytes also widens the prospects for NMR spectroscopy: accelerating the discovery of next-generation catalysts by using NMR to investigate their efficiency and degradative mechanism in performance, and investigating green electrolytes, such as those derived from renewable feedstocks, under conditions as close as possible to real working conditions may further improve the sustainability of the entire system in CO₂ reduction.

Finally, the development of in situ and *operando* NMR techniques is an important frontier. Recent advancements in probe design, such as

Table 5

¹H NMR and ¹³C NMR chemical shifts for formate, methanol, formaldehyde, ethanol and acetate.

Compound	¹ H NMR chemical shifts (δ , ppm)	Multiplicity	¹³ C NMR chemical shifts (δ , ppm)	Reference number
Formate	8.3–8.5 (HCO)	Singlet (s)	~170–180 (COO ⁻)	[105,111,113,119]
Methanol	3.3–3.5 (CH ₃)	Singlet (s)	~50 (CH ₃)	[71,81,87,130,132–134,137]
Formaldehyde	~4.4 (HCHO-bisulfite adduct)	Singlet (s)	N/A	[66,162]
Ethanol	1.0–1.3 (CH ₃)	Triplet (t)	~18 (CH ₃)	[74,163,175,181,182,184,191]
	3.3–3.8 (CH ₂)	Quartet (q)	~58 (CH ₂)	
Acetate	1.9–2.2 (CH ₃)	Singlet (s)	~20–22 (CH ₃)	[204,210,217]
			~170–180 (COO ⁻)	

Table 6
Faradaic Efficiency (FE) Equations.

Eq. no.	Equation	Variables description	Product (internal standard)	Refs.
(2)	$FE = \frac{2FVC}{Q} \times 100\%$	F : Faraday constant V : Sample volume C : Product concentration Q : Total charge	Formate/formic acid (DMSO)	[16]
(3)	$FE = \frac{nF\eta}{Jt} \times 100\%$	n : Number of transferred electrons η : Moles of product J : Current t : Time of electrolysis c : Concentration of formate	Formate/formic acid (DMSO)	[84]
(4)	$FE_{HCOO^-} = \frac{n \times F \times V \times c}{1000 \times M \times Q}$	M : Molar mass of formate V : Electrolyte volume	Formate/formic acid (DMSO)	[85]
(5)	$FE = \frac{2 \times F \times \eta}{Q}$	η : Concentration of formate	Formate/formic acid (DMF)	[112]
(6)	$FE = \frac{N \times c \times V \times F}{Q}$	N : Electrons transferred c : Formate concentration	Formate/formic acid (Phenol)	[113]
(7)	$FE = \frac{znF}{Q}$	z : Electrons per product molecule n : Moles of product	Methanol (DMSO)	[81]
(9)	$FE = \frac{C_{methanol} \times V \times N_A \times 6e}{N_{total}}$	$C_{methanol}$: Concentration N_A : Avogadro's number N_{total} : Total charge	Methanol (DMSO)	[129]
(10)	$FE_i = \frac{Q_i}{Q_{total}} = \frac{N_i \times n \times F}{Q_{total}}$	Q_i : charge for product i N_i : moles of product i	Methanol (DMSO)	[130]
(11)	$FE = \frac{C_{Me} \times V_{liq} \times n \times F}{Q}$	C_{Me} : Methanol concentration V_{liq} : Electrolyte volume	Methanol (DMSO)	[132]
(13)	$FE = \frac{nFC_iV}{Q}$	C_i : Product concentration n : Electrons per molecule C_{ref} : Reference concentration	Methanol (DMSO/phenol)	[142]
(14)	$FE = C_{ref} \cdot \frac{I_p}{I_R} \cdot \frac{H_R}{H_p} \cdot \frac{nFV}{Q} \cdot \frac{5}{4} \times 100$	I_p/I_R : Peak ratio H_R/H_p : Proton count ratio 5/4: Dilution factor n : Electrons for product j	Methanol (DMSO/phenol)	[131]
(17)	$FE = \frac{n_jFC_iV}{Q_t}$	C_i : Concentration of methanol Q_t : Total charge N : Required number of electrons to produce product	Methanol (4-nitrophenol)	[72]
(20)	$FE = \frac{N}{N_{Total}} \times 100\%$	N_{total} : Total electrons	Methanol (TMS)	[146]
(21)	$FE = \frac{n \times F \times N}{Q}$	$C_{ethanol}$: Transferred electrons n : Moles of ethanol	Ethanol (DMSO)	[189]
(22)	$FE_i = \frac{q_i}{q_{total}} = \frac{96485 \times C_i \times V \times z_i}{q_{total}}$	96,485: Faradaic constant C_i : Product concentration	Ethanol (DMSO)	[187]

Table 6 (continued)

Eq. no.	Equation	Variables description	Product (internal standard)	Refs.
(25)	$FE = n \times F \times V \times 100 \times j^{-1}$	V : Catholyte volume z_i : Transferred electrons j : Current density V : Electrolyte volume M : Molarity	Ethanol (DMSO/phenol)	[193]
(26)	$FE\% = \frac{nMVF}{0.9tJ_{tot}} \times 100$	J_{tot} : Total current density t : Time m : Mass concentration	Acetate (DMSO)	[201]
(27)	$FE = \frac{mV}{M} \times \frac{nNF}{Q}$	V : Volume of anolyte M : Molar mass N : Product amount	Acetate (DMSO)	[204]
(28)	$FE = n \cdot N \cdot \frac{F}{Q} \times 100\%$	n : transferred electrons per molecule	Acetate (DMSO)	[206]

planar stripline detectors, enable spatially resolved measurements and integration with electrochemical cells, facilitating real-time monitoring of electrolyte chemistry and interfacial processes [224]. A ground-breaking study by Xu et al. [225] employed *operando* electrocatalytic NMR to track oxygen, carbon, and hydrogen species in real time, revealing a water-assisted formate formation mechanism. By introducing Bi/In adsorption sites in Cu-based catalysts, adsorbed H₂O molecules directly participate in regenerating COOH[−] intermediates, boosting formate selectivity from 34.2 % to 98 %. This demonstrates NMR's unique capability to resolve atom-specific pathways in complex reaction networks [225]. These methods allow the observation of reaction dynamics in real time; for the first time, one is able to directly observe catalyst behavior, the formation of reaction intermediates, and the evolution of products during electrochemical processes. Better in situ NMR hardware and software would go a long way toward improving our capabilities to correlate reaction conditions to product outcomes, thereby driving the design of highly optimized and selective CO₂ reduction systems.

CRedit authorship contribution statement

Aymen S. Abu Hatab: Writing – review & editing, Writing – original draft, Validation, Data curation, Conceptualization. **Yahia H. Ahmad**: Writing – original draft. **Mohamed F. Mady**: Writing – review & editing, Conceptualization. **Yasser Hassan**: Writing – original draft. **Abdelrahman Zkria**: Writing – original draft. **Alessandro Sinopoli**: Writing – original draft. **Aboubakr M. Abdullah**: Writing – original draft. **Siham Y. Al-Qaradawi**: Writing – original draft. **Tsuyoshi Yoshitake**: Writing – original draft. **Mazen Khaled**: Writing – review & editing, Supervision, Project administration, Funding acquisition, Conceptualization.

Declaration of competing interest

The authors declare that they have no known competing financial interests or personal relationships that could have appeared to influence the work reported in this paper.

Acknowledgements

This work was made possible by the Qatar-Japan Research Collaboration Research Program, funded by Marubeni, under grant number M-QJRC-2023-312. The statements made herein are solely the

responsibility of the authors. Open Access funding is provided by the Qatar National Library.

Data availability

No data was used for the research described in the article.

References

- [1] D.T. Whipple, P.J.A. Kenis, Prospects of CO₂ utilization via direct heterogeneous electrochemical reduction, *J. Phys. Chem. Lett.* 1 (24) (2010) 3451–3458, <https://doi.org/10.1021/jz1012627>.
- [2] F. He, S. Tong, Z. Luo, H. Ding, Z. Cheng, C. Li, Z. Qi, Accelerating net-zero carbon emissions by electrochemical reduction of carbon dioxide, *J. Energy Chem.* 79 (2023) 398–409, <https://doi.org/10.1016/j.ijechem.2023.01.020>.
- [3] S. Hernández, M. Amin Farkhondeh, F. Sastre, M. Makkee, G. Saracco, N. Russo, Syngas production from electrochemical reduction of CO₂: current status and prospective implementation, *Green Chem.* 19 (10) (2017) 2326–2346, <https://doi.org/10.1039/C7GC00398F>.
- [4] C. Long, X. Li, J. Guo, Y. Shi, S. Liu, Z. Tang, Electrochemical reduction of CO₂ over heterogeneous catalysts in aqueous solution: recent progress and perspectives, *Small Methods* 3 (3) (2019) 1800369, <https://doi.org/10.1002/smt.201800369>.
- [5] K. Malik, S. Singh, S. Basu, A. Verma, Electrochemical reduction of CO₂ for synthesis of green fuel, *WIREs Energy Environ* 6 (4) (2017) e244, <https://doi.org/10.1002/wene.244>.
- [6] S.A. Farooqi, A.S. Farooqi, S. Sajjad, C. Yan, A.B. Victor, Electrochemical reduction of carbon dioxide into valuable chemicals: a review, *Environ. Chem. Lett.* 21 (3) (2023) 1515–1553, <https://doi.org/10.1007/s10311-023-01565-7>.
- [7] A. Somoza-Tornos, O.J. Guerra, A.M. Crow, W.A. Smith, B.-M. Hodge, Process modeling, techno-economic assessment, and life cycle assessment of the electrochemical reduction of CO₂: a review, *iScience* 24 (7) (2021), <https://doi.org/10.1016/j.isci.2021.102813>.
- [8] S. Jin, Z. Hao, K. Zhang, Z. Yan, J. Chen, Advances and challenges for the electrochemical reduction of CO₂ to CO: from fundamentals to industrialization, *Angew. Chem. Int. Ed.* 60 (38) (2021) 20627–20648, <https://doi.org/10.1002/anie.202101818>.
- [9] S. Liang, L. Huang, Y. Gao, Q. Wang, B. Liu, Electrochemical reduction of CO₂ to CO over transition metal/N-doped carbon catalysts: the active sites and reaction mechanism, *Adv. Sci.* 8 (24) (2021) 2102886, <https://doi.org/10.1002/advs.202102886>.
- [10] S.A. Mahyoub, F.A. Qaraah, C. Chen, F. Zhang, S. Yan, Z. Cheng, An overview on the recent developments of ag-based electrodes in the electrochemical reduction of CO₂ to CO, *Sustainable Energy Fuels* 4 (1) (2020) 50–67, <https://doi.org/10.1039/C9SE00594C>.
- [11] S. Lu, Y. Zhang, M.F. Mady, O. Egwu Eleri, W. Mekonnen Tucho, M. Mazur, A. Li, F. Lou, M. Gu, Z. Yu, Sulfur-decorated Ni–N–C catalyst for Electrocatalytic CO₂ reduction with near 100% CO selectivity, *ChemSusChem* 15 (19) (2022) e202200870, <https://doi.org/10.1002/cssc.202200870>.
- [12] M. Arsalan, D. Ewis, M.M. Ba-Abbad, M. Khaled, A. Amhamed, M.H. El-Naas, Efficient electrochemical conversion of CO₂ into formic acid using colloidal NiCo@rGO catalyst, *Res. Eng. Des.* 21 (2024) 101824, <https://doi.org/10.1016/j.rineng.2024.101824>.
- [13] M. Arsalan, D. Ewis, N. Mahmud, M.M. Ba-Abbad, M. Khaled, M.H. El-Naas, Enhanced electrochemical conversion of CO₂ into formic acid using PbSO₄/AtSn electrode: catalyst synthesis and process optimization, *J. Environ. Chem. Eng.* 11 (6) (2023) 111352, <https://doi.org/10.1016/j.jece.2023.111352>.
- [14] J. Chung, D.H. Won, J. Koh, E.-H. Kim, S.I. Woo, Hierarchical Cu pillar electrodes for electrochemical CO₂ reduction to formic acid with low overpotential, *Phys. Chem. Chem. Phys.* 18 (8) (2016) 6252–6258, <https://doi.org/10.1039/C5CP07964K>.
- [15] C. Dai, L. Sun, J. Song, H. Liao, A.C. Fisher, Z.J. Xu, Selective Electroreduction of carbon dioxide to formic acid on cobalt-decorated copper thin films, *Small Methods* 3 (11) (2019) 1900362, <https://doi.org/10.1002/smt.201900362>.
- [16] B. Jia, Z. Chen, C. Li, Z. Li, X. Zhou, T. Wang, W. Yang, L. Sun, B. Zhang, Indium Cyanamide for industrial-grade CO₂ Electroreduction to formic acid, *J. Am. Chem. Soc.* 145 (25) (2023) 14101–14111, <https://doi.org/10.1021/jacs.3c04288>.
- [17] R. Kortlever, I. Peters, S. Koper, M.T.M. Koper, Electrochemical CO₂ reduction to formic acid at Low Overpotential and with high faradaic efficiency on carbon-supported bimetallic Pd–Pt nanoparticles, *ACS Catal.* 5 (7) (2015) 3916–3923, <https://doi.org/10.1021/acscatal.5b00602>.
- [18] S. Dongare, N. Singh, H. Bhunia, P.K. Bajpai, A.K. Das, Electrochemical reduction of carbon dioxide to ethanol: a review, *ChemistrySelect* 6 (42) (2021) 11603–11629, <https://doi.org/10.1002/slct.202102829>.
- [19] Z. Zhang, L. Bian, H. Tian, Y. Liu, Y. Bando, Y. Yamauchi, Z.-L. Wang, Tailoring the surface and interface structures of copper-based catalysts for electrochemical reduction of CO₂ to ethylene and ethanol, *Small* 18 (18) (2022) 2107450, <https://doi.org/10.1002/smll.202107450>.
- [20] M. Orlić, C. Hochenauer, R. Nagpal, V. Subotić, Electrochemical reduction of CO₂: a roadmap to formic and acetic acid synthesis for efficient hydrogen storage, *Energy Convers. Manag.* 314 (2024) 118601, <https://doi.org/10.1016/j.enconman.2024.118601>.
- [21] G. Feng, W. Chen, B. Wang, Y. Song, G. Li, J. Fang, W. Wei, Y. Sun, Oxygenates from the electrochemical reduction of carbon dioxide, *Chem. Asian J.* 13 (16) (2018) 1992–2008, <https://doi.org/10.1002/asia.201800637>.
- [22] X. Fu, J. Zhang, Y. Kang, Electrochemical reduction of CO₂ towards multi-carbon products via a two-step process, *React. Chem. Eng.* 6 (4) (2021) 612–628, <https://doi.org/10.1039/D1RE00001B>.
- [23] P. Bhatia, S. Dharaskar, A.P. Unnarkat, CO₂ reduction routes to value-added oxygenates: a review, *Environ. Sci. Pollut. Res.* 28 (44) (2021) 61929–61950, <https://doi.org/10.1007/s11356-021-16003-w>.
- [24] L.R.L. Ting, B.S. Yeo, Recent advances in understanding mechanisms for the electrochemical reduction of carbon dioxide, *Curr Opin, Electrochem* 8 (2018) 126–134, <https://doi.org/10.1016/j.coelec.2018.04.011>.
- [25] R. Kortlever, J. Shen, K.J.P. Schouten, F. Calle-Vallejo, M.T.M. Koper, Catalysts and reaction pathways for the electrochemical reduction of carbon dioxide, *J. Phys. Chem. Lett.* 6 (20) (2015) 4073–4082, <https://doi.org/10.1021/acs.jpclett.5b01559>.
- [26] G.M. Tomboc, S. Choi, T. Kwon, Y.J. Hwang, K. Lee, Potential link between Cu surface and selective CO₂ Electroreduction: perspective on future Electrocatalyst designs, *Adv. Mater.* 32 (17) (2020) 1908398, <https://doi.org/10.1002/adma.201908398>.
- [27] F. Pan, X. Yang, T. O'Carroll, H. Li, K.-J. Chen, G. Wu, Carbon catalysts for electrochemical CO₂ reduction toward multicarbon products, *Adv. Energy Mater.* 12 (24) (2022) 2200586, <https://doi.org/10.1002/aenm.202200586>.
- [28] M. Umeda, Y. Niitsuma, T. Horikawa, S. Matsuda, M. Osawa, Electrochemical reduction of CO₂ to methane on platinum catalysts without Overpotentials: strategies for improving conversion efficiency, *ACS Appl Energy Mater* 3 (1) (2020) 1119–1127, <https://doi.org/10.1021/acsaem.9b02178>.
- [29] D.A. Torelli, S.A. Francis, J.C. Crompton, A. Javier, J.R. Thompson, B. S. Brunswig, M.P. Soriaga, N.S. Lewis, Nickel–gallium-catalyzed electrochemical reduction of CO₂ to highly reduced products at Low Overpotentials, *ACS Catal.* 6 (3) (2016) 2100–2104, <https://doi.org/10.1021/acscatal.5b02888>.
- [30] A. Vasilieff, Y. Zhu, X. Zhi, Y. Zhao, L. Ge, H.M. Chen, Y. Zheng, S.-Z. Qiao, Electrochemical reduction of CO₂ to ethane through stabilization of an Ethoxy intermediate, *Angew. Chem. Int. Ed.* 59 (44) (2020) 19649–19653, <https://doi.org/10.1002/anie.202004846>.
- [31] P.K. Giesbrecht, D.E. Herbert, Electrochemical reduction of carbon dioxide to methanol in the presence of Benzannulated Dihydropyridine additives, *ACS Energy Lett.* 2 (3) (2017) 549–555, <https://doi.org/10.1021/acsenenergylett.7b00047>.
- [32] M. Wang, K. Torbensen, D. Salvatore, S. Ren, D. Joulié, F. Dumoulin, D. Mendoza, B. Lassalle-Kaiser, U. Işci, C.P. Berlinguette, M. Robert, CO₂ electrochemical catalytic reduction with a highly active cobalt phthalocyanine, *Nat. Commun.* 10 (1) (2019) 3602, <https://doi.org/10.1038/s41467-019-11542-w>.
- [33] E. Bertheussen, Y. Abghoui, Z.P. Jovanov, A.-S. Varela, I.E.L. Stephens, I. Chorkendorff, Quantification of liquid products from the electroreduction of CO₂ and CO using static headspace-gas chromatography and nuclear magnetic resonance spectroscopy, *Catal. Today* 288 (2017) 54–62, <https://doi.org/10.1016/j.cattod.2017.02.029>.
- [34] L. Ji, L. Li, X. Ji, Y. Zhang, S. Mou, T. Wu, Q. Liu, B. Li, X. Zhu, Y. Luo, X. Shi, A. M. Asiri, X. Sun, Highly selective electrochemical reduction of CO₂ to alcohols on an FeP Nanoarray, *Angew. Chem. Int. Ed.* 59 (2) (2020) 758–762, <https://doi.org/10.1002/anie.201912836>.
- [35] K.P. Kuhl, E.R. Cave, D.N. Abram, T.F. Jaramillo, New insights into the electrochemical reduction of carbon dioxide on metallic copper surfaces, *Energy Environ. Sci.* 5 (5) (2012) 7050–7059, <https://doi.org/10.1039/C2EE21234J>.
- [36] R.A. Geioushy, M.M. Khaled, K. Alhooshani, A.S. Hakeem, A. Rinaldi, Graphene/ZnO/Cu₂O electrocatalyst for selective conversion of CO₂ into n-propanol, *Electrochim. Acta* 245 (2017) 456–462, <https://doi.org/10.1016/j.electacta.2017.05.185>.
- [37] A.A. Pawar, H.A. Bandal, A. Rajkamal, H. Kim, Understanding the impact of reaction parameters on electrochemical reduction of CO₂ to methanol: activity relationship of cuprite/polyaniline electrodes, *J. Electroanal. Chem.* 946 (2023) 117721, <https://doi.org/10.1016/j.jelechem.2023.117721>.
- [38] A. Roy, H.S. Jadhav, S. J. Gil, Cu₂O/CuO Electrocatalyst for electrochemical reduction of carbon dioxide to methanol, *Electroanalysis* 33 (3) (2021) 705–712, <https://doi.org/10.1002/elan.202060265>.
- [39] Y. Qiao, D. Hochfizer, J. Kibsgaard, I. Chorkendorff, B. Seger, Real-time detection of acetaldehyde in electrochemical CO reduction on Cu single crystals, *ACS Energy Lett.* 9 (3) (2024) 880–887, <https://doi.org/10.1021/acsenenergylett.3c02549>.
- [40] M. Elyashberg, Identification and structure elucidation by NMR spectroscopy, *TrAC, trends, Anal. Chem.* 69 (2015) 88–97, <https://doi.org/10.1016/j.trac.2015.02.014>.
- [41] E.E. Kwan, S.G. Huang, Structural elucidation with NMR spectroscopy: practical strategies for organic chemists, *Eur. J. Org. Chem.* 2008 (16) (2008) 2671–2688, <https://doi.org/10.1002/ejoc.200700966>.
- [42] Z. Huang, T. Bi, H. Jiang, H. Liu, Review on NMR as a tool to analyse natural products extract directly: molecular structure elucidation and biological activity analysis, *Phytochem. Anal.* 35 (1) (2024) 5–16, <https://doi.org/10.1002/pca.3292>.
- [43] R.M. Maggio, N.L. Calvo, S.E. Vignaduzzo, T.S. Kaufman, Pharmaceutical impurities and degradation products: uses and applications of NMR techniques, *J. Pharm. Biomed. Anal.* 101 (2014) 102–122, <https://doi.org/10.1016/j.jpba.2014.04.016>.

- [44] G.F. Pauli, S.-N. Chen, C. Simmler, D.C. Lankin, T. Gödecke, B.U. Jaki, J. B. Friesen, J.B. McAlpine, J.G. Napolitano, Importance of purity evaluation and the potential of Quantitative ^1H NMR as a purity assay, *J. Med. Chem.* 57 (22) (2014) 9220–9231, <https://doi.org/10.1021/jm500734a>.
- [45] S. Ahlawat, K.R. Mote, N.-A. Lakomek, V. Agarwal, Solid-state NMR: methods for biological solids, *Chem. Rev.* 122 (10) (2022) 9643–9737, <https://doi.org/10.1021/acs.chemrev.1c00852>.
- [46] L. Liang, Y. Ji, K. Chen, P. Gao, Z. Zhao, G. Hou, Solid-state NMR dipolar and chemical shift anisotropy recoupling techniques for structural and dynamical studies in biological systems, *Chem. Rev.* 122 (10) (2022) 9880–9942, <https://doi.org/10.1021/acs.chemrev.1c00779>.
- [47] A.R. Camacho-Zarco, V. Schnapka, S. Guseva, A. Abyzov, W. Adamski, S. Milles, M.R. Jensen, L. Zidek, N. Salvi, M. Blackledge, NMR provides unique insight into the functional dynamics and interactions of intrinsically disordered proteins, *Chem. Rev.* 122 (10) (2022) 9331–9356, <https://doi.org/10.1021/acs.chemrev.1c01023>.
- [48] E. Viciano, J.A. Martínez-Lao, E. López-Lao, I. Fernández, F.M. Arrabal-Campos, Development of an earth-field nuclear magnetic resonance spectrometer: paving the way for AI-enhanced Low-field nuclear magnetic resonance technology, *Sensors* 24 (17) (2024) 5537, <https://doi.org/10.3390/s24175537>.
- [49] I.H. Hameed, A.F. Al-Rubaye, Kadhim MJJJJoCPR, Research. Uses of nuclear magnetic resonance spectroscopy technique in pharmaceutical analysis: A review, *Int J Current Pharm Rev Res* 8 (2) (2017) 79–84.
- [50] N. Bross-Walch, T. Kühn, D. Moskau, O.J.C. Zerbe, Biodiversity. Strategies and tools for structure determination of natural products using modern methods of NMR spectroscopy, *Chem Biodiversity* 2 (2) (2005) 147–177.
- [51] Su Rehman, S. Xu, H. Xu, T. Tao, Y. Li, Z. Yu, K. Ma, W. Xu, J. Wang, The Role of NMR in Metal Organic Frameworks: Deep Insights into Dynamics, Structure and Mapping of Functional Groups, *Mater Today Adv* 16 (2022) 100287, <https://doi.org/10.1016/j.mtadv.2022.100287>.
- [52] Dračinský M. Chapter, One - The chemical bond: The perspective of NMR spectroscopy, in: G.A. Webb (Ed.), *Annual Reports on NMR Spectroscopy vol. 90*, Academic Press, 2017, pp. 1–40.
- [53] B. Blümich, K. Singh, Desktop NMR and its applications from materials science to organic chemistry, *Angew. Chem. Int. Ed.* 57 (24) (2018) 6996–7010, <https://doi.org/10.1002/anie.201707084>.
- [54] T. Castaing-Cordier, V. Ladroue, F. Besacier, A. Bulete, D. Jacquemin, P. Giraudeau, J. Farjon, High-field and benchtop NMR spectroscopy for the characterization of new psychoactive substances, *Forensic Sci. Int.* 321 (2021) 110718, <https://doi.org/10.1016/j.forsciint.2021.110718>.
- [55] Y. Nikolaev, N. Ripin, M. Soste, P. Picotti, D. Iber, F.H.T. Allain, Systems NMR: single-sample quantification of RNA, proteins and metabolites for biomolecular network analysis, *Nat. Methods* 16 (8) (2019) 743–749, <https://doi.org/10.1038/s41592-019-0495-7>.
- [56] Y. Yamaoka, T. Nagata, T. Sakamoto, M. Katahira, Recent progress of in-cell NMR of nucleic acids in living human cells, *Biophys. Rev.* 12 (2) (2020) 411–417, <https://doi.org/10.1007/s12551-020-00664-x>.
- [57] M. Baldus, Molecular interactions investigated by multi-dimensional solid-state NMR, *Curr. Opin. Struct. Biol.* 16 (5) (2006) 618–623, <https://doi.org/10.1016/j.sbi.2006.08.003>.
- [58] T. Sugiki, N. Kobayashi, T. Fujiwara, Modern Technologies of Solution Nuclear Magnetic Resonance Spectroscopy for three-dimensional structure determination of proteins open avenues for life scientists, *Comput Struct, Biotechnol. J.* 15 (2017) 328–339, <https://doi.org/10.1016/j.csbj.2017.04.001>.
- [59] A. Sekhar, L.E. Kay, NMR paves the way for atomic level descriptions of sparsely populated, transiently formed biomolecular conformers, *PNAS* 110 (32) (2013) 12867–12874, <https://doi.org/10.1073/pnas.1305688110>.
- [60] T.K.S. Kumar, C. Yu, Monitoring protein folding at atomic resolution, *Acc. Chem. Res.* 37 (12) (2004) 929–936, <https://doi.org/10.1021/ar020156z>.
- [61] M.J. Smith, C.B. Marshall, F.-X. Theillet, A. Binolfi, P. Selenko, M. Ikura, Real-time NMR monitoring of biological activities in complex physiological environments, *Curr. Opin. Struct. Biol.* 32 (2015) 39–47, <https://doi.org/10.1016/j.sbi.2015.02.003>.
- [62] C.A. Lepre, J.M. Moore, J.W. Peng, Theory and applications of NMR-based screening in pharmaceutical research, *Chem. Rev.* 104 (8) (2004) 3641–3676, <https://doi.org/10.1021/cr030409h>.
- [63] A. Tampieri, M. Szabó, F. Medina, H. Gulyás, A brief introduction to the basics of NMR spectroscopy and selected examples of its applications to materials characterization, *Phys. Sci. Rev.* 6 (1) (2020) 20190086, <https://doi.org/10.1515/psr-2019-0086>.
- [64] P. Preikschat, A.J. Martín, B.S. Yeo, J. Pérez-Ramírez, NMR-based quantification of liquid products in CO_2 electroreduction on phosphate-derived nickel catalysts, *Commun Chem* 6 (1) (2023) 147, <https://doi.org/10.1038/s42004-023-00948-9>.
- [65] A.R.E. Hansen, K. Enemark-Rasmussen, F.A.A. Mulder, P.R. Jensen, S. Meier, Versatile procedures for reliable NMR quantification of CO_2 Electroreduction products, *J. Phys. Chem. C* 126 (27) (2022) 11026–11032, <https://doi.org/10.1021/acs.jpcc.2c03448>.
- [66] T. Chatterjee, E. Boutin, M. Robert, Manifesto for the routine use of NMR for the liquid product analysis of aqueous CO_2 reduction: from comprehensive chemical shift data to formaldehyde quantification in water, *Dalton Trans.* 49 (14) (2020) 4257–4265, <https://doi.org/10.1039/C9DT04749B>.
- [67] F. Dalitz, M. Cudaj, M. Maiwald, G. Guthausen, Process and reaction monitoring by low-field NMR spectroscopy, *Prog Nucl Magn Reson, Spectrosc* 60 (2012) 52–70, <https://doi.org/10.1016/j.pnmrs.2011.11.003>.
- [68] T.J. Henderson, N.M.R. Quantitative, Spectroscopy using coaxial inserts containing a reference standard: purity determinations for military nerve agents, *Anal. Chem.* 74 (1) (2002) 191–198, <https://doi.org/10.1021/ac010809+>.
- [69] T. Tsujiguchi, Y. Kawabe, S. Jeong, T. Ohto, S. Kukuniri, H. Kuramochi, Y. Takahashi, T. Nishiuchi, H. Masuda, M. Wakasaka, K. Hu, G. Elumalai, J.-i. Fujita, Y. Ito, Acceleration of electrochemical CO_2 reduction to Formate at the Sn/reduced graphene oxide Interface, *ACS Catal.* 11 (6) (2021) 3310–3318, <https://doi.org/10.1021/acscatal.0c04887>.
- [70] Z. Yang, C. Yang, J. Han, W. Zhao, S. Shao, S. Li, H. Gao, H. Xie, X. Zhang, Boosting electrochemical CO_2 reduction to formate using SnO_2 /graphene oxide with amide linkages, *J. Mater. Chem. A* 9 (35) (2021) 19681–19686, <https://doi.org/10.1039/D1TA02780H>.
- [71] E. Boutin, M. Wang, J.C. Lin, M. Mesnage, D. Mendoza, B. Lassalle-Kaiser, C. Hahn, T.F. Jaramillo, M. Robert, Aqueous electrochemical reduction of carbon dioxide and carbon monoxide into methanol with cobalt Phthalocyanine, *Angew. Chem. Int. Ed.* 58 (45) (2019) 16172–16176, <https://doi.org/10.1002/anie.201909257>.
- [72] S. Payra, S. Shenoy, C. Chakraborty, K. Tarafder, S. Roy, Structure-sensitive Electrocatalytic reduction of CO_2 to methanol over carbon-supported intermetallic PtZn Nano-alloys, *ACS Appl. Mater. Interfaces* 12 (17) (2020) 19402–19414, <https://doi.org/10.1021/acsami.0c00521>.
- [73] J. Du, S. Li, S. Liu, Y. Xin, B. Chen, H. Liu, B. Han, Selective electrochemical reduction of carbon dioxide to ethanol via a relay catalytic platform, *Chem. Sci.* 11 (19) (2020) 5098–5104, <https://doi.org/10.1039/D0SC01133A>.
- [74] N. Theaker, J.M. Strain, B. Kumar, J.P. Brian, S. Kumari, J.M. Spurgeon, Heterogeneously catalyzed two-step cascade electrochemical reduction of CO_2 to ethanol, *Electrochim. Acta* 274 (2018) 1–8, <https://doi.org/10.1016/j.electacta.2018.04.072>.
- [75] N. Dutta, D. Bagchi, G. Chawla, S.C. Peter, A guideline to determine faradaic efficiency in electrochemical CO_2 reduction, *ACS Energy Lett.* 9 (1) (2024) 323–328, <https://doi.org/10.1021/acsenenergyl.3c02362>.
- [76] M. Olkopp, A. Löwe, C.M.S. Lobo, S. Baranyai, T. Khoza, M. Auinger, E. Klemm, Producing formic acid at low pH values by electrochemical CO_2 reduction, *J CO2 Util* 56 (2022) 101823, <https://doi.org/10.1016/j.jcou.2021.101823>.
- [77] B. Böhlen, N. Daems, Z. Su, A. Chen, J. Lipkowski, T. Breugelmans, In situ Spectroelectrochemical study of acetate formation by CO_2 reduction using Bi catalyst in amine-based capture solution, *ChemSusChem* 17 (20) (2024) e202400437, <https://doi.org/10.1002/cssc.202400437>.
- [78] B. Zha, C. Li, J. Li, Efficient electrochemical reduction of CO_2 into formate and acetate in polyoxometalate catholyte with indium catalyst, *J. Catal.* 382 (2020) 69–76, <https://doi.org/10.1016/j.jcat.2019.12.010>.
- [79] A.N. Grace, S.Y. Choi, M. Vinoba, M. Bhagiyalakshmi, D.H. Chu, Y. Yoon, S. C. Nam, S.K. Jeong, Electrochemical reduction of carbon dioxide at low overpotential on a polyaniline/ Cu_2O nanocomposite based electrode, *Appl. Energy* 120 (2014) 85–94, <https://doi.org/10.1016/j.apenergy.2014.01.022>.
- [80] Y. Liu, S. Chen, X. Quan, H. Yu, Efficient electrochemical reduction of carbon dioxide to acetate on nitrogen-doped Nanodiamond, *J. Am. Chem. Soc.* 137 (36) (2015) 11631–11636, <https://doi.org/10.1021/jacs.5b02975>.
- [81] S. Mou, T. Wu, J. Xie, Y. Zhang, L. Ji, H. Huang, T. Wang, Y. Luo, X. Xiong, B. Tang, X. Sun, Boron phosphide nanoparticles: a nonmetal catalyst for high-selectivity electrochemical reduction of CO_2 to CH_3OH , *Adv. Mater.* 31 (36) (2019) 1903499, <https://doi.org/10.1002/adma.201903499>.
- [82] S.K. Bharti, R. Roy, Quantitative ^1H NMR spectroscopy, *TRAC, trends, Anal. Chem.* 35 (2012) 5–26, <https://doi.org/10.1016/j.trac.2012.02.007>.
- [83] M.Q. Alkoshab, E. Thomou, I. Abdulazeez, M.H. Suliman, K. Spyrou, W. Iali, K. Alhooshani, T.N. Baroud, Low Overpotential electrochemical reduction of CO_2 to ethanol enabled by $\text{Cu/Cu}_2\text{O}$ nanoparticles embedded in nitrogen-doped carbon cuboids, *Nanomaterials* 13 (2) (2023) 230, <https://doi.org/10.3390/nano13020230>.
- [84] T.N. Nguyen, B.N. Khirak, Z. Xu, A. Farzi, S.M. Sadaf, A. Seifitokaldani, C.-T. Dinh, Multi-metallic layered catalysts for stable electrochemical CO_2 reduction to Formate and formic acid, *ChemSusChem* 17 (2024) e202301894, <https://doi.org/10.1002/cssc.202301894>.
- [85] L. Li, A. Ozden, S. Guo, García de Arquer FP, Wang C, Zhang M, Zhang J, Jiang H, Wang W, Dong H, Sinton D, Sargent E.H, Zhong M., Stable, active CO_2 reduction to formate via redox-modulated stabilization of active sites, *Nat. Commun.* 12 (1) (2021) 5223, <https://doi.org/10.1038/s41467-021-25573-9>.
- [86] M. Schatz, J.F. Kochs, S. Jovanovic, R.-A. Eichel, J. Granwehr, Interplay of local pH and cation hydrolysis during electrochemical CO_2 reduction visualized by in operando chemical shift-resolved magnetic resonance imaging, *J. Phys. Chem. C* 127 (38) (2023) 18986–18996, <https://doi.org/10.1021/acs.jpcc.3c03563>.
- [87] D. Bagchi, J. Raj, A.K. Singh, A. Cherevotan, S. Roy, K.S. Manoj, C.P. Vinod, S. C. Peter, Structure-tailored surface oxide on Cu-Ga Intermetallics enhances CO_2 reduction selectivity to methanol at ultralow potential, *Adv. Mater.* 34 (19) (2022) 2109426, <https://doi.org/10.1002/adma.202109426>.
- [88] P. Giraudeau, V. Silvestre, S. Akoka, Optimizing water suppression for quantitative NMR-based metabolomics: a tutorial review, *Metabolomics* 11 (5) (2015) 1041–1055, <https://doi.org/10.1007/s11306-015-0794-7>.
- [89] G. Zheng, W.S. Price, Solvent signal suppression in NMR, *Prog. Nucl. Magn. Reson. Spectrosc.* 56 (3) (2010) 267–288, <https://doi.org/10.1016/j.pnmrs.2010.01.001>.
- [90] J.A. Aguilar, S.J. Kenwright, Robust NMR water signal suppression for demanding analytical applications, *Analyst* 141 (1) (2016) 236–242, <https://doi.org/10.1039/C5AN02121A>.

- [91] B. Gouilleux, B. Charrier, S. Akoka, P. Giraudeau, Gradient-based solvent suppression methods on a benchtop spectrometer, *Magn. Reson. Chem.* 55 (2) (2017) 91–98, <https://doi.org/10.1002/mrc.4493>.
- [92] X. Han, T. Zhang, J. Arbiol, Metal-organic framework-derived single atom catalysts for electrocatalytic reduction of carbon dioxide to C1 products, *Energy Adv.* 2 (2) (2023) 252–267, <https://doi.org/10.1039/D2YA00284A>.
- [93] J. Han, X. Bai, X. Xu, X. Bai, A. Husile, S. Zhang, L. Qi, J. Guan, Advances and challenges in the electrochemical reduction of carbon dioxide, *Chem. Sci.* 15 (21) (2024) 7870–7907, <https://doi.org/10.1039/D4SC01931H>.
- [94] D.U. Nielsen, X.-M. Hu, K. Daasbjerg, T. Skrydstrup, Chemically and electrochemically catalysed conversion of CO₂ to CO with follow-up utilization to value-added chemicals, *Nat Catal* 1 (4) (2018) 244–254, <https://doi.org/10.1038/s41929-018-0051-3>.
- [95] D. Li, H. Zhang, H. Xiang, S. Rasul, J.-M. Fontmorin, P. Izadi, A. Roldan, R. Taylor, Y. Feng, L. Banerji, A. Cowan, E.H. Yu, J. Xuan, How to go beyond C1 products with electrochemical reduction of CO₂, *Sustainable Energy Fuels* 5 (23) (2021) 5893–5914, <https://doi.org/10.1039/D1SE00861G>.
- [96] T. Hatsukade, K.P. Kuhl, E.R. Cave, D.N. Abram, T.F. Jaramillo, Insights into the electrocatalytic reduction of CO₂ on metallic silver surfaces, *Phys. Chem. Chem. Phys.* 16 (27) (2014) 13814–13819, <https://doi.org/10.1039/C4CP00692E>.
- [97] M. Ma, B.J. Trześniewski, J. Xie, W.A. Smith, Selective and efficient reduction of carbon dioxide to carbon monoxide on oxide-derived nanostructured silver Electrochemicals, *Angew. Chem. Int. Ed.* 55 (33) (2016) 9748–9752, <https://doi.org/10.1002/anie.201604654>.
- [98] Y. Mun, S. Lee, A. Cho, S. Kim, J.W. Han, J. Lee, Cu-Pd alloy nanoparticles as highly selective catalysts for efficient electrochemical reduction of CO₂ to CO, *Appl. Catal. B Environ.* 246 (2019) 82–88, <https://doi.org/10.1016/j.apcatb.2019.01.021>.
- [99] J. Rosen, G.S. Hutchings, Q. Lu, S. Rivera, Y. Zhou, D.G. Vlachos, F. Jiao, Mechanistic insights into the electrochemical reduction of CO₂ to CO on nanostructured Ag surfaces, *ACS Catal.* 5 (7) (2015) 4293–4299, <https://doi.org/10.1021/acscatal.5b00840>.
- [100] S. Rasul, D.H. Anjum, A. Jedidi, Y. Minenkov, L. Cavallo, K. Takanabe, A Highly Selective Copper–Indium Bimetallic Electrocatalyst for the Electrochemical Reduction of Aqueous CO₂ to CO, *Angew. Chem. Int. Ed.* 54 (7) (2015) 2146–2150, <https://doi.org/10.1002/anie.201410233>.
- [101] B. Qin, Y. Li, H. Wang, G. Yang, Y. Cao, H. Yu, Q. Zhang, H. Liang, F. Peng, Efficient electrochemical reduction of CO₂ into CO promoted by sulfur vacancies, *Nano Energy* 60 (2019) 43–51, <https://doi.org/10.1016/j.nanoen.2019.03.024>.
- [102] B.-X. Dong, S.-L. Qian, F.-Y. Bu, Y.-C. Wu, L.-G. Feng, Y.-L. Teng, W.-L. Liu, Z.-W. Li, Electrochemical Reduction of CO₂ to CO by a Heterogeneous Catalyst of Fe–Porphyrin-Based Metal–Organic Framework, *ACS Appl. Energy Mater* 1 (9) (2018) 4662–4669, <https://doi.org/10.1021/acsaem.8b00797>.
- [103] S. Van Daele, L. Hintjens, S. Hoekx, B. Bohlén, S. Neukermans, N. Daems, J. Hereijgers, T. Breugelmans, How flue gas impurities affect the electrochemical reduction of CO₂ to CO and formate, *Appl. Catal. B Environ.* 341 (2024) 123345, <https://doi.org/10.1016/j.apcatb.2023.123345>.
- [104] S. Lu, Y. Zhang, M.F. Mady, W. Mekonnen Tucho, F. Lou, Z. Yu, Efficient electrochemical reduction of CO₂ to CO by Ag-decorated B-doped g-C₃N₄: a combined theoretical and experimental study, *Ind. Eng. Chem. Res.* 61 (29) (2022) 10400–10408, <https://doi.org/10.1021/acs.iecr.2c00152>.
- [105] P. Lu, X. Tan, H. Zhao, Q. Xiang, K. Liu, X. Zhao, X. Yin, X. Li, X. Hai, S. Xi, A.T. S. Wee, S.J. Pennycook, X. Yu, M. Yuan, J. Wu, G. Zhang, S.C. Smith, Z. Yin, Atomically dispersed indium sites for selective CO₂ Electroreduction to formic acid, *ACS Nano* 15 (3) (2021) 5671–5678, <https://doi.org/10.1021/acsnano.1c00858>.
- [106] Z. Wang, H. Li, T. Dong, Y. Geng, X. Tian, R. Chang, J. Lai, S. Feng, L. Wang, Efficient acidic CO₂ electroreduction to formic acid by modulating electrode structure at industrial-level current, *Chem. Eng. J.* 489 (2024) 151238, <https://doi.org/10.1016/j.cej.2024.151238>.
- [107] M. Zhong, K. Tran, Y. Min, C. Wang, Z. Wang, C.-T. Dinh, P. De Luna, Z. Yu, A. S. Rasouli, P. Brodersen, S. Sun, O. Voznyy, C.-S. Tan, M. Askerka, F. Che, M. Liu, A. Seifitokaldani, Y. Pang, S.-C. Lo, A. Ip, Z. Ulissi, E.H. Sargent, Accelerated discovery of CO₂ electrocatalysts using active machine learning, *Nature* 581 (7807) (2020) 178–183, <https://doi.org/10.1038/s41586-020-2242-8>.
- [108] P.-A. Hsieh, P.-J. Chen, L.-M. Lyu, S.-Y. Chen, M.-C. Tseng, M.-Y. Chung, W.-H. Chiang, J.-L. Chen, C.-H. Kuo, Enhanced production of formic acid in electrochemical CO₂ reduction over Pd-doped BiOCl Nanosheets, *ACS Appl. Mater. Interfaces* 13 (49) (2021) 58799–58808, <https://doi.org/10.1021/acsaami.1c20009>.
- [109] S. Yang, H. An, S. Arnouts, H. Wang, X. Yu, J. de Ruiter, S. Bals, T. Altantzis, B. M. Weckhuysen, W. van der Stam, Halide-guided active site exposure in bismuth electrocatalysts for selective CO₂ conversion into formic acid, *Nat Catal* 6 (9) (2023) 796–806, <https://doi.org/10.1038/s41929-023-01008-0>.
- [110] Z. Xia, M. Freeman, D. Zhang, B. Yang, L. Lei, Z. Li, Y. Hou, Highly selective electrochemical conversion of CO₂ to HCOOH on dendritic indium foams, *ChemElectroChem* 5 (2) (2018) 253–259, <https://doi.org/10.1002/celec.201700935>.
- [111] T. Yan, H. Pan, Z. Liu, P. Kang, Phase-inversion induced 3D electrode for direct acidic Electroreduction CO₂ to formic acid, *Small* 19 (23) (2023) 2207650, <https://doi.org/10.1002/sml.202207650>.
- [112] G. Wen, D.U. Lee, B. Ren, F.M. Hassan, G. Jiang, Z.P. Cano, J. Gostick, E. Croiset, Z. Bai, L. Yang, Z. Chen, Orbital interactions in Bi–Sn bimetallic Electrocatalysts for highly selective electrochemical CO₂ reduction toward Formate production, *Adv. Energy Mater.* 8 (31) (2018) 1802427, <https://doi.org/10.1002/aenm.201802427>.
- [113] B. Jiang, X.-G. Zhang, K. Jiang, D.-Y. Wu, W.-B. Cai, Boosting Formate production in Electrocatalytic CO₂ reduction over wide potential window on Pd surfaces, *J. Am. Chem. Soc.* 140 (8) (2018) 2880–2889, <https://doi.org/10.1021/jacs.7b12506>.
- [114] T.-W. Jiang, Y.-W. Zhou, X.-Y. Ma, X. Qin, H. Li, C. Ding, B. Jiang, K. Jiang, W.-B. Cai, Spectrometric study of electrochemical CO₂ reduction on Pd and Pd-B electrodes, *ACS Catal.* 11 (2) (2021) 840–848, <https://doi.org/10.1021/acscatal.0c03725>.
- [115] A.W. Nichols, S. Chatterjee, M. Sabat, C.W. Machan, Electrocatalytic reduction of CO₂ to Formate by an Iron Schiff Base complex, *Inorg. Chem.* 57 (4) (2018) 2111–2121, <https://doi.org/10.1021/acs.inorgchem.7b02955>.
- [116] X. Wei, Y. Li, L. Chen, J. Shi, Formic acid electro-synthesis by concurrent cathodic CO₂ reduction and anodic CH₃OH oxidation, *Angew. Chem. Int. Ed.* 60 (6) (2021) 3148–3155, <https://doi.org/10.1002/anie.202012066>.
- [117] D.T. Hofmann, Y. Liang, S.S. Uttarwar, M. Gautam, S. Pishgar, S. Gulati, C. A. Grapperhaus, J.M. Spurgeon, The pH and potential dependence of Pb-catalyzed electrochemical CO₂ reduction to methyl Formate in a dual methanol/water electrolyte, *ChemSusChem* 15 (5) (2022) e202102289, <https://doi.org/10.1002/cssc.202102289>.
- [118] H.-J. Yang, H. Yang, Y.-H. Hong, P.-Y. Zhang, T. Wang, L.-N. Chen, F.-Y. Zhang, Q.-H. Wu, N. Tian, Z.-Y. Zhou, S.-G. Sun, Promoting ethylene selectivity from CO₂ Electroreduction on CuO supported onto CO₂ capture materials, *ChemSusChem* 11 (5) (2018) 881–887, <https://doi.org/10.1002/cssc.201702338>.
- [119] R.R. Garcia, G.F.S. dos Santos, A.C. Neto, J. Ribeiro, Synthesis of electrocatalysts based on M_xO_y and M_xO_y/C (M = Sn, Cu, and Co) with potential for application in CO₂ reduction, *J. Solid State Electrochem.* (2024), <https://doi.org/10.1007/s10008-024-05903-9>.
- [120] A. Hailu, A.A. Tamijani, S.E. Mason, S.K. Shaw, Efficient conversion of CO₂ to Formate using inexpensive and easily prepared post-transition metal alloy catalysts, *Energy Fuel* 34 (3) (2020) 3467–3476, <https://doi.org/10.1021/acs.energyfuels.9b03783>.
- [121] F. Dalena, A. Senatore, A. Marino, A. Gordan, M. Basile, A. Basile, Chapter 1 - methanol production and applications: An overview, in: A. Basile (Ed.), *Dalena F, editors, Elsevier, Methanol*, 2018, pp. 3–28.
- [122] A.M. El-Zeftawy, Focus on the chemical value of methanol, *Journal of King Saud University - Eng. Sci.* 7 (1995) 209–254, [https://doi.org/10.1016/S1018-3639\(18\)31058-4](https://doi.org/10.1016/S1018-3639(18)31058-4).
- [123] I. Ganesh, Conversion of carbon dioxide into methanol – a potential liquid fuel: fundamental challenges and opportunities (a review), *Renew. Sust. Energ. Rev.* 31 (2014) 221–257, <https://doi.org/10.1016/j.rser.2013.11.045>.
- [124] S. Back, H. Kim, Y. Jung, Selective heterogeneous CO₂ Electroreduction to methanol, *ACS Catal.* 5 (2) (2015) 965–971, <https://doi.org/10.1021/cs501600x>.
- [125] T.-Y. Chang, R.-M. Liang, P.-W. Wu, J.-Y. Chen, Y.-C. Hsieh, Electrochemical reduction of CO₂ by Cu₂O-catalyzed carbon clothes, *Mater. Lett.* 63 (12) (2009) 1001–1003, <https://doi.org/10.1016/j.matlet.2009.01.067>.
- [126] F. Martínez, C. Jiménez, J. García, R. Camarillo, J.J.E.E. Rincón, M. Journal, A preliminary study on electrocatalytic conversion of CO₂ into fuels, *Environ. Eng. Manag. J.* 13 (10) (2014) 2477–2485.
- [127] R.F. Zarandi, B. Rezaei, H.S. Ghaziaskar, A.A. Ensafi, Electrochemical conversion of CO₂ to methanol using a glassy carbon electrode, modified by Pt/histamine-reduced graphene oxide, *Int. J. Hydrog. Energy* 44 (59) (2019) 30820–30831, <https://doi.org/10.1016/j.ijhydene.2019.09.237>.
- [128] K. Kim, P. Wagner, K. Wagner, A.J. Mozer, Electrochemical CO₂ reduction catalyzed by copper molecular complexes: the influence of ligand structure, *Energy Fuel* 36 (9) (2022) 4653–4676, <https://doi.org/10.1021/acs.energyfuels.2c00400>.
- [129] Z. Liang, J. Wang, P. Tang, W. Tang, L. Liu, M. Shakouri, X. Wang, J. Llorca, S. Zhao, M. Heggen, R.E. Dunin-Borkowski, A. Cabot, H.B. Wu, J. Arbiol, Molecular engineering to introduce carbonyl between nickel salenphen active sites to enhance electrochemical CO₂ reduction to methanol, *Appl. Catal. B Environ.* 314 (2022) 121451, <https://doi.org/10.1016/j.apcatb.2022.121451>.
- [130] X. Ren, J. Zhao, X. Li, J. Shao, B. Pan, A. Salamé, E. Boutin, T. Groizard, S. Wang, J. Ding, X. Zhang, W.-Y. Huang, W.-J. Zeng, C. Liu, Y. Li, S.-F. Hung, Y. Huang, M. Robert, B. Liu, In-situ spectroscopic probe of the intrinsic structure feature of single-atom center in electrochemical CO/CO₂ reduction to methanol, *Nat. Commun.* 14 (1) (2023) 3401, <https://doi.org/10.1038/s41467-023-39153-6>.
- [131] T. Chan, C.J. Kong, A.J. King, F. Babbe, R.R. Prabhakar, C.P. Kubiak, J.W. Ager, Role of mass transport in electrochemical CO₂ reduction to methanol using immobilized cobalt Phthalocyanine, *ACS Appl. Energy Mater* 7 (8) (2024) 3091–3098, <https://doi.org/10.1021/acsaem.3c02979>.
- [132] L. Yao, K.E. Rivera-Cruz, P.M. Zimmerman, N. Singh, C.C.L. McCrory, Electrochemical CO₂ reduction to methanol by cobalt Phthalocyanine: quantifying CO₂ and CO binding strengths and their influence on methanol production, *ACS Catal.* 14 (1) (2024) 366–372, <https://doi.org/10.1021/acscatal.3c04957>.
- [133] Y. Song, P. Guo, T. Ma, J. Su, L. Huang, W. Guo, Y. Liu, G. Li, Y. Xin, Q. Zhang, S. Zhang, H. Shen, X. Feng, D. Yang, J. Tian, S.K. Ravi, B.Z. Tang, R. Ye, Ultrathin, cationic covalent organic Nanosheets for enhanced CO₂ Electroreduction to methanol, *Adv. Mater.* 36 (17) (2024) 2310037, <https://doi.org/10.1002/adma.202310037>.
- [134] W. Zhang, Q. Qin, L. Dai, R. Qin, X. Zhao, X. Chen, D. Ou, J. Chen, T.T. Chuong, B. Wu, N. Zheng, Electrochemical reduction of carbon dioxide to methanol on hierarchical Pd/SnO₂ Nanosheets with abundant Pd–O–Sn interfaces, *Angew. Chem. Int. Ed.* 57 (30) (2018) 9475–9479, <https://doi.org/10.1002/anie.201804142>.

- [135] N.R. Babji, E.O. McCusker, G.T. Whiteker, B. Canturk, N. Choy, L.C. Creemer, C.V. D. Amicis, N.M. Hewlett, P.L. Johnson, J.A. Knobelsdorf, F. Li, B.A. Lorsbach, B. M. Nugent, S.J. Ryan, M.R. Smith, Q. Yang, NMR chemical shifts of trace impurities: industrially preferred solvents used in process and green chemistry, *Org. Process. Res. Dev.* 20 (3) (2016) 661–667, <https://doi.org/10.1021/acs.oprd.5b00417>.
- [136] G.R. Fulmer, A.J.M. Miller, N.H. Sherden, H.E. Gottlieb, A. Nudelman, B. M. Stoltz, J.E. Bercaw, K.I. Goldberg, NMR chemical shifts of trace impurities: common laboratory solvents, organics, and gases in deuterated solvents relevant to the organometallic chemist, *Organometallics* 29 (9) (2010) 2176–2179, <https://doi.org/10.1021/om100106e>.
- [137] J. Huang, Q. Hu, X. Guo, Q. Zeng, L. Wang, Rethinking $\text{CO}(\text{CO}_3)_{0.5}(\text{OH})\cdot 0.11\text{H}_2\text{O}$: a new property for highly selective electrochemical reduction of carbon dioxide to methanol in aqueous solution, *Green Chem.* 20 (13) (2018) 2967–2972, <https://doi.org/10.1039/C7GC03744A>.
- [138] Z. Cao, J.S. Derrick, J. Xu, R. Gao, M. Gong, E.M. Nichols, P.T. Smith, X. Liu, X. Wen, C. Copéret, C.J. Chang, Chelating N-heterocyclic Carbene ligands enable tuning of Electrocatalytic CO_2 reduction to Formate and carbon monoxide: surface organometallic chemistry, *Angew. Chem. Int. Ed.* 57 (18) (2018) 4981–4985, <https://doi.org/10.1002/anie.201800367>.
- [139] X. Yang, J. Cheng, X. Yang, Y. Xu, W. Sun, J. Zhou, MOF-derived Cu_2O heterogeneous electrocatalyst with moderate intermediates adsorption for highly selective reduction of CO_2 to methanol, *Chem. Eng. J.* 431 (2022) 134171, <https://doi.org/10.1016/j.cej.2021.134171>.
- [140] Q.H. Low, N.W.X. Loo, F. Calle-Vallejo, B.S. Yeo, Enhanced Electroreduction of carbon dioxide to methanol using zinc dendrites pulse-deposited on silver foam, *Angew. Chem. Int. Ed.* 58 (8) (2019) 2256–2260, <https://doi.org/10.1002/anie.201810991>.
- [141] G. Zhang, T. Wang, M. Zhang, L. Li, D. Cheng, S. Zhen, Y. Wang, J. Qin, Z.-J. Zhao, J. Gong, Selective CO_2 electroreduction to methanol via enhanced oxygen bonding, *Nat. Commun.* 13 (1) (2022) 7768, <https://doi.org/10.1038/s41467-022-35450-8>.
- [142] J. Zhang, W. Luo, A. Züttel, Crossover of liquid products from electrochemical CO_2 reduction through gas diffusion electrode and anion exchange membrane, *J. Catal.* 385 (2020) 140–145, <https://doi.org/10.1016/j.jcat.2020.03.013>.
- [143] J.T. Perryman, J.C. Ortiz-Rodríguez, J.W. Jude, F.P. Hyler, R.C. Davis, A. Mehta, A.R. Kulikarni, C.J. Priddy, J.M. Velázquez, Metal-promoted Mo_6S_8 clusters: a platform for probing ensemble effects on the electrochemical conversion of CO_2 and CO to methanol, *Mater. Horiz.* 7 (1) (2020) 193–202, <https://doi.org/10.1039/C9MH00745H>.
- [144] M. Nur Hossain, S. Chen, A. Chen, Thermal-assisted synthesis of unique Cu nanodendrites for the efficient electrochemical reduction of CO_2 , *Appl. Catal. B Environ.* 259 (2019) 118096, <https://doi.org/10.1016/j.apcatb.2019.118096>.
- [145] D. Yang, Q. Zhu, C. Chen, H. Liu, Z. Liu, Z. Zhao, X. Zhang, S. Liu, B. Han, Selective electroreduction of carbon dioxide to methanol on copper selenide nanocatalysts, *Nat. Commun.* 10 (1) (2019) 677, <https://doi.org/10.1038/s41467-019-08653-9>.
- [146] L. Lu, X. Sun, J. Ma, D. Yang, H. Wu, B. Zhang, J. Zhang, B. Han, Highly Efficient Electroreduction of CO_2 to Methanol on Palladium–Copper Bimetallic Aerogels, *Angew. Chem. Int. Ed.* 57 (43) (2018) 14149–14153, <https://doi.org/10.1002/anie.201808964>.
- [147] X. Sun, Q. Zhu, X. Kang, H. Liu, Q. Qian, Z. Zhang, B. Han, Molybdenum–Bismuth Bimetallic Chalcogenide Nanosheets for Highly Efficient Electrocatalytic Reduction of Carbon Dioxide to Methanol, *Angew. Chem. Int. Ed.* 55 (23) (2016) 6771–6775, <https://doi.org/10.1002/anie.201603034>.
- [148] V. Rizzo, V. Pincirol, Quantitative NMR in synthetic and combinatorial chemistry, *J. Pharm. Biomed. Anal.* 38 (5) (2005) 851–857, <https://doi.org/10.1016/j.jpba.2005.01.045>.
- [149] F.A. Lipskerov, E.V. Sheshukova, T.V. Komarova, Approaches to formaldehyde measurement: from liquid biological samples to cells and organisms, *Int. J. Mol. Sci.* 23 (12) (2022) 6642, <https://doi.org/10.3390/ijms23126642>.
- [150] W. Li, X.-F. Wu, Formaldehyde as C1 Synthon in Organic Synthesis, 2022 2022/03/28. (The Chemical Transformations of C 1 Compounds), 2025.
- [151] A. Prodi, F. Rui, A. Belloni Fortina, M.T. Corradin, Filon F. Larese, Sensitization to formaldehyde in northeastern Italy, 1996 to 2012, *Dermatitis* 27 (1) (2016) 21–25, <https://doi.org/10.1097/DER.0000000000000158>.
- [152] W.J. Rea, K.D. Patel, Reversibility of chronic disease and hypersensitivity, in: *The Environmental Aspects of Chemical Sensitivity*, 1st ed. vol. 4, CRC Press, 2018.
- [153] A.K. Haghi, D. Balköse, O.V. Mukbaniani, A.G. Mercader, *Applied Chemistry and Chemical Engineering. Mathematical and Analytical Techniques*. Vol. 1. 1st ed. Apple Academic Press, 2018.
- [154] A.M. Bahmanpour, A. Hoadley, A. Tanksale, Critical review and exergy analysis of formaldehyde production processes, *Rev. Chem. Eng.* 30 (6) (2014) 583–604, <https://doi.org/10.1515/revce-2014-0022>.
- [155] H.I. Mahdi, N.N. Ramlie, Santos DHDS, D.A. Giannakoudakis, L.H. de Oliveira, R. Selvasembian, Azelee NIW, A. Bazargan, L. Meili, Formaldehyde production using methanol and heterogeneous solid catalysts: a comprehensive review, *Mol Catal* 537 (2023) 112944, <https://doi.org/10.1016/j.mcat.2023.112944>.
- [156] J. Quiroz Torres, S. Royer, J.-P. Bellat, J.-M. Giraudon, J.-F. Lamonier, Formaldehyde: catalytic oxidation as a promising soft way of elimination, *ChemSusChem* 6 (4) (2013) 578–592, <https://doi.org/10.1002/cssc.201200809>.
- [157] K. Nakata, T. Ozaki, C. Terashima, A. Fujishima, Y. Einaga, High-yield electrochemical production of formaldehyde from CO_2 and seawater, *Angew. Chem. Int. Ed.* 53 (3) (2014) 871–874, <https://doi.org/10.1002/anie.201308657>.
- [158] L. Yao, Y. Pan, D. Wu, A. Bentalib, J. Li, B. Liu, Z. Peng, Balancing CO chemisorption with hydrogen electrochemical adsorption on Pt alloy catalyst for improving direct CO reduction to formaldehyde, *Chem. Eng. J.* 446 (2022) 137131, <https://doi.org/10.1016/j.cej.2022.137131>.
- [159] M. Girardi, S. Blanchard, S. Griveau, P. Simon, M. Fontecave, F. Bedioui, A. Proust, Electro-assisted reduction of CO_2 to CO and formaldehyde by $(\text{TOA})_6[\alpha\text{-SiW}_{11}\text{O}_{39}\text{Co}(\text{I})]$ Polyoxometalate, *Eur. J. Inorg. Chem.* 2015 (22) (2015) 3642–3648, <https://doi.org/10.1002/ejic.201500389>.
- [160] L. Deng, Z. Wang, X. Jiang, J. Xu, Z. Zhou, X. Li, Z. You, M. Ding, T. Shishido, X. Liu, M. Xu, Catalytic aqueous CO_2 reduction to formaldehyde at Ru surface on hydroxyl-groups-rich LDH under mild conditions, *Appl. Catal. B Environ.* 322 (2023) 122124, <https://doi.org/10.1016/j.apcatb.2022.122124>.
- [161] D. Xiang, D. Magana, R.B. Dyer, CO_2 reduction catalyzed by Mercaptopteridine on glassy carbon, *J. Am. Chem. Soc.* 136 (40) (2014) 14007–14010, <https://doi.org/10.1021/ja5081103>.
- [162] L. Yao, Y. Pan, X. Shen, D. Wu, A. Bentalib, Z. Peng, Utilizing hydrogen underpotential deposition in CO reduction for highly selective formaldehyde production under ambient conditions, *Green Chem.* 22 (17) (2020) 5639–5647, <https://doi.org/10.1039/D0GC001412E>.
- [163] S. Gonglach, S. Paul, M. Haas, F. Pillwein, S.S. Sreejith, S. Barman, R. De, S. Müllegger, P. Gerschel, U.-P. Apfel, H. Coskun, A. Aljabour, P. Stadler, W. Schöfberger, S. Roy, Molecular cobalt corrole complex for the heterogeneous electrocatalytic reduction of carbon dioxide, *Nat. Commun.* 10 (1) (2019) 3864, <https://doi.org/10.1038/s41467-019-11868-5>.
- [164] E. Boutin, A. Salamé, L. Merakeb, T. Chatterjee, M. Robert, On the existence and role of formaldehyde during aqueous electrochemical reduction of carbon monoxide to methanol by cobalt Phthalocyanine, *Chem. Eur. J.* 28 (27) (2022) e202200697, <https://doi.org/10.1002/chem.202200697>.
- [165] S. Zhao, H.-Q. Liang, X.-M. Hu, S. Li, K. Daasbjerg, Challenges and prospects in the catalytic conversion of carbon dioxide to formaldehyde, *Angew. Chem. Int. Ed.* 61 (46) (2022) e202204008, <https://doi.org/10.1002/anie.202204008>.
- [166] A. Singh, A. Zamader, R. Khakpour, K. Laasonen, M. Busch, M. Robert, Molecular electrochemical catalysis of CO -to-formaldehyde conversion with a cobalt complex, *J. Am. Chem. Soc.* 146 (32) (2024) 22129–22133, <https://doi.org/10.1021/jacs.4c06878>.
- [167] Y. Lin, T. Wang, L. Zhang, G. Zhang, L. Li, Q. Chang, Z. Pang, H. Gao, K. Huang, P. Zhang, Z.-J. Zhao, C. Pei, J. Gong, Tunable CO_2 electroreduction to ethanol and ethylene with controllable interfacial wettability, *Nat. Commun.* 14 (1) (2023) 3575, <https://doi.org/10.1038/s41467-023-39351-2>.
- [168] A.D. Handoko, K.W. Chan, B.S. Yeo, $-\text{CH}_3$ mediated pathway for the Electroreduction of CO_2 to ethane and ethanol on thick oxide-derived copper catalysts at Low Overpotentials, *ACS Energy Lett.* 2 (9) (2017) 2103–2109, <https://doi.org/10.1021/acscenergylett.7b00514>.
- [169] L. Yang, X. Lv, C. Peng, S. Kong, F. Huang, Y. Tang, L. Zhang, G. Zheng, Promoting CO_2 Electroreduction to acetate by an amine-terminal, Dendrimer-Functionalized Cu Catalyst, *ACS Cent Sci* 9 (10) (2023) 1905–1912, <https://doi.org/10.1021/acscentsci.3c00826>.
- [170] H.-T. Kim, J. Park, J. Mun, H. Shin, D.-H. Roh, J. Kwon, S. Kim, S.-J. Kim, G. Lee, S.-J. Kang, T.-H. Kwon, Selective Electroreduction of CO_2 to C_2+ alcohols using graphitic frustrated Lewis pair catalyst, *ACS Catal.* 14 (13) (2024) 10392–10402, <https://doi.org/10.1021/acscatal.3c04275>.
- [171] I.A. Idowu, K. Hashim, A. Shaw, L.J.R. Nunes, Enhancing the fuel properties of beverage wastes as non-edible feedstock for biofuel production, *Biofuels* 13 (6) (2022) 763–770, <https://doi.org/10.1080/17597269.2021.1923934>.
- [172] T.-D. Hoang, N. Nghiem, Recent developments and current status of commercial production of fuel ethanol, *Fermentation* 7 (4) (2021) 314, <https://doi.org/10.3390/fermentation7040314>.
- [173] C. Manochio, B.R. Andrade, R.P. Rodriguez, B.S. Moraes, Ethanol from biomass: a comparative overview, *Renew. Sust. Energ. Rev.* 80 (2017) 743–755, <https://doi.org/10.1016/j.rser.2017.05.063>.
- [174] Y. Nakagawa, N. Tajima, K. Hirao, A theoretical study of catalytic hydration reactions of ethylene, *J. Comput. Chem.* 21 (14) (2000) 1292–1304, [https://doi.org/10.1002/1096-987X\(20001115\)21:14<1292::AID-JCC8>3.0.CO;2-5](https://doi.org/10.1002/1096-987X(20001115)21:14<1292::AID-JCC8>3.0.CO;2-5).
- [175] S. Dongare, N. Singh, H. Bhunia, P.K. Bajpai, Electrochemical reduction of CO_2 using oxide based Cu and Zn bimetallic catalyst, *Electrochim. Acta* 392 (2021) 138988, <https://doi.org/10.1016/j.electacta.2021.138988>.
- [176] Robens E, Hecker B, Kungl H, Tempel H, Eichel R-A. Bimetallic Copper–Silver Catalysts for the Electrochemical Reduction of CO_2 to Ethanol, *ACS Appl Energy Mater* 6(14) (2023) 7571–7577. doi: <https://doi.org/10.1021/acsaem.3c00985>.
- [177] X. Zhao, G. Hao, Q. Fang, X. Lang, D. Li, D. Zhong, J. Li, Q. Zhao, Boosting $^*\text{CO}$ coverage on Cu octahedra enclosed by Cu(111) for efficient CO_2 electroreduction to $\text{C}_2\text{H}_5\text{OH}$, *Appl. Surf. Sci.* 664 (2024) 160202, <https://doi.org/10.1016/j.apsusc.2024.160202>.
- [178] Y. Song, R. Peng, D.K. Hensley, P.V. Bonnesen, L. Liang, Z. Wu, H.M. Meyer Iii, M. Chi, C. Ma, B.G. Sumpter, A.J. Rondinone, High-selectivity electrochemical conversion of CO_2 to ethanol using a copper nanoparticle/N-doped graphene electrode, *ChemistrySelect* 1 (19) (2016) 6055–6061, <https://doi.org/10.1002/slct.201601169>.
- [179] J. Yuan, M.-P. Yang, W.-Y. Zhi, H. Wang, H. Wang, J.-X. Lu, Efficient electrochemical reduction of CO_2 to ethanol on Cu nanoparticles decorated on N-doped graphene oxide catalysts, *J CO2 Util* 33 (2019) 452–460, <https://doi.org/10.1016/j.jcou.2019.07.014>.
- [180] M. Li, N. Song, W. Luo, J. Chen, W. Jiang, J. Yang, Engineering surface Oxophilicity of copper for electrochemical CO_2 reduction to ethanol, *Adv. Sci.* 10 (2) (2023) 2204579, <https://doi.org/10.1002/adv.202204579>.
- [181] J. Ding, H. Bin Yang, X.-L. Ma, S. Liu, W. Liu, Q. Mao, Y. Huang, J. Li, T. Zhang, B. Liu, A tin-based tandem electrocatalyst for CO_2 reduction to ethanol with 80%

- selectivity, *Nat. Energy* 8 (12) (2023) 1386–1394, <https://doi.org/10.1038/s41560-023-01389-3>.
- [182] H. Xu, D. Rebolgar, H. He, L. Chong, Y. Liu, C. Liu, C.-J. Sun, T. Li, J.V. Muntean, R.E. Winans, D.-J. Liu, T. Xu, Highly selective electrocatalytic CO₂ reduction to ethanol by metallic clusters dynamically formed from atomically dispersed copper, *Nat. Energy* 5 (8) (2020) 623–632, <https://doi.org/10.1038/s41560-020-0666-x>.
- [183] Y. Liu, X. Fan, A. Nayak, Y. Wang, B. Shan, X. Quan, T.J. Meyer, Steering CO₂ electroreduction toward ethanol production by a surface-bound Ru polypyridyl carbene catalyst on N-doped porous carbon, *PNAS* 116 (52) (2019) 26353–26358, <https://doi.org/10.1073/pnas.1907740116>.
- [184] F. Li, Y.C. Li, Z. Wang, J. Li, D.-H. Nam, Y. Lum, M. Luo, X. Wang, A. Ozden, S.-F. Hung, B. Chen, Y. Wang, J. Wicks, Y. Xu, Y. Li, C.M. Gabardo, C.-T. Dinh, Y. Wang, T.-T. Zhuang, D. Sinton, E.H. Sargent, Cooperative CO₂-to-ethanol conversion via enriched intermediates at molecule–metal catalyst interfaces, *Nat. Catal.* 3 (1) (2020) 75–82, <https://doi.org/10.1038/s41929-019-0383-7>.
- [185] Y.C. Li, Z. Wang, T. Yuan, D.-H. Nam, M. Luo, J. Wicks, B. Chen, J. Li, F. Li, F.P. G. de Arquer, Y. Wang, C.-T. Dinh, O. Voznyy, D. Sinton, E.H. Sargent, Binding site diversity promotes CO₂ Electroreduction to ethanol, *J. Am. Chem. Soc.* 141 (21) (2019) 8584–8591, <https://doi.org/10.1021/jacs.9b02945>.
- [186] X. Wang, Z. Wang, F.P. García de Arquer, C.-T. Dinh, A. Ozden, Y.C. Li, D.-H. Nam, J. Li, Y.-S. Liu, J. Wicks, Z. Chen, M. Chi, B. Chen, Y. Wang, J. Tam, J. Y. Howe, A. Proppe, P. Todorović, F. Li, T.-T. Zhuang, C.M. Gabardo, A. R. Kirmani, C. McCallum, S.-F. Hung, Y. Lum, M. Luo, Y. Min, A. Xu, C.P. O'Brien, B. Stephen, B. Sun, A.H. Ip, L.J. Richter, S.O. Kelley, D. Sinton, E.H. Sargent, Efficient electrically powered CO₂-to-ethanol via suppression of deoxygenation, *Nat. Energy* 5 (6) (2020) 478–486, <https://doi.org/10.1038/s41560-020-0607-8>.
- [187] W. Ma, S. Xie, T. Liu, Q. Fan, J. Ye, F. Sun, Z. Jiang, Q. Zhang, J. Cheng, Y. Wang, Electrocatalytic reduction of CO₂ to ethylene and ethanol through hydrogen-assisted C–C coupling over fluorine-modified copper, *Nat. Catal.* 3 (6) (2020) 478–487, <https://doi.org/10.1038/s41929-020-0450-0>.
- [188] X. Su, Z. Jiang, J. Zhou, H. Liu, D. Zhou, H. Shang, X. Ni, Z. Peng, F. Yang, W. Chen, Z. Qi, D. Wang, Y. Wang, Complementary operando spectroscopy identification of in-situ generated metastable charge-asymmetry Cu₂-CuN₃ clusters for CO₂ reduction to ethanol, *Nat. Commun.* 13 (1) (2022) 1322, <https://doi.org/10.1038/s41467-022-29035-8>.
- [189] S. Shen, X. Peng, L. Song, Y. Qiu, C. Li, L. Zhuo, J. He, J. Ren, X. Liu, J. Luo, AuCu alloy nanoparticle embedded Cu Submicrocone arrays for selective conversion of CO₂ to ethanol, *Small* 15 (37) (2019) 190229, <https://doi.org/10.1002/smll.201902229>.
- [190] W. Xia, Y. Xie, S. Jia, S. Han, R. Qi, T. Chen, X. Xing, T. Yao, D. Zhou, X. Dong, J. Zhai, J. Li, J. He, D. Jiang, Y. Yamauchi, M. He, H. Wu, B. Han, Adjacent Copper Single Atoms Promote C–C Coupling in Electrochemical CO₂ Reduction for the Efficient Conversion of Ethanol, *J. Am. Chem. Soc.* 145 (31) (2023) 17253–17264, <https://doi.org/10.1021/jacs.3c04612>.
- [191] K. Lv, Y. Fan, Y. Zhu, Y. Yuan, J. Wang, Y. Zhu, Q. Zhang, Elastic ag-anchored N-doped graphene/carbon foam for the selective electrochemical reduction of carbon dioxide to ethanol, *J. Mater. Chem. A* 6 (12) (2018) 5025–5031, <https://doi.org/10.1039/C7TA10802H>.
- [192] W. Zhu, K. Zhao, S. Liu, M. Liu, F. Peng, P. An, B. Qin, H. Zhou, H. Li, Z. He, Low-overpotential selective reduction of CO₂ to ethanol on electrodeposited Cu₂Au nanowire arrays, *J. Energy Chem.* 37 (2019) 176–182, <https://doi.org/10.1016/j.ijechem.2019.03.030>.
- [193] C. Kim, K.M. Cho, K. Park, J.Y. Kim, G.-T. Yun, F.M. Toma, I. Gereige, H.-T. Jung, Cu/Cu₂O interconnected porous aerogel catalyst for highly productive Electrosynthesis of ethanol from CO₂, *Adv. Funct. Mater.* 31 (32) (2021) 2102142, <https://doi.org/10.1002/adfm.202102142>.
- [194] J. Yuan, J.-J. Zhang, M.-P. Yang, W.-J. Meng, H. Wang, J.-X. Lu, CuO nanoparticles supported on TiO₂ with high efficiency for CO₂ electrochemical reduction to ethanol, *Catalysts* 8 (4) (2018) 171, <https://doi.org/10.3390/catal8040171>.
- [195] T.A. Ivandini, Electrochemical conversion of CO₂ at metal-modified boron-doped diamond electrodes, *AIP Conf. Proc.* 2023 (1) (2018) 020102, <https://doi.org/10.1063/1.5064099>.
- [196] X. Wang, Y. Chen, F. Li, R.K. Miao, J.E. Huang, Z. Zhao, X.-Y. Li, R. Dorakhan, S. Chu, J. Wu, S. Zheng, W. Ni, D. Kim, S. Park, Y. Liang, A. Ozden, P. Ou, Y. Hou, D. Sinton, E.H. Sargent, Site-selective protonation enables efficient carbon monoxide electroreduction to acetate, *Nat. Commun.* 15 (1) (2024) 616, <https://doi.org/10.1038/s41467-024-44727-z>.
- [197] Z.-X. Li, X.-F. Qiu, P.-Q. Liao, Efficient electroreduction of CO₂ to acetate with relative purity of 100% by ultrasmall Cu₂O nanoparticle on a conductive metal-organic framework, *Chin. Chem. Lett.* (2024) 110473, <https://doi.org/10.1016/j.ccllet.2024.110473>.
- [198] H.-L. Zhu, J.-R. Huang, M.-D. Zhang, C. Yu, P.-Q. Liao, X.-M. Chen, Continuously produced highly concentrated and pure acetic acid aqueous solution via direct Electroreduction of CO₂, *J. Am. Chem. Soc.* 146 (1) (2024) 1144–1152, <https://doi.org/10.1021/jacs.3c12423>.
- [199] R. De, S. Gonglach, S. Paul, M. Haas, S.S. Sreejith, P. Gerschel, U.-P. Apfel, T. H. Vuong, J. Rabeah, S. Roy, W. Schöfberger, Electrocatalytic reduction of CO₂ to acetic acid by a molecular manganese Corrole complex, *Angew. Chem. Int. Ed.* 59 (26) (2020) 10527–10534, <https://doi.org/10.1002/anie.20200601>.
- [200] Y. Wang, J. Zhao, C. Cao, J. Ding, R. Wang, J. Zeng, J. Bao, B. Liu, Amino-functionalized Cu for efficient electrochemical reduction of CO to acetate, *ACS Catal.* 13 (6) (2023) 3532–3540, <https://doi.org/10.1021/acscatal.2c05140>.
- [201] D. Zang, Q. Li, G. Dai, M. Zeng, Y. Huang, Y. Wei, Interface engineering of MoS₂/Cu heterostructures toward highly selective electrochemical reduction of carbon dioxide into acetate, *Appl. Catal. B Environ.* 281 (2021) 119426, <https://doi.org/10.1016/j.apcatb.2020.119426>.
- [202] W. Luc, X. Fu, J. Shi, J.-J. Lv, M. Jouny, B.H. Ko, Y. Xu, Q. Tu, X. Hu, J. Wu, Q. Yue, Y. Liu, F. Jiao, Y. Kang, Two-dimensional copper nanosheets for electrochemical reduction of carbon monoxide to acetate, *Nat. Catal.* 2 (5) (2019) 423–430, <https://doi.org/10.1038/s41929-019-0269-8>.
- [203] H.H. Heenen, H. Shin, G. Kastlunger, S. Overa, J.A. Gauthier, F. Jiao, K. Chan, The mechanism for acetate formation in electrochemical CO₂ reduction on Cu: selectivity with potential, pH, and nanostructuring, *Energy Environ. Sci.* 15 (9) (2022) 3978–3990, <https://doi.org/10.1039/D2EE01485H>.
- [204] X.-F. Qiu, J.-R. Huang, C. Yu, Z.-H. Zhao, H.-L. Zhu, Z. Ke, P.-Q. Liao, X.-M. Chen, A stable and conductive covalent organic framework with isolated active sites for highly selective Electroreduction of carbon dioxide to acetate, *Angew. Chem. Int. Ed.* 61 (36) (2022) e202206470, <https://doi.org/10.1002/anie.202206470>.
- [205] W. Rong, H. Zou, S. Tan, E. Hu, F. Li, C. Tang, H. Dai, S. Wei, Y. Ji, L. Duan, Few-atom copper catalyst for the electrochemical reduction of CO to acetate: synergistic catalysis between neighboring Cu atoms, *CCS Chem.* 5 (5) (2022) 1176–1188, <https://doi.org/10.31635/ccschem.022.202201910>.
- [206] Y. Wang, D. Wang, C.J. Dares, S.L. Marquard, M.V. Sheridan, T.J. Meyer, CO₂ reduction to acetate in mixtures of ultrasmall (Cu)_m(Ag)_m bimetallic nanoparticles, *PNAS* 115 (2) (2018) 278–283, <https://doi.org/10.1073/pnas.1713962115>.
- [207] M. Abidinejad, T. Yuan, K. Tang, S. Duangdangchote, A. Farzi, H.-P. Iglesias van Montfort, M. Li, J. Middelkoop, M. Wolff, A. Seifitokaldani, O. Voznyy, T. Burdyny, Electroreduction of carbon dioxide to acetate using Heterogenized hydrophilic manganese porphyrins, *Chem. Eur. J.* 29 (14) (2023) e202203977, <https://doi.org/10.1002/chem.202203977>.
- [208] J.-X. Wu, S.-Z. Hou, X.-D. Zhang, M. Xu, H.-F. Yang, P.-S. Cao, Z.-Y. Gu, Cathodized copper porphyrin metal-organic framework nanosheets for selective formate and acetate production from CO₂ electroreduction, *Chem. Sci.* 10 (7) (2019) 2199–2205, <https://doi.org/10.1039/C8SC04344B>.
- [209] Q. Sun, Y. Zhao, X. Tan, C. Jia, Z. Su, Q. Meyer, M.I. Ahmed, C. Zhao, Atomically dispersed Cu–Au alloy for efficient Electrocatalytic reduction of carbon monoxide to acetate, *ACS Catal.* 13 (8) (2023) 5689–5696, <https://doi.org/10.1021/acscatal.2c06145>.
- [210] W. Sun, C. Li, H. Zhao, The targeted multi-electrons transfer for acetic acid and ethanol obtained with (n-Bu₄N)₃SVW₁₁O₄₀ and in synergistic catalysis in CO₂ electroreduction, *J. Power Sources* 517 (2022) 230665, <https://doi.org/10.1016/j.jpowsour.2021.230665>.
- [211] M. Serafini, F. Mariani, A. Fasolini, E.T. Brandi, E. Scavetta, F. Basile, D. Tonelli, Electrosynthesized CuMgAl layered double hydroxides as new catalysts for the electrochemical reduction of CO₂, *Adv. Funct. Mater.* 33 (29) (2023) 2300345, <https://doi.org/10.1002/adfm.202300345>.
- [212] J. Liu, X. Guo, Z. Lyu, R.-B. Song, P. Zhou, S. Ding, Y. Zhou, L.-P. Jiang, Y. Lin, W. Zhu, A novel tandem reactor design based on nano-cu electrocatalysts and microbial biocatalysts for converting CO₂ into ethylene and acetate, *Green Chem.* 25 (14) (2023) 5712–5720, <https://doi.org/10.1039/D3GC01025B>.
- [213] J.Z.Y. Tan, A.K. Virdee, J.M. Andresen, M.M. Maroto-Valer, Core-shell nanostructured Cu-based bi-metallic electrocatalysts for co-production of ethylene and acetate, *Faraday Discuss.* 247 (0) (2023) 216–226, <https://doi.org/10.1039/D3FD00058C>.
- [214] W. Tian, N. Li, D. Chen, Q. Xu, H. Li, C. Yan, J. Lu, Vibration-driven reduction of CO₂ to acetate with 100% selectivity by SnS Nanobelt Piezocatalysts, *Angew. Chem. Int. Ed.* 62 (33) (2023) e202306964, <https://doi.org/10.1002/anie.202306964>.
- [215] S. Guo, Y. Liu, Y. Huang, H. Wang, E. Murphy, L. Lafontaine, J.L. Chen, I. V. Zhenyuk, P. Atanassov, Promoting electrolysis of carbon monoxide toward acetate and 1-propanol in flow Electrolyzer, *ACS Energy Lett.* 8 (2) (2023) 935–942, <https://doi.org/10.1021/acsenergylett.2c02502>.
- [216] X. Fu, Y. Wang, H. Shen, Y. Yu, F. Xu, G. Zhou, W. Xie, R. Qin, C. Dun, C.W. Pao, J. L. Chen, Y. Liu, J. Guo, Q. Yue, J.J. Urban, C. Wang, Y. Kang, Chemical upgrade of carbon monoxide to acetate on an atomically dispersed copper catalyst via CO-insertion, *Mater. Today Phys.* 19 (2021) 100418, <https://doi.org/10.1016/j.mtphys.2021.100418>.
- [217] H.-L. Zhu, H.-Y. Chen, Y.-X. Han, Z.-H. Zhao, P.-Q. Liao, X.-M. Chen, A porous π–π stacking framework with Dicooper(I) sites and adjacent proton relays for Electroreduction of CO₂ to C₂₊ products, *J. Am. Chem. Soc.* 144 (29) (2022) 13319–13326, <https://doi.org/10.1021/jacs.2c04670>.
- [218] A. Caligiani, D. Acquotti, G. Palla, V. Bocchi, Identification and quantification of the main organic components of vinegars by high resolution ¹H NMR spectroscopy, *Anal. Chim. Acta* 585 (1) (2007) 110–119, <https://doi.org/10.1016/j.aca.2006.12.016>.
- [219] J.E.A. Rodrigues, G.L. Erny, A.S. Barros, V.I. Esteves, T. Brandão, A.A. Ferreira, E. Cabrita, A.M. Gil, Quantification of organic acids in beer by nuclear magnetic resonance (NMR)-based methods, *Anal. Chim. Acta* 674 (2) (2010) 166–175, <https://doi.org/10.1016/j.aca.2010.06.029>.
- [220] I.C. Jones, G.J. Sharman, J. Pidgeon, ¹H and ¹³C NMR data to aid the identification and quantification of residual solvents by NMR spectroscopy, *Magn. Reson. Chem.* 43 (6) (2005) 497–509, <https://doi.org/10.1002/mrc.1578>.
- [221] M. Grootveld, B. Percival, M. Gibson, Y. Osman, M. Edgar, M. Molinari, M. L. Mather, F. Casanova, P.B. Wilson, Progress in low-field benchtop NMR spectroscopy in chemical and biochemical analysis, *Anal. Chim. Acta* 1067 (2019) 11–30, <https://doi.org/10.1016/j.aca.2019.02.026>.
- [222] C. Castiello, P. Junghanns, A. Mergel, C. Jacob, C. Ducho, S. Valente, D. Rotili, R. Fioravanti, C. Zwergel, A. Mai, GreenMedChem: the challenge in the next

- decade toward eco-friendly compounds and processes in drug design, *Green Chem.* 25 (6) (2023) 2109–2169, <https://doi.org/10.1039/D2GC03772F>.
- [223] S. Jovanovic, P. Jakes, S. Merz, D.T. Daniel, R.-A. Eichel, J. Granwehr, In operando NMR investigations of the aqueous electrolyte chemistry during electrolytic CO₂ reduction, *Commun Chem* 6 (1) (2023) 268, <https://doi.org/10.1038/s42004-023-01065-3>.
- [224] Z. Zhu, R. Luo, E.W. Zhao, Operando NMR methods for studying electrocatalysis, *Magn. Reson. Lett* 4 (2) (2024) 100096, <https://doi.org/10.1016/j.mrl.2023.12.004>.
- [225] B.B. Xu, Y. Liu, Y. Liu, X. You, H. Zhou, Y.N. Xu, P.F. Liu, H.F. Wang, H.G. Yang, X.L. Wang, Y.F. Yao, Operando electrochemical NMR spectroscopy reveals a water-assisted formate formation mechanism, *Chem* 10 (10) (2024) 3114–3130, <https://doi.org/10.1016/j.chempr.2024.06.001>.